

University of Alberta

**Thermokinetic Modeling of the HCCI Cycle:  
Predicting the Ignition Timing**

by

**Patrick Kirchen**



A thesis submitted to the Faculty of Graduate Studies and Research in  
partial fulfillment of the requirements for the degree of Master of Science

Department of Mechanical Engineering

Edmonton Alberta

Fall 2004



Library and  
Archives Canada

Bibliothèque et  
Archives Canada

Published Heritage  
Branch

Direction du  
Patrimoine de l'édition

395 Wellington Street  
Ottawa ON K1A 0N4  
Canada

395, rue Wellington  
Ottawa ON K1A 0N4  
Canada

*Your file* *Votre référence*  
*ISBN: 0-612-95784-5*  
*Our file* *Notre référence*  
*ISBN: 0-612-95784-5*

The author has granted a non-exclusive license allowing the Library and Archives Canada to reproduce, loan, distribute or sell copies of this thesis in microform, paper or electronic formats.

L'auteur a accordé une licence non exclusive permettant à la Bibliothèque et Archives Canada de reproduire, prêter, distribuer ou vendre des copies de cette thèse sous la forme de microfiche/film, de reproduction sur papier ou sur format électronique.

The author retains ownership of the copyright in this thesis. Neither the thesis nor substantial extracts from it may be printed or otherwise reproduced without the author's permission.

L'auteur conserve la propriété du droit d'auteur qui protège cette thèse. Ni la thèse ni des extraits substantiels de celle-ci ne doivent être imprimés ou autrement reproduits sans son autorisation.

---

In compliance with the Canadian Privacy Act some supporting forms may have been removed from this thesis.

Conformément à la loi canadienne sur la protection de la vie privée, quelques formulaires secondaires ont été enlevés de cette thèse.

While these forms may be included in the document page count, their removal does not represent any loss of content from the thesis.

Bien que ces formulaires aient inclus dans la pagination, il n'y aura aucun contenu manquant.

# Canada

"... they who are Friends do not what they *think* they must,  
but what they *must*."

-*Henry David Thoreau*

To my wife Krystal

## Acknowledgements

I would like to take this opportunity to thank some of the many people who have helped or encouraged this work, whether they knew it or not.

I am deeply indebted to my supervisor, Dr. Bob Koch, not only for his financial support, but also for his guidance in all things academic. He has given me the freedom to explore different topics as I saw fit, but at the same time helped me stay focussed on our goals. Dr. Larry Kostiuk has been able to find time to help me with both technical and personal dilemmas, for which I am greatly appreciative. I would also like to thank Dr. Doug Dale and Mr. Mark Ackerman as they are the ones responsible for introducing the world of research to me, as well as Dr. Alan Nelson for his work as an external examiner.

My sanity, or what's left of it, is attributed to Mr. David Arthur and my other lab mates. These are the guys that I can count on for a beer, a coffee, or a laugh. The friendships formed during these last two and a half years will not soon end.

My family, both immediate and inherited, have always been supportive of my decisions, including this degree. Without your support, Mom, Dad, Chris, Heather, Dave, Sandra, and Kerri, this would have been a most impossible task.

If there is one person whom I cannot thank enough, it is my wife Krystal. She has had to put up with an absent (both physically and mentally) boyfriend, fiancé, and husband, but despite this has been the one that keeps me going. Her love, support, and friendship remind me that there is more to life than what is on these pages. Thank you, Krystal.

Much of the computational work presented in this thesis was carried out using the Westgrid High Performance Computing Network, allowing the work to progress at a much accelerated pace. The ability to access this Network is gratefully acknowledged.

# Contents

<b>1</b>	<b>Introduction</b>	<b>1</b>
1.1	Background . . . . .	1
1.2	Overview of This Thesis . . . . .	4
1.3	Layout of the Thesis . . . . .	5
<b>2</b>	<b>Literature Review</b>	<b>7</b>
2.1	The HCCI Cycle: A Brief History . . . . .	7
2.2	Controlling HCCI Combustion . . . . .	12
2.2.1	Octane Number . . . . .	12
2.2.2	Initial Temperature . . . . .	13
2.2.3	Engine Speed . . . . .	14
2.2.4	Compression Ratio . . . . .	15
2.2.5	Equivalence Ratio . . . . .	16
2.2.6	Initial Pressure . . . . .	17
2.2.7	EGR . . . . .	18
2.3	Modeling of the HCCI Cycle . . . . .	20
2.3.1	Modeling of the Combustion Process . . . . .	21
2.3.2	Thermodynamic Models . . . . .	27
2.4	Summary . . . . .	30
<b>3</b>	<b>Background Theory</b>	<b>34</b>
3.1	Introduction . . . . .	34
3.2	Thermodynamic Modeling . . . . .	35
3.2.1	Energy Balance . . . . .	36
3.2.2	Boundary Work . . . . .	40
3.2.3	Internal Energy . . . . .	41
3.2.4	Energy Balance - Revisited . . . . .	42
3.3	Thermodynamic Properties . . . . .	43
3.3.1	Estimating the Specific Heat . . . . .	44
3.3.2	Determination of NASA Polynomials . . . . .	47
3.4	Chemical Kinetics . . . . .	49
3.4.1	Kinetic Modeling . . . . .	49

## CONTENTS

---

3.4.2	Hydrocarbon Ignition and Combustion . . . . .	54
3.4.3	A Skeletal Kinetic Mechanism . . . . .	59
3.5	The Complete Thermokinetic Model . . . . .	62
3.5.1	Initial Conditions . . . . .	64
3.5.2	Solution Methodology . . . . .	66
3.6	Summary . . . . .	67
<b>4</b>	<b>Validation of the Thermokinetic Model</b>	<b>73</b>
4.1	Introduction . . . . .	73
4.2	Equilibrium Validation . . . . .	74
4.2.1	Equilibrium Calculations . . . . .	75
4.2.2	Results . . . . .	76
4.3	Ignition Delay Validation . . . . .	77
4.3.1	Rapid Compression Machine Validation . . . . .	78
4.3.2	Shock Tube Validation . . . . .	81
4.4	HCCI Validation . . . . .	84
4.4.1	Calculating the HCCI Ignition Timing . . . . .	85
4.4.2	Results . . . . .	89
4.5	Summary . . . . .	94
<b>5</b>	<b>Applications of the Thermokinetic Model</b>	<b>96</b>
5.1	Introduction . . . . .	96
5.2	Parameter Variations . . . . .	97
5.3	Dimensional Analysis . . . . .	98
5.3.1	Initial Pressure . . . . .	100
5.3.2	Initial Temperature . . . . .	100
5.3.3	Engine Speed . . . . .	101
5.3.4	EGR Rate . . . . .	102
5.3.5	Equivalence Ratio . . . . .	106
5.3.6	Ignition Delay . . . . .	107
5.3.7	Evaluation of Dimensionless Parameters . . . . .	107
5.4	Predicting the Ignition Timing Parametrically . . . . .	110
5.4.1	Implementing the Ignition Correlation . . . . .	113
5.5	Summary . . . . .	114
<b>6</b>	<b>Conclusions and Future Work</b>	<b>116</b>
6.1	Conclusions . . . . .	116
6.1.1	Thermokinetic Model . . . . .	117
6.1.2	Parameter Variations . . . . .	118
6.2	Future Work . . . . .	119
6.2.1	Thermokinetic Model . . . . .	119
<b>A</b>	<b>Sample Calculations</b>	<b>132</b>

## CONTENTS

---

A.1	Estimation of the Specific Heat of Iso-Octane . . . . .	132
A.2	Example using the Ignition Correlation . . . . .	134
A.2.1	Problem Statement . . . . .	134
A.2.2	Solution . . . . .	134
A.2.3	Determining the Required Temperature . . . . .	137
A.3	Calculation Specific Heats . . . . .	138
A.3.1	Combustion Equation . . . . .	138
<b>B</b>	<b>Extrapolated <math>c_p</math> Fits</b>	<b>140</b>
<b>C</b>	<b>Computer Programs</b>	<b>150</b>

# List of Tables

3.1	Matlab ODE solvers . . . . .	67
3.2	Complete skeletal chemical kinetic mechanism . . . . .	68
4.1	Initial conditions for equilibrium validation . . . . .	76
4.2	Initial conditions for rapid compression machine validation . . . . .	80
4.3	CFR engine configuration . . . . .	86
4.4	HCCI validation conditions . . . . .	87
5.1	Parameter variation ranges . . . . .	98
5.2	Effect of EGR on specific heat capacity . . . . .	103
5.3	Ignition correlation validation parameters . . . . .	111
A.1	Ignition correlation validation parameters . . . . .	134
C.1	List of Computer Programs . . . . .	151

# List of Figures

1.1	The HCCI Cycle . . . . .	2
2.1	Comparison of chemical kinetic mechanism reduction methods . . .	25
3.1	One zone thermodynamic system . . . . .	37
3.2	Characteristics of hydrocarbon autoignition . . . . .	58
3.3	The negative temperature coefficient region . . . . .	59
3.4	Schematic of chemical kinetic mechanism . . . . .	61
3.5	Schematic of the thermokinetic model . . . . .	63
4.1	Combustion temperature validation with STANJAN . . . . .	77
4.2	Roll-up vortex containment in a rapid compression machine . . . . .	81
4.3	Ignition delay validation with rapid compression machine results . .	82
4.4	Shock tube schematic . . . . .	83
4.5	Ignition delay validation using shock tube measurements . . . . .	84
4.6	Experimental HCCI apparatus . . . . .	86
4.7	Illustration of the 50 cycle mean pressure trace . . . . .	90
4.8	HCCI validation using 20PRF . . . . .	91
4.9	HCCI validation using 40PRF . . . . .	92
4.10	HCCI validation using 60PRF . . . . .	93
4.11	Comparison of simulated and experimental exothermicity . . . . .	94
5.1	Effect of isothermal EGR . . . . .	103
5.2	Effect of isothermal EGR with constant specific heat capacity . . .	104
5.3	The different effects of EGR . . . . .	106
5.4	Relationship between the parameters $\Pi_1$ and $\Pi_2$ . . . . .	109
5.5	Correlation for predicting condition required for ignition timing . .	111
B.1	Estimation of $c_p$ for $C_3H_7CHO$ . . . . .	141
B.2	Estimation of $c_p$ for $C_3H_7O_2$ . . . . .	141
B.3	Estimation of $c_p$ for $C_3H_7OOH$ . . . . .	142
B.4	Estimation of $c_p$ for $C_7H_{14}O$ . . . . .	142
B.5	Estimation of $c_p$ for $C_7H_{14}OOH$ . . . . .	143

## LIST OF FIGURES

---

B.6	Estimation of $c_p$ for $C_7H_{15}OO$ . . . . .	143
B.7	Estimation of $c_p$ for $C_7H_{15}OOH$ . . . . .	144
B.8	Estimation of $c_p$ for $C_8H_{16}O$ . . . . .	144
B.9	Estimation of $c_p$ for $C_8H_{16}OOH$ . . . . .	145
B.10	Estimation of $c_p$ for $C_8H_{17}O$ . . . . .	145
B.11	Estimation of $c_p$ for $C_8H_{17}OO$ . . . . .	146
B.12	Estimation of $c_p$ for $C_8H_{17}OOH$ . . . . .	146
B.13	Estimation of $c_p$ for $OC_7H_{13}O$ . . . . .	147
B.14	Estimation of $c_p$ for $OC_7H_{13}OOH$ . . . . .	147
B.15	Estimation of $c_p$ for $OC_8H_{15}O$ . . . . .	148
B.16	Estimation of $c_p$ for $OC_8H_{15}OOH$ . . . . .	148
B.17	Estimation of $c_p$ for $OOC_7H_{14}OOH$ . . . . .	149
B.18	Estimation of $c_p$ for $OOC_8H_{16}OOH$ . . . . .	149

# Nomenclature

## Symbols

$\alpha$	Thermal diffusivity of fluid
$\eta_{th}$	Thermal Efficiency
$\frac{dQ_{HT}}{dt}$	Wall heat transfer rate
$\frac{dU}{dt}$	Rate of change of internal energy
$\mu$	Dynamic fluid viscosity
$\nu$	Kinematic fluid viscosity $\frac{\mu}{\rho}$
$\bar{S}_p$	Mean piston velocity
$\Phi$	Fuel/Air Equivalence Ratio
$\rho$	Density
$\theta$	Crank Angle
$a$	Coefficient
$b$	Coefficient
$c$	Coefficient
$C_p$	Specific Heat
$CR$	Compression Ratio
$f_c$	Cutoff Frequency
$h$	Convective heat transfer coefficient
$k$	Ratio of specific heat $\frac{c_p}{c_v}$

## NOMENCLATURE

---

$k_f$	Thermal conductivity of the fluid K
$L$	Characteristic length
$l$	Connecting rod length
$N$	Engine Speed
$N_i$	Number of moles of the $i^{th}$ specie
$Nu$	Nusselt number
$ON$	Octane Number
$P$	Pressure
$P_o$	Initial Mixture Pressure
$Pr$	Prandtl number
$r_c$	Crank throw radius
$R_u$	Universal Gas Constant
$Re$	Reynolds number
$T$	Temperature
$T_o$	Initial Temperature
$U$	Internal energy
$V$	Characteristic velocity
$V_c$	Clearance volume
$w$	Characteristic fluid velocity
$W_{boundary}$	Boundary work

## Abbreviations

AERR	Average Energy Release Rate
ATAC	Active Thermo-Atmosphere Combustion
BOC	Beginning Of Compression
CAD	Crank Angle Degrees

## NOMENCLATURE

---

CFD	Computational Fluid Dynamics
CFR	Cooperative Fuels Research
EGR	Exhaust Gas Recirculation
EVO	Exhaust Valve Closing
IMEP	Indicated Mean Effective Pressure
IVC	Intake Valve Closing
IVP	Initial Value Problem
ODE	Ordinary Differential Equation
PRF	Primary Reference Fuel
uHC	unburned Hydrocarbons
VVT	Variable Valve Train

# Chapter 1

## Introduction

### 1.1 Background

Increasingly stringent vehicle emission regulations require that the current use of fossil fuels become more efficient and produce fewer emissions. In order to meet these constraints, alternative combustion processes such as the Homogenous Charge Compression Ignition (HCCI) cycle are being investigated. The HCCI cycle has the potential for reduced fuel consumption (through increased efficiency) and  $\text{NO}_x$  emissions compared to current Spark Ignition (SI) engine designs. In addition, it does not require a significant change in fueling infrastructure or vehicle design, as is this case with other potential technologies such as hydrogen.

The HCCI cycle is a modified version of the SI engine in which the combustion event is initiated not through an electric spark, but rather by the high temperatures and pressure achieved during compression. The basic HCCI process is outlined in Figure 1.1. First, a homogenous mixture of fuel and air is drawn into the combustion chamber during the intake stroke (1). Next, the intake valve closes and the piston begins to move upwards, compressing the mixture and increasing

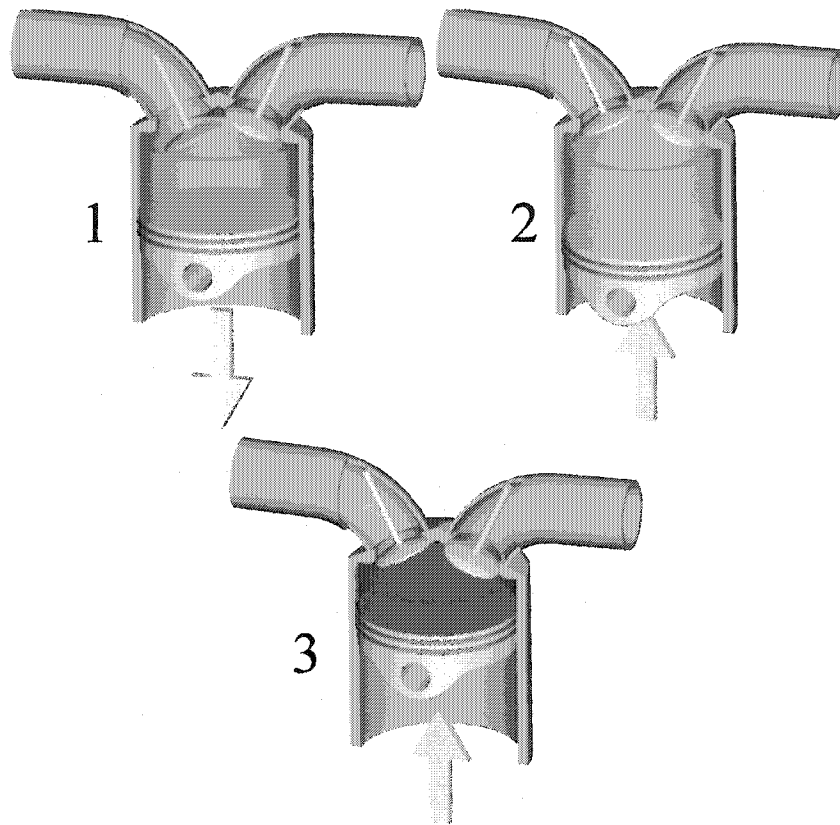


Figure 1.1: Clockwise from top left: (1) A homogeneous fuel/air mixture is drawn into the cylinder during the intake stroke of the HCCI cycle. (2) The upward motion of the piston compresses the fuel/air mixture, increasing the mixture temperature and pressure. (3) The mixture autoignites and combusts uniformly throughout the combustion chamber.

the mixture temperature and pressure(2). As the piston approaches the end of its upwards stroke, the mixture temperature and pressure are such that the mixture autoignites uniformly throughout the entire combustion chamber (3). The hot combustion gases expand, forcing the piston back down, turning the engine crank, and thus providing useful mechanical work. Once the piston reaches the bottom of this expansion stroke, the exhaust valve opens, the piston begins to move upwards again and expels the exhaust gases through the exhaust valve. At the top

## CHAPTER 1: INTRODUCTION

---

of the stroke, the exhaust valve closes, the intake valve opens, and the cycle begins again. In order to ensure proper ignition timing, the mixture properties at the beginning of compression must accurately controlled. For example, the mixture temperature and pressure at the beginning of compression must be sufficiently high that ignition takes place, but not so high that the ignition occurs too early.

The uniform ignition and combustion processes result in several limitations of the HCCI cycle. Spontaneous combustion of the mixture leads to high rates of pressure rise relative to those in conventional SI or Diesel engines. As this high rate of pressure rise can lead to engine damage, the fuel/air mixture is diluted using excess air or recirculated exhaust gases. Diluting the mixture decreases the in-cylinder fuel quantity and reduces the useful work output of the engine. This limits the HCCI cycle to loads lower than those attainable with SI and Diesel engines. Because of this reduced power density (i.e. useful work output per unit engine displacement) the HCCI cycle is likely to be implemented in an SI/HCCI hybrid configuration. The engine would operate in SI mode for high load and startup and then switch to HCCI for part load operation.

A means of controlling the HCCI cycle, particularly the ignition timing, is required before this cycle can be used for applications outside of the laboratory. Such a control system would be used to maintain a constant ignition timing across all desired engine speeds and loads by adjusting engine parameters such as the equivalence ratio and initial mixture temperature so that the ignition timing does not vary. At steady state operation this implies that only slight variations are required, but during transient operation considerable variations in the parameters are required. The parameters must be varied on a cycle by cycle basis so that the ignition timing can be controlled for every combustion event.

The focus of this investigation is using a thermokinetic model to understand the

effects of various parameters on the ignition timing. The timing of the combustion event relative to the position of the piston must be such that is not too early, in which case useful work is lost as the hot combustion products are compressed, nor too late, in which case not all of the chemical energy in the fuel will be utilized. Unlike the SI and Diesel cycles, the HCCI cycle does not have any means of directly controlling the ignition timing. In an SI engine the spark timing can be used to directly control the timing of the combustion event, while in a Diesel engine the timing of the fuel injection in to the hot cylinder gases is used. The HCCI cycle requires that the mixture conditions at the beginning of compression are such that ignition occurs at the appropriate time. In order to determine which conditions are required, it is necessary to understand the individual and combined effects of engine parameters and mixture properties. Once these effects are understood, it is possible to use them to control the ignition timing, and hence performance, of the HCCI cycle.

### 1.2 Overview of This Thesis

In this investigation, a computer simulation of the HCCI engine cycle is developed and used to predict the effects of various engine parameters on the ignition timing. In particular, a *thermokinetic* model is formed by combining a thermodynamic model representing the thermodynamic state of the mixture within the combustion chamber, with a chemical kinetic mechanism (a set of chemical reactions) representing the change of the mixture composition as a function of time. A new chemical kinetic mechanism is developed with an emphasis on computational efficiency and the ability to predict ignition and combustion processes for arbitrary blends of n-heptane and iso-octane. Before the thermokinetic model is used to investigate the effects of engine parameters on the ignition timing, it is validated

against independent combustion temperature and ignition delay results. The combustion temperatures are validated for an idealized case, while the ignition delays are compared to experimental ignition delay measurements for simplified combustion systems (Park & Keck 1990, Fieweger et al. 1997). The overall performance of the thermokinetic model is validated with experimental HCCI pressure histories from Atkins (2004). It should be noted that the goal of the thermokinetic model is not to precisely predict the ignition timing, but rather to provide qualitative predictions of the effects of the engine parameters on the ignition timing.

Using the validated model, engine parameters deemed relevant to the ignition process are varied independently to elucidate their effect on the ignition timing. The results of this parameter variation are evaluated using a dimensional analysis to form a correlation describing the relative magnitudes of each of the parameters required for a given ignition timing. The benefit of such a correlation is that it is not necessary to iteratively determine the required conditions, but rather they can be quickly determined using this algebraic relationship. The correlation also elucidates the relationships between the various parameters and can be used as part of an algorithm for controlling the HCCI cycle in a real engine.

### 1.3 Layout of the Thesis

Chapter two presents a literature review to provide a background of the HCCI cycle, not only from a perspective of what it is, but also how it works, what affects it, and how can it be controlled. Both experimental and numerical investigations are discussed, as are the different methods of modeling the HCCI cycle. Following this review, chapter three discusses the theory used to develop the thermokinetic model of the HCCI cycle. This includes the derivation of the thermodynamic model, as well as a discussion of chemical kinetic mechanisms and their solution.

## CHAPTER 1: INTRODUCTION

---

The validation of the thermokinetic model with known results for combustion temperatures and ignition delays is discussed in chapter 4. Chapter 5 discusses the parameter variations and the correlation of the parameters affecting the ignition delay. An example in which the correlation is used to determine the conditions required for a given ignition timing is also presented. Finally, chapter 6 presents the conclusions of this work and gives some suggestions for future paths of this research.

## Chapter 2

# Literature Review

### 2.1 The HCCI Cycle: A Brief History

The HCCI<sup>1</sup> cycle modifies the traditional SI cycle to use the compression process to initiate combustion rather than an electric discharge across spark plug gap. In this sense it is very much a combination of the Spark Ignition (SI) and Diesel engines. A homogenous charge fuel air mixture is compressed by an upward moving piston as in a SI engine, but unlike the SI engine the combustion event is initiated by the elevated temperature and pressure reached through compression, as in a Diesel engine. In a Diesel engine, however, the timing of the combustion event can be controlled by changing the timing of the fuel injection. In an HCCI engine, there is no such direct mechanism by which the combustion timing can be controlled.

One of the earliest intentional implementations of this cycle was done under lean operation in a two stroke engine by Onishi et al. (1979), which they termed

---

<sup>1</sup>Many names have been proposed for the process now commonly referred to as HCCI, several of which will be introduced. However, in order to maintain consistency with other current publications the process will be referred to as HCCI in this work.

Active Thermo-Atmosphere Combustion (ATAC). In order to achieve HCCI operation, hot exhaust gases were retained and increased the mean charge temperature at the beginning of compression. These higher temperatures are, in part, what led to the autoignition of the mixture. If too much exhaust gas was retained, autoignition did not occur as the combustion temperatures, and hence the mean temperature at the beginning of compression decreased. Among the advantages seen using this form of HCCI, compared to SI or Diesel operation, were the decreased  $\text{NO}_x$ , unburned hydrocarbon (uHC) and particulate emissions, as well as reduced fuel consumption and increased combustion stability. The increased combustion stability is evidenced by lower cycle to cycle variations in the combustion process. Through the use of schlieren photography, Onishi et al. noted that the combustion event was unlike that of SI or Diesel engines. Rather than combustion occurring as a flame propagating through the mixture (as in the case of SI engines) or a diffusion flame (as in the case of Diesel engines), there were multiple ignition points throughout the combustion chamber leading to an almost uniform oxidation of the combustion reactants. From the photographic investigation, it was also noted that there was no flame front and that the combustion duration was not defined by the flame propagation speed, but rather by the chemical kinetics governing the ignition and combustion processes. This uniform combustion is attainable with leaner mixtures than possible with SI engines (while still maintaining adequate combustion stability), resulting in an increased thermal efficiency. The Otto cycle, which the HCCI engine cycle closely approximates, has an ideal thermal efficiency defined by (Cengel & Boles 1998):

$$\eta_{th} = 1 - \frac{1}{CR^{k-1}} \quad (2.1)$$

where  $\eta_{th}$  is the thermal efficiency,  $CR$  is the compression ratio, and  $k$  is the

ratio of specific heat capacities of the fuel/air mixture. As the mixture is made increasingly lean,  $k$  increases, thereby increasing the thermal efficiency.

Unlike SI and Diesel engines where there is a distinct control mechanism by which the combustion can be initiated (i.e. the spark event in the SI engine, and the fuel injection in the Diesel engine), the HCCI engine has no such mechanism. For a combustion event to take place, it is necessary that both the temperature and the mixture composition in the cylinder are accurately controlled (Onishi et al. 1979). The thermodynamic state of the mixture during the compression process is largely defined by the thermodynamic state of the mixture at the beginning of compression, requiring that the mixture state at the beginning of compression be carefully selected to ensure ignition.

Because the combustion process is governed by the rate of the chemical reactions (i.e. the chemical kinetics) rather than heat and mass diffusion as in flames, it can be more rapid than combustion events in SI and Diesel engines. This rapid combustion and associated high rate of pressure rise can damage the engine and cause undesired acoustic noise from the engine. In order to slow the combustion and avoid engine damage, diluted mixtures are used (Najt & Foster 1983). This is achieved either by operating under lean conditions where there is excess air in the cylinder, or by diluting the mixture with exhaust gases from a previous combustion event. In a two stroke engine the latter is inherently the case due to high Exhaust Gas Recirculation (EGR) fractions (Onishi et al. 1979).

When lean mixtures or high EGR fractions are used, the fuel mass and hence output of the engine are reduced, limiting HCCI to loads lower than those obtainable using SI or Diesel engines. As the mixture is made increasingly lean, the combustion temperature decreases and lowers the exhaust temperature. As two stroke engines have high EGR rates, a decrease in the exhaust temperature

results in a decrease in the mixture temperature, creating unfavorable conditions for autoignition. Leaner mixtures have lower fuel concentrations, reducing the likelihood of the fuel and air molecules colliding and reacting. Alternatively, as stoichiometric mixtures and low EGR fractions are used, the combustion rate increases and may damage the engine. Thus there are both upper and lower load limits on the use of the HCCI engine. The upper load limit is in place to prevent engine damage, while the lower load limit prevents misfires and the associated increase in fuel consumption and uHC emissions.

HCCI engines can be operated with leaner mixtures than SI engines as lean operation in an SI engine is limited by increased combustion durations and incomplete combustion. These lean mixtures results in lower combustion temperatures and hence lower  $\text{NO}_x$  emissions as the critical temperature for thermal  $\text{NO}_x$  formation of approximately 1700K (Warnatz et al. 2001) is not reached. The lower combustion temperatures also result in lower heat transfer rates to the cylinder walls and hence reduced fuel consumption as less of the fuel's energy is lost as heat. The lower combustion temperatures do have a disadvantage since the relatively slow, temperature dependant oxidation of CO to  $\text{CO}_2$  may not reach completion. This has particular consequence as the conversion of CO to  $\text{CO}_2$  is responsible for the majority of the exothermicity (Dryer & Glassman 1977). Not all of the fuel's chemical energy will be used if this CO oxidation is not complete, reducing the efficiency of the engine.

Both the HCCI and the Diesel cycle can operate at overall lean conditions, but differ in that Diesel combustion takes place through a diffusion flame at locally stoichiometric conditions, leading to higher combustion temperatures and hence  $\text{NO}_x$  emissions. Due to the heterogeneous nature of Diesel combustion, there can be quantities of fuel that are only partially oxidized, leading to high particulate

emissions and reduced thermal efficiency.

The reduction in uHC emissions noted by Onishi et al. (1979) is a phenomena realized only in two stroke engines. In a two stroke engine, the majority of unburned hydrocarbon emissions come from misfires or incomplete combustion events. As HCCI operation increases the combustion stability and reduces the number of misfires, the uHC emissions are reduced.

When Najt & Foster (1983) investigated HCCI in a four stroke engine, they referred to it as Compression-Ignited Homogeneous Charge combustion, and found many of the same traits seen by Onishi et al. One exception to this was that the uHC emissions did not see the same reduction as in the two stroke engine. In a four stroke engine, the uHC emissions are predominantly due to unburned portions of the mixture being trapped in crevice regions during compression and combustion and then being released, unburned, during the expansion stroke (Heywood 1988). The temperature in an SI engine during the expansion stroke is generally hot enough to oxidize some of the trapped mixture, but this does not occur to the same extent in HCCI engines due the lower exhaust temperatures.

The focus of the research presented in this thesis is that of implementing the HCCI cycle in modern four stroke engines, and as such the remainder of the literature review will consider only four stroke applications of the HCCI cycle. HCCI combustion in four stroke engines holds the potential to reduce emissions and fuel consumption, but first requires that the ignition and combustion processes are controlled. The ignition timing has a significant effect on the efficiency of the HCCI cycle and the HCCI cycle can only be realistically implemented once the ignition timing is understood and can be controlled.

## 2.2 Controlling HCCI Combustion

As the HCCI ignition and combustion processes are kinetically controlled, they are strongly influenced by the temperature and pressure history of the mixture, as well as the chemical kinetic properties of the mixture itself. For a given fuel/air mixture, ignition occurs only after the mixture is subject to a suitably high temperature for a suitably long period of time. Changing the temperature or pressure history, or the composition of the fuel/air mixture, also changes the ignition timing. Physical parameters such as the initial mixture temperature ( $T_o$ ), compression ratio ( $CR$ ), engine speed ( $N$ ), fuel octane number ( $ON$ ), fuel/air equivalence ratio ( $\Phi$ ), initial mixture pressure ( $P_o$ ), and the EGR fraction can be used to vary the mixture temperature, pressure and composition. When used together or separately, each of these affect the ignition timing providing some degree of control. The individual effect of each of these parameters on the ignition timing are discussed below.

The thermodynamic state (temperature, pressure and composition) of the mixture at the beginning of compression is considered as it is representative of the thermodynamic state during compression. In some cases the initial mixture state within the cylinder can be based on the state of the mixture as measured in the intake manifold. However, while the manifold temperature and pressure may be indicative of the in-cylinder values, they are not necessarily the same as there may be pressure fluctuations and temperature variations throughout the intake system.

### 2.2.1 Octane Number

The octane number of a fuel is the volumetric iso-octane fraction in a binary n-heptane/iso-octane mixture which autoignites under the same conditions as the fuel being considered (Heywood 1988). For example, an arbitrary fuel which au-

toignites under the same conditions as a mixture with 92% (by volume) iso-octane and 8% n-heptane, will have an octane number of 92. Fuels with higher octane numbers will have a higher resistance to autoignition, as iso-octane autoignites less readily than n-heptane. In this discussion, references to different octane numbers refer to different iso-octane and n-heptane mixtures. Commercially available gasoline is commonly approximated for numerical and experimental investigations using different blends of iso-octane and n-heptane, which are referred to as the Primary Reference Fuels (PRFs). A PRF blend of 20% iso-octane and 80% n-heptane is referred to as 20PRF.

As the octane number is a measure of the ability of a mixture to autoignite, a means of varying the octane number also provides a means of controlling the ignition timing. Tunestål et al. (2002) implemented a system in which two fuel injectors were used, one for n-heptane and one for iso-octane, thereby controlling the octane number of the fuel by changing the relative injection quantities. By changing the octane number during engine operation, they were able to control the ignition timing.

Changing the fuel octane number has also been used to increase the operating region of the HCCI engine. For example, Atkins (2004) carried out experimental equivalence ratio and EGR sweeps for three different PRFs on a Cooperative Fuel Research (CFR) engine. Atkins found that by increasing the octane number, less mixture dilution was required to ensure proper ignition timing, which increased the attainable load. Effectively, low octane number fuels can be used for low load operation and high octane fuels for higher load operation.

### 2.2.2 Initial Temperature

As chemical kinetic processes are highly temperature dependant, the initial temperature has a significant impact on the ignition timing of the HCCI engine. In

early investigations by Najt & Foster (1983) and Thring (1989), intake air heating was required for autoignition to occur. The initial mixture temperature can be used to keep the ignition timing constant as other engine parameters are changed. For example, Aceves et al. (2001) varied the fuel mass flow rate to obtain different loads and varied the intake air temperature to maintain an acceptable ignition timing for the different loads. Relying on intake air heating to achieve HCCI combustion results in considerable energy being used in heating the air which reduces the overall efficiency of the engine. By supplying power to the heater, the thermal efficiency of the engine is decreased, as less useful mechanical work is realized for the same input of chemical energy. By heating the intake charge, the density of the charge is also decreased, requiring larger engine displacements to obtain the same load. Larger, and hence heavier, engines are undesirable for mobile applications as the increased engine mass leads to higher fuel consumption.

From a control standpoint there is a considerable lag between a change in the heater output and a change in the mixture temperature in the cylinder due to the large air volume between the heater and the cylinder. Haraldsson et al. (2004) were able to rapidly change the intake air temperature by controlling the fractions of hot and cold air inducted into the engine, as opposed to varying the output of a heater. While this technique removes the lag due to the thermal mass of the heater, there was a delay of four cycles prior to seeing any change in the ignition timing, due to the large intake system volume.

### 2.2.3 Engine Speed

The engine speed is not considered an ignition timing control mechanism, but its effect on ignition timing must be understood and accounted for when investigating the control of HCCI ignition. For a mixture with a given thermodynamic

state, a certain period of time will elapse before the mixture ignites. This period of time, known as the induction period, is the time during which relatively slow chemical reactions take place and produce the radicals required for ignition and combustion (this is discussed in greater detail in section 3.4.2). Changing the engine speed changes the time that the mixture is exposed to the elevated temperatures and pressures. Thus, as the engine speed changes, the thermodynamic state of the mixture must be changed to compensate for the changes in available induction time so that a constant ignition timing may be attained.

In a numerical investigation, Sjöberg & Dec (2003) varied the intake temperature in order to maintain a constant crank angle at which 50% of the fuel/air mass was burned (which is indicative of the ignition timing) at various engine speeds. An intake temperature of 140°C was required at 2400rpm, but for an engine speed of 600rpm an intake temperature of only 95°C was required. Decreased engine speeds exposed the mixture to high temperatures and pressure for longer periods of time, requiring lower intake temperatures. While Sjöberg & Dec varied the intake temperature to compensate for the changes in engine speed, any parameter which changes the thermodynamic state (such as pressure, equivalence ratio, or EGR rate) of the charge could have been used to maintain a constant ignition timing.

### 2.2.4 Compression Ratio

Higher compression ratios are one method of ensuring autoignition of common fuels, such as gasoline, with higher octane numbers. Increasing the compression ratio increases chemical kinetic activity by increasing the end of compression temperature and pressure. As HCCI is realistically achievable at only part loads, one possible implementation is a combined HCCI/SI engine (Martinez-Frias

et al. 2001). In a combined HCCI/SI engine, selecting the compression ratio is a compromise as too high of a compression ratio will lead to knock under full load SI operation and too low of a compression ratio will inhibit ignition under HCCI operation if the same fuel is used for both engine modes.

Haraldsson et al. (2003) used a variable compression ratio engine with which they were able to adjust the compression ratio mechanically from 9:1 to 21:1, while the engine was operating. Control of the ignition timing by varying the compression ratio was possible with this engine. The change in ignition timing was only limited by the rate at which the compression ratio was changed.

### 2.2.5 Equivalence Ratio

The equivalence ratio is a measure of the mass based air/fuel ratio, relative to stoichiometric conditions. The equivalence ratio specifies the fuel concentration within the cylinder, which affects the ignition timing, combustion duration and engine load. A decrease in the fuel concentration (i.e. lean operation) leads to retarded ignition timing and increased combustion durations as there is a smaller probability that the fuel molecules will collide and react with the oxygen molecules. By decreasing the fuel concentration, the useful work output of the engine is also decreased. If the equivalence ratio is changed to control the engine load, other parameters must be adjusted to maintain desirable ignition timing. Martinez-Frias et al. (2001) carried out a numerical investigation in which the equivalence ratio, EGR rate, and intake pressure were optimized to obtain HCCI operation at different load/speed points. An increase in equivalence ratio at a constant speed increased the engine load, but also required that higher EGR fractions be used in order to maintain a constant ignition timing.

### 2.2.6 Initial Pressure

Conventional SI engines vary the intake pressure using a throttle valve to control the engine load. However, throttling the intake reduces the thermal efficiency of the engine as the air must be pulled past the restrictive valve. An HCCI engine can be operated unthrottled, using the equivalence ratio to vary the load, reducing the pumping losses and increasing the efficiency.

Though rarely done, the initial charge pressure can be used as a control mechanism for HCCI ignition timing. An increase in the initial pressure will increase the air and fuel concentrations within the cylinder and therefore increase the reaction rates and advance the ignition timing. Higher intake pressures will also lead to higher compression temperatures, further increasing the reaction rate.

Variations in the intake pressure are more commonly used to extend the operating region of the engine. For example, Sun et al. (2004), Hyvönen et al. (2003) and Olsson et al. (2004) boosted the intake pressure using either super- or turbochargers and were able to increase the upper load attainable from HCCI engines. By increasing the intake pressure it is still possible to operate under lean conditions and realize the associated benefits while attaining higher loads. Olsson et al. (2004) were able to reach an Indicated Mean Effective Pressure<sup>2</sup> (IMEP) as high as 17bar by increasing the intake pressure (compared to the naturally aspirated maximum IMEP of approximately 5bar). The drawback to this method is the higher pumping losses due to the increased exhaust pressure required to drive turbocharger. As the exhaust temperature is low during HCCI operation, it is necessary to increase the exhaust back pressure to increase the turbo efficiency.

---

<sup>2</sup>IMEP is a measure of the engine output, which is independent of the engine displacement. This makes it possible to compare engines of the same type, but of different displacements. For example, if two SI engines, of different displacements, are both operating at full load, they will both have an IMEP in the area of 12bar.

Increasing the exhaust pressure decreases the thermal efficiency as more work must be done to expel the exhaust gases. By using a turbocharger specifically designed for HCCI or variable turbine geometry, some of these losses can be reduced.

Similarly, the initial pressure can be used to extend the lower HCCI load limit. In their optimization study, Martinez-Frias et al. (2001) found that operation at lower loads was possible by decreasing the mixture pressure and increasing the equivalence ratio.

### 2.2.7 EGR

The effect of EGR on the combustion process is multifold and was investigated by Zhao et al. (2001) using a numerical investigation in which various properties of both the fresh and EGR mixture were modified. Zhao et al. describe the effects of EGR as follows:

**Charge Heating** When sufficiently hot exhaust gases are used they increase the temperature of the fuel/air mixture. This has the same effects on the ignition timing and combustion duration as intake air heating, with the difference that an external heater is not required. By recovering some of the thermal energy from the hot exhaust gases, the efficiency of the engine is improved. The charge heating effect holds the most potential for ignition control using EGR.

**Thermal Effect** EGR introduces  $H_2O$  and  $CO_2$  to the fresh fuel/air mixture, increasing the specific heat of the mixture. It has been noted both experimentally (for example, (Atkins 2004)) and numerically (for example, (Zhao et al. 2001)), that an increase in isothermal EGR (greater EGR fraction, but no change in the mixture temperature) will retard the ignition timing. This investigation has found that the increase in specific heat capacity slows the

temperature increase during the slow chemical activity preceding ignition, hence retarding the ignition (see section 5.3.4).

**Dilution Effect** EGR replaces oxygen with chemical species that are inert during the low temperature compression and ignition processes. This leads to reduced chemical activity and retarded ignition timing.

**Chemical Effect** Some of the EGR components (i.e.  $\text{H}_2\text{O}$ ,  $\text{CO}$ ,  $\text{CO}_2$ ) can dissociate and become chemically active, leading to an advancement of the ignition timing. In general, the temperatures seen during compression are too low for this effect to have implications on the ignition timing, though the additional active chemical species decrease the combustion duration.

Through their simulation study, Zhao et al. (2001) found that the ignition timing is predominantly effected by the charge heating and thermal effects, and less sensitive to the chemical and dilution effects. The combustion duration is most affected by the charge heating effect, but the chemical, dilution and thermal effects are also important. The thermal and dilution effects both increase the combustion duration. The former due the higher specific heat capacity requiring more energy to increase the temperature of the mixture (and hence accelerate the combustion process), and the later due to the higher inert gas fractions decreasing the concentration of active species.

EGR can be introduced in the cylinder in two different ways. It can be routed from the exhaust manifold to the intake manifold and then drawn into the cylinder with the fresh charge, a process termed external EGR. Alternatively, it can be retained in cylinder by either closing the exhaust valve early and not expelling all of the exhaust gases, or the exhaust valve can be closed late (i.e. during the intake stroke) and some of the exhaust gases drawn back into the cylinder from the

exhaust manifold. Increasing the EGR fraction through such methods is referred to as internal EGR. Internal EGR has the advantage that it is subjected to less heat transfer, resulting in a higher capacity for charge heating than external EGR. A Variable Valve Train (VVT) is one method by which the fraction of internal EGR can be varied at different engine operating points. External EGR requires less modifications to a conventional engine as it generally involves routing some of the exhaust gases through a control valve back to the intake manifold. External EGR is widely employed on SI engines to control  $\text{NO}_x$  emissions, but the VVTs required for internal EGR are not commercially produced.

Chen et al. (2003) use an experimental VVT system to vary the internal EGR fraction and thereby control the ignition timing. Increases in the internal EGR fraction advanced the ignition timing due to the higher mixture temperatures. They found that for a given engine speed and equivalence ratio, there existed a minimum required amount of internal EGR below which ignition will not occur, as the charge was not hot enough.

### 2.3 Modeling of the HCCI Cycle

Modeling of the HCCI cycle requires coupling a thermodynamic model, which describes the conservation of energy, with some means of describing the energy released by the combustion process, generally using either chemical kinetics (to describe the change in mixture composition) or empirical relationships. The thermodynamic model is used to describe the thermodynamic state (i.e. temperature, pressure, and composition) of the mixture. The spatial variation of the thermodynamic state of the mixture, is represented using one or more thermodynamic zones.

The ignition and combustion processes can be represented using a set of chem-

ical reactions, known as chemical kinetic mechanisms, to describe the change in mixture composition as a function of time. This knowledge of the mixture composition is used by the thermodynamic model to describe the temperature and pressure changes during the combustion process. The combination of a thermodynamic model with a chemical kinetic mechanism is referred to as a *thermokinetic* model.

Rather than using chemical kinetic mechanisms, simple empirical equations can be used to describe the exothermicity of the combustion event as a function of time, based on experimental measurements. The following discussion will first focus on the different methods of modeling the combustion process, and then on the different types of thermodynamic models.

### 2.3.1 Modeling of the Combustion Process

The combustion process in an HCCI engine is very similar to the autoignition and combustion of end gases in SI engine knock (Eng 2003) as the thermokinetic process is fundamentally the same: a homogeneous fuel/air mixture is compressed, increasing the temperature and pressure until it autoignites. Therefore, much of the research carried out to describe the phenomena of knock is directly applicable to the autoignition process in an HCCI engine. Sets of chemical reactions referred to as chemical kinetic mechanisms, have been developed to describe these ignition and combustion processes. These mechanisms can range from relatively simple skeletal mechanisms consisting on the order of 100 reactions (for example, Zheng et al. (2002)), to detailed mechanisms consisting of several thousand reactions (for example, Slavinskaya & Haidn (2003)). Through the use of these mechanisms it is possible to describe the changing mixture composition and hence exothermicity (i.e. energy release).

Experimental combustion data can be used, generally in the form of a pressure trace, to develop a relationship describing the exothermicity of the combustion process. Rather than describing the chemical reactions responsible for the exothermicity, these empirical relationships describe the exothermicity as a function of time. The historical development and use of both the chemical kinetic and empirical methods are described in greater detail below.

### Chemical Kinetics

Chemical kinetic mechanisms used to describe the autoignition process in an HCCI engine are typically based on prior SI knock investigations. Two distinct approaches to the development of kinetic mechanisms exist: a detailed approach in which many fundamental reaction steps are considered; or a skeletal approach in which only the relevant reactions (for the conditions being considered) are accounted for. Detailed kinetic mechanisms are valid over wide ranges of thermodynamic states, but results in large numbers of differential equations requiring simultaneous solution. If a detailed mechanism contains all the relevant reactions describing the chemical process, it can be used for extrapolative purposes. Extrapolative investigations are those in which a model is being used for predictive purposes for conditions outside of the region in which it was validated. When only qualitative results or many simulations are required, such as for control system development, smaller and less computationally expensive mechanisms are desired. As control system development is the focus of this investigation, only the smaller, skeletal mechanisms are discussed in detail. Interested readers are referred to Curran et al. (1998) and (2002) as starting points for detailed kinetic mechanisms for n-heptane and iso-octane, respectively, or Westbrook (2000) for a review of the topic.

One of the skeletal mechanisms describing the phenomenological ignition kinetics of hydrocarbon/air mixtures is that of Halstead et al. (1977) and is commonly referred to as the “Shell Model”, as the research was carried out at Shell Research Limited. Reaction rate coefficients were fit to a general, fuel *non*-specific mechanism based on experimental ignition delay measurements. Using this technique, it was possible to predict the ignition timing as well as various ignition phenomena such as two stage ignition (these phenomena will be discussed in further detail in section 3.4.2). Halstead et al. commented on the existence of a *degenerate chain branching* mechanism, a mechanism in which chain branching occurs, but at a relatively slow rate<sup>3</sup>. It should be noted that the presence of degenerate chain branching in hydrocarbon oxidation was first discussed by Semenov (1935).

Benson (1981) described the ignition process using fundamental reactions as well, but did not determine the reaction rate parameters by fitting them to experimental ignition delays. Rather, Benson used published values or theoretical estimates. Hu & Keck (1987), using the mechanism presented by Benson, were able to predict the ignition delay and noted that the rate of the isomerization of the hydroperoxy radical was what defined the different induction periods for different fuels. Using empirical ignition delay data, they predicted the isomerization reaction rate parameters for different fuels. Li et al. (1992) and (1996) found, using this mechanism, that the fuel consumption was too high (nearly 100% vs. the 50% consumption measured experimentally for the given conditions) and that the exothermicity was too low, when compared to experimental investigations. By extending the model to include CO formation mechanisms, they were able to im-

---

<sup>3</sup>Chain branching reactions are those in which the number of radicals produced by the reaction is greater than the number of radicals consumed by the reaction. This net increase in the number of radicals accelerates the chemical kinetic behavior as the radicals are much more reactive than their chemically stable counterparts. See section 3.4.2 for a further discussion of this topic.

prove the exothermicity and fuel consumption agreement. Using Li et al.'s (1992) version of the Hu & Keck mechanism for the ignition process, Zheng et al. (2001) and (2002) formed a skeletal mechanism describing the autoignition and oxidation of PRFs. In order to describe the post-ignition large molecule decomposition and high temperature chemistry, they used the general alkane mechanism presented by Griffiths et al. (1994). In general, the higher temperature oxidation is independent of the initial fuel as alkanes decompose into the same smaller molecules after ignition. Zheng et al. (2002) represented the PRF blend as a single molecule, with its own associated rate parameters. Subsequent changes of the fuel blend required that a new set of rate parameters be determined for the fuel specific reactions. Tanaka et al. (2003) developed a reduced mechanism for the HCCI ignition and oxidation of PRF's in which the chemistry of both fuels is included separately, allowing arbitrary PRF blends to be modeled. Tanaka et al. used global reactions to convert the intermediate species produced during ignition into combustion products (i.e. CO, H<sub>2</sub>O, CO<sub>2</sub>). Global reactions effectively describe several reactions with only one reaction. While global reactions have the advantage of reducing the mechanism size, they are only suited to conditions for which they were derived, and are not well suited to extrapolative purposes.

While the preceding discussion has focussed on *phenomenological* skeletal kinetic mechanisms, it is also possible to use *reduced* skeletal kinetic mechanisms. Figure 2.1 illustrates the difference between these two methods of developing skeletal mechanisms. In the phenomenological mechanisms, reactions deemed to be important are added until the mechanism adequately describes the process (in this case HCCI autoignition). In the case of reduced mechanisms, reactions are progressively removed until a smaller mechanism, still capable of describing the desired process, is formed.

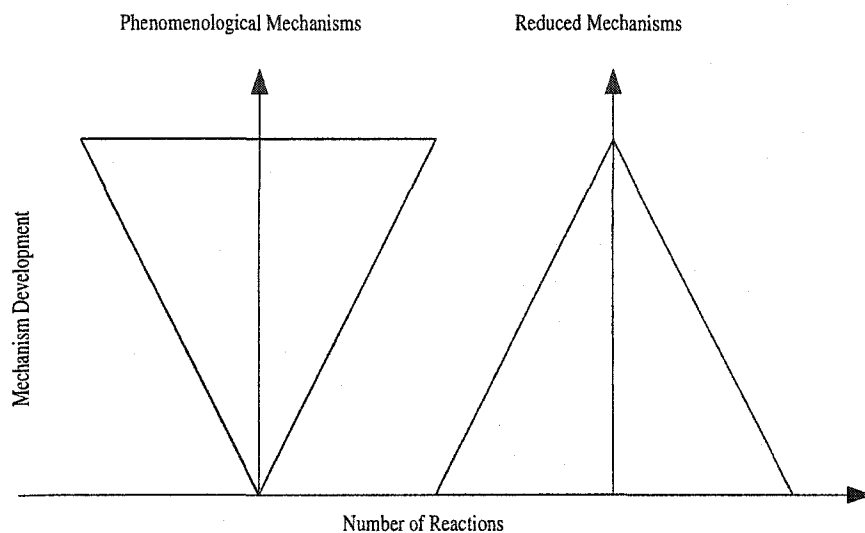


Figure 2.1: A comparison of the phenomenological and reduction methods for forming skeletal kinetic mechanisms.

In general, there are three methods by which a mechanism can be reduced. A sensitivity analysis can be used to determine the sensitivity of a control variable, such as ignition delay, to various system parameters, such as species concentrations or reaction rates. Reactions or species not influencing the control variable are removed. Similarly, a reaction-flow analysis determines which reaction paths are important, and which can be removed. A quasi steady state approximation is used to combine several reactions if there are intermediate species with short life times (i.e. they are consumed as soon as they are formed). An example of such a reduction is that of an n-heptane mechanism by Soyhan et al. (2002), in which the mechanism was reduced from 510 reactions and 74 species to 16 global reactions and 19 species. Using the reduced mechanism, they were able to predict the ignition timing to within 3 Crank Angle Degrees (CAD) of the ignition timing determined using the full mechanism. Similar to global reactions, reduced mechanisms are only valid for the conditions considered in the reduction analysis.

### Empirical Methods

Rather than determining the temporal variation of specie concentrations to predict the exothermicity, it is also possible to describe the exothermicity as energy added to the system. This is done by specifying the shape of the mass fraction burned curve, a practice often used for SI engine modeling. The most common approximation of the mass fraction burned curve is that using the Vibe (1970) function

$$x(\theta) = \frac{m_{burned}}{m_{total}} = 1 - \exp\left(-6.908 \left(\frac{\theta - \theta_{ign}}{\Delta\theta_{comb}}\right)^{m+1}\right) \quad (2.2)$$

where  $x$  is the mass fraction burned,  $\theta$  is the instantaneous crank angle,  $\theta_{ign}$  is the ignition crank angle,  $\Delta\theta_{comb}$  is the combustion duration in degrees crank angle, and  $m$  is a parameter governing the shape of the mass fraction burned curve.

The parameter  $m$  is usually determined from experimental investigations, which limits the extrapolative ability of the model. The major difficulty in implementing the Vibe function for HCCI combustion, is the lack of any mechanism by which the ignition timing can be predicted. When equation 2.2 is used for SI engine modeling,  $\Delta\theta_{comb}$  is approximately constant, and  $\theta_{ign}$  is specified by the spark timing. These values are generally not well known before combustion takes place in an HCCI engine. If the dependence of the Vibe equation parameters on various engine parameters is well known, it is possible to use the Vibe function for qualitative investigations (Bulaty & Glanzmann 1984).

An alternative empirical method of representing the HCCI combustion process was presented by Najt & Foster (1983), where the ignition timing is predicted using a set of four reactions from the Shell Model (Halstead et al. (1977)), and the exothermicity by an Average Energy Release Rate (AERR). The AERR was based on the oxidation kinetics of CO to CO<sub>2</sub> and an experimentally determined

coefficient. Using these two models, Najt & Foster were able to investigate the effect of various engine parameters on the ignition timing and combustion duration.

### 2.3.2 Thermodynamic Models

The different chemical kinetic mechanisms discussed above describe the variation of the specie concentrations, while a thermodynamic model describes the relationship between the mixture temperature, pressure, and composition. The control mass (i.e. the mixture within the combustion chamber) can be approximated with variable volume systems using either single- or multi-zone models, or Computational Fluid Dynamics (CFD) codes. The difference between these three different types of models is the accuracy with which the spatial variation of the thermodynamic state is represented. Furthermore, each of the different types of thermodynamic models describe processes such as heat transfer differently.

#### Single Zone

Single zone models assume that the thermodynamic state of the mixture is uniform throughout the combustion chamber. No spatial variations in the temperature, pressure, or mixture composition (for example equivalence ratio or EGR) are considered. The in-cylinder fluid motion is neglected and empirical correlations based on engine parameters, such as that by Woschni (1967), are used to approximate the heat transfer process.

Such a thermodynamic model was used by Aceves et al. (1999) along with a kinetic mechanism for natural gas to investigate the effect of compression ratio on HCCI combustion. Using this model, they found that the single zone approximation was not capable of predicting combustion durations, peak pressures, and CO and uHC emissions as they were all affected by the lower temperatures within the

boundary layer regions, which were not modeled. The combustion duration was under predicted by the model because, contrary to the one zone assumption, the entire mixture does not ignite and combust concurrently. Rather, different regions throughout the mixture have different temperatures and compositions, leading to slightly different ignition times. The mixture within the boundary layer regions will ignite later due to the lower temperatures, thus extending the combustion duration. The lower temperatures within the boundary layers are also the mechanism responsible for the incomplete combustion, seen as CO and uHC emissions. By not accounting for the lower temperature regions within the boundary layers, the single zone model also assumes that all of the fuel reacts. As this is not the case and some of the fuel within the cooler regions does not react, the peak pressure and temperature are over-predicted by single zone models. Despite these issues, the single zone model is able to predict the effects of various engine parameters on the ignition timing (Aceves et al. 1999).

Zhao et al. (2001) used a single zone model to thoroughly investigate the effects of EGR in an HCCI engine. In such an investigation the qualitative trends are more relevant than quantitative values and the ability to carry out a multitude of simulations quickly is desired. Much of Zhao et al.'s (2001) investigation was carried out numerically and could not have been done experimentally, as the composition of EGR was altered to investigate various chemical and thermodynamic effects. Single zone models are generally used when the application requires approximate or qualitative predictions, or to reduce computational requirements. While single zone models do not provide precise, quantitative values, they are an effective tool to further the understanding of HCCI ignition.

### Multi-Zone

To improve the ability of the thermodynamic model to predict the HCCI combustion process, the combustion chamber can be divided into multiple thermodynamic zones, each with its own thermodynamic state. Fiveland & Assanis (2001) created a two zone model which divided the combustion chamber into an adiabatic core volume and an outer boundary layer region. The boundary layer thickness was determined based on in-cylinder fluid motion measurements and used to determine the mass of the mixture trapped within the boundary layer. This mass affects the peak pressure, combustion duration, and CO and uHC emissions. The temperature profile through the boundary layer was used to determine the conductive heat transfer, while the convective heat transfer was determined using turbulence models. Using this two zone model with detailed chemical kinetic mechanisms, Fiveland & Assanis were able to predict the ignition timing as well as peak pressures and combustion durations.

Flowers et al. (2003) investigated the effects of the number of zones on the simulation accuracy by comparing the simulation results with experimental results. Simulations with 10, 20, and 40 zones were used to discretize the temperature distribution throughout the combustion chamber, which was determined using a CFD software package. The CFD and chemical kinetic models were uncoupled and the CFD analysis was used only to determine the temperature distribution during compression. This temperature distribution was then used to determine the geometry of the zones used in the multizone simulation. Using this multi-zone model, accurate predictions of the peak pressure and burn durations were possible with 10 zones (to within 1.4% of the experimental peak pressure and 21% of the experimental combustion duration). No significant improvements were obtained by using more than ten zones. Even when 40 zones were used, the CO emissions

were still under predicted by 84%, likely due the lower temperature regions (i.e. crevice and boundary layer regions) not being discretized finely enough.

### CFD

By coupling a detailed kinetic mechanism with a CFD package, Kong & Reitz (2003) were able predict the CO and uHC emissions in a direct injected HCCI engine. More importantly, the use of CFD allows the physical mechanism by which the CO and uHC are formed to be investigated. The CFD simulation verified that the CO and uHC emissions are largely due to the lower temperatures within the crevice regions. The advantage of using a CFD model over a multi-zone model is that the temperature and species concentration distributions throughout the cylinder do not have to be estimated and can be finely discretized in the crevice and boundary layer regions. These distributions are determined based on engine geometry and operating conditions. By using CFD, the effects of fluid motion are also included and can be used to accurately predict the convective heat transfer. The disadvantage of coupling the many discrete zones of a CFD model with a chemical kinetic mechanism, is that it leads to high computational requirements.

## 2.4 Summary

The HCCI cycle is a modified version of the SI cycle in which the mixture autoignites due to the high compression temperatures and pressures. The combustion process in an HCCI engine differs considerably from that of an SI engine since the mixture combusts uniformly throughout the chamber, rather than by a flame propagating through the cylinder. This uniform combustion process results in high rates of pressure rise and possible engine damage unless the fuel/air mixture is diluted using either excess air or EGR. Because the mixture is diluted, the

HCCI engine has a lower power density (i.e. useful power/engine mass) and will likely be implemented in a combined HCCI/SI configuration. One advantage of the diluted mixture is that the combustion temperature is reduced, resulting in lower  $\text{NO}_x$  emissions and heat transfer to the cylinder walls. Furthermore, because the engine can be operated under lean conditions, the thermal efficiency is also increased.

Numerous engine parameters affect the operation of the HCCI engine as they influence the ignition timing and combustion duration:

**Octane Number** The octane number is a measure of a fuel's autoignition properties. As the octane number is increased, the likelihood of a fuel autoigniting also increases. Thus, by varying the octane number, it is possible to control the ignition timing. The octane number can also be used to extend the load range of the HCCI engine.

**Initial Temperature** The initial temperature of the mixture affects the rate of the chemical reactions, therefore influencing both the ignition timing and combustion duration. As the temperature is increased, the kinetic rate is also increased, advancing the ignition timing and reducing the combustion duration. It is difficult to use an intake air heater to vary the initial temperature as the sole control mechanism because there is considerable lag between changes in the heater output and the in-cylinder mixture temperature.

**Engine Speed** The engine speed is not a control mechanism as such, but does it does have implications on the ignition process. Changing the engine speed changes the time (in seconds) during which the autoignition process can take place and requires changes in engine parameters to maintain a constant ignition timing (in CAD).

**Compression Ratio** The compression ratio affects the end of compression temperature and pressure, and hence autoignition timing. Implementations of variable compression ratio strategies found that the response of the ignition timing is limited by the rate at which the compression ratio can be changed.

**Equivalence Ratio** The equivalence ratio is a measure of the relative fuel/air quantities. Variations in the equivalence ratio have been used to control the engine load, while other parameters such as the EGR rate, were used to maintain a constant ignition timing.

**Initial Pressure** The initial mixture pressure influences the mixture concentration and hence the likelihood of the fuel molecules reacting with the oxygen molecules. Higher pressures advance the ignition timing, while lower pressure retard it. The initial pressure has also been used to extend the HCCI load range by throttling to achieve lower loads, and by turbo- or supercharging to achieve higher loads.

**EGR** Recirculated exhaust gases affect the combustion process by: changing the initial temperature and specific heat of the mixture, introducing chemically active species ( $\text{CO}$ ,  $\text{CO}_2$ , and  $\text{H}_2\text{O}$ ), and diluting the fuel/air mixture. The most dominant of these effects is that of changing the initial mixture temperature (the charge heating effect).

Modeling of the HCCI cycle is accomplished by coupling a thermodynamic model with either a chemical kinetic mechanism, or empirical relationships to describe the combustion process. When a chemical kinetic mechanism is used, the model is termed a *thermokinetic* model. Chemical kinetic mechanisms can range from small skeletal mechanisms (either phenomenological or reduced), to large detailed mechanisms. Detailed mechanisms are computationally expensive

but may be used for extrapolative purposes, while skeletal mechanisms have lower computational requirements but are limited to applications for which they were developed. Chemical kinetic mechanisms describe the underlying physical process of ignition and can be used for extrapolative investigations. Empirical relationships, which rely on correlations from experimental measurements, can be used to describe the combustion process but are generally not well suited to extrapolative investigations.

Thermodynamic models can represent the combustion chamber as a single spatially uniform zone, or it can be discretized to describe spatial variations in the thermodynamic state. The single zone model is well suited to determining the qualitative effects of engine parameters on the ignition timing, but not the subsequent combustion process (i.e. the peak pressure and temperature, combustion duration, and exhaust gas composition). In order to more accurately model the high temperature combustion process, further spatial discretization of the combustion chamber is required to account for the effects of the cooler boundary layer regions. The use of CFD models coupled with chemical kinetic mechanisms, while computationally expensive, allows accurate investigations to be made. By using a multi-zone thermodynamic approximation of the system, a compromise between computational requirements and accuracy can be reached.

## Chapter 3

# Background Theory

### 3.1 Introduction

Before developing an engine model to predict engine operation and performance, it is useful to understand the physical processes taking place within the cylinder. Generally, the aim of the model is to characterize the thermodynamic state within the cylinder by determining the mixture temperature, pressure, and composition. These parameters are inter-dependant and are affected by processes such as piston motion, heat transfer, and combustion. Energy can be added through heat transfer with the cylinder walls, the combustion process, or work can be done by the system through expansion of the hot combustion gases.

This chapter discusses the details of the thermokinetic model developed in this thesis. A first law (conservation of energy) analysis, in which the different energy sources and sinks are considered, is used to derive an equation describing the thermodynamic state of the cylinder contents. This requires knowledge of the thermodynamic properties of the mixture, which in some cases are not known and must be estimated using additivity rules based on statistical thermodynamics.

These properties are presented in a manner that is efficient for numerical solutions.

The exothermicity and compositional changes due to combustion are also considered. Given a chemical kinetic mechanism, the temporal variation of the mixture composition is determined, by accounting for the effects of temperature and pressure on the reaction rates. A chemical kinetic mechanism was developed by combining existing sub-mechanisms for hydrocarbon ignition and combustion. The resulting mechanism can be used for arbitrary PRF blends without having to calculate new reaction parameters for each fuel blend. The mechanism describes low temperature ignition phenomena, such as induction periods, multistage ignition and negative temperature coefficient regions, as well as the high temperature processes such as CO oxidation.

### 3.2 Thermodynamic Modeling

Thermodynamic models of internal combustion engines can range in complexity from a simple single zone model with the assumption of uniform thermodynamic state throughout the cylinder, to multidimensional CFD models used to predict the fluid motion and heat and mass transport. In this investigation, a single zone approximation was chosen as it is well suited to determining the qualitative effects of engine parameters on the ignition timing in an HCCI engine, despite the limitations discussed in chapter 2. The nature of the HCCI cycle lends itself well to this type of model, as the fuel/air mixture can be assumed to be uniform and to combust concurrently at multiple points and that the thermodynamic state of the mixture changes uniformly with respect to time. This is in contrast to SI and Diesel engines in which, at any time during combustion, there is both a fresh fuel/air mixture component and an burned gas component. The one zone approximation neglects fluid motion and mass transfer and assumes a con-

stant thermodynamic state throughout the cylinder, reducing the computational requirements and development time of the model.

Only the high pressure phases of the HCCI cycle, from Intake Valve Closing (IVC) to Exhaust Valve Opening (EVO) are considered in this investigation. This includes the compression, ignition, combustion and expansion phases of the cycle. For this system, a differential equation describing the mixture temperature of the single zone is developed based on a first law analysis for a constant mass system.

### 3.2.1 Energy Balance

The single zone model used to describe the system is shown in Figure 3.1. The control volume, denoted by the dashed lines, is subject to the following assumptions:

1. The thermodynamic state is uniform throughout the control volume. Spatial variations in temperature, pressure, or mixture composition are not considered.
2. The mass of the system is constant, none of mixture can enter or leave the control boundaries. This implies that blow-by of the mixture past gaps in the cylinder rings is neglected.
3. All species in the mixture are in the gas phase and can be treated as ideal gases.

Using these assumptions, the change in internal energy,  $\frac{dU}{dt}$ , can be described using

$$\frac{dU}{dt} = \frac{dQ_{HT}}{dt} - \dot{W}_{boundary} \quad (3.1)$$

where  $\frac{dQ_{HT}}{dt}$  is the rate at which energy is added to the system through heat transfer with the cylinder wall and,  $\dot{W}_{boundary}$  is the rate at which boundary (or

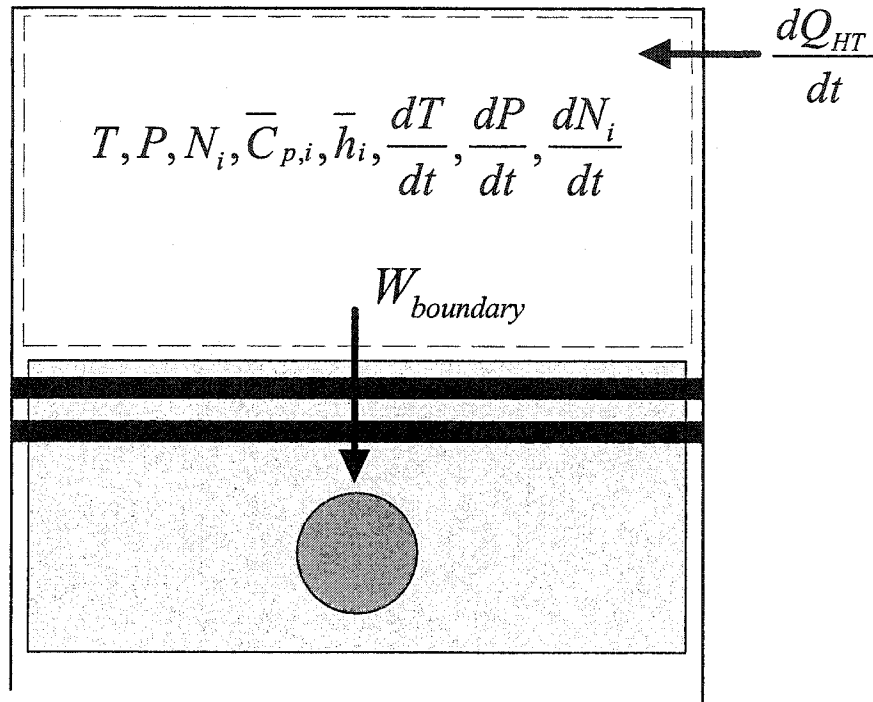


Figure 3.1: Control mass used in the one zone model. The thermodynamic state is assumed to be constant throughout the entire volume.

expansion) work is being done by the control mass on the moving piston. The determination of each of these three terms are discussed in detail below.

### Heat Transfer

The heat transfer process during the compression stroke in an HCCI engine is the same as that in an SI or Diesel engine. The majority of heat transfer is through the convective mode to due to fluid motion relative to the cylinder walls. This can be approximated using a form of the Reynolds Flow Analogy (Borman & Nishiwaki 1987):

$$Nu = aRe^bPr^c \quad (3.2)$$

$$\frac{hL}{k_f} = a \left( \frac{\rho VL}{\mu} \right)^b \left( \frac{\nu}{\alpha} \right)^c$$

where  $Nu$  is the Nusselt number,  $Re$  is the Reynolds number, and  $Pr$  is the Prandtl number. Equation 3.2 can be rearranged to solve for  $h$ , the convective heat transfer coefficient, based on the fluid properties ( $k_f$ , thermal conductivity;  $\rho$ , density;  $\mu$ , dynamic viscosity;  $\nu$ , kinematic viscosity;  $\alpha$ , thermal diffusivity) and the characteristic length and fluid velocities of the system,  $L$  and  $V$ , respectively. The coefficients  $a$ ,  $b$ , and  $c$  are determined from empirical investigations.

The definition of the characteristic length and velocities depends on how detailed an investigation was used to determine the empirical constants. Examples of characteristic lengths are the cylinder bore (Woschni 1967) or the macro scale of in-cylinder turbulence (Assanis & Heywood 1986), and the mean piston velocity or turbulent fluid velocity for characteristic velocities. Indeed, the level of accuracy of the heat transfer correlation used depends largely on the knowledge of the in-cylinder fluid motion. The reader is referenced to Borman & Nishiwaki (1987) for a more complete discussion of engine heat transfer correlations.

As knowledge of the in-cylinder fluid motion for this investigation was very limited, the Woschni (1967) heat transfer correlation was used. The characteristic length and velocity are defined as the bore diameter and mean piston speed, respectively. The Woschni heat transfer correlation is based on a form of the Reynolds Flow Analogy specific to turbulent flow in which the coefficients are determined from experimental measurements of the heat transfer in a Diesel engine. Woschni assumes the following form of equation 3.2:

$$Nu = CRe^m \tag{3.3}$$

where  $C$  and  $m$  are experimentally determined coefficients. By defining the thermal conductivity, density, and viscosities in terms of the mixture temperature and pressure, Woschni (1967) was able to determine the convective heat transfer

coefficient,  $h$ , from equation 3.3 to be:

$$h = C (d^{m-1} P^m w^m T^{0.75-1.62m}) \quad (3.4)$$

For turbulent flow,  $m$  is arbitrarily set to 0.8 and the constant  $C$  is used to characterize the fluid velocity,  $w$ , for the different phases of the cycle (i.e. compression, combustion, expansion, gas exchange). Woschni has defined the characteristic fluid velocity as follows:

$$w = C_1 \bar{S}_p + C_2 \frac{V_d T_r}{P_r V_r} (P - P_m) \quad (3.5)$$

Where  $\bar{S}_p$  is the mean piston speed,  $V_d$  is the displaced volume of the engine,  $T_r$ ,  $P_r$ , and  $V_r$  are the reference mixture temperature pressure, and volume, respectively (at IVC for example), and  $(P - P_m)$  is the increase in pressure due to combustion. The second term is the contribution to the fluid motion due to the change in fluid density during combustion. The coefficients  $C_1$ , and  $C_2$  are defined as follows:

$$\begin{cases} C_1 = 6.18, & C_2 = 0 & \text{For gas exchange} \\ C_1 = 2.28, & C_2 = 0 & \text{For compression stroke} \\ C_1 = 2.28, & C_2 = 3.24 \times 10^{-3} & \text{For combustion and expansion} \end{cases} \quad (3.6)$$

Since only a closed system is considered in this investigation, the heat transfer during the gas exchange process is not relevant. The influence of the density change on the fluid motion is not considered as the density of the mixture is assumed to change uniformly. Without a density gradient in the mixture, there is not any additional fluid movement due to the combustion process. The original empirical measurements were taken from a Diesel engine (Woschni 1967), which

has much higher radiative heat transfer components and is accounted for in  $C_2$ . As both the high radiation heat transfer and combustion induced fluid motion are not present in the HCCI cycle (Assanis & Heywood 1986),  $C_2$  was set to zero in the thermokinetic model.

### 3.2.2 Boundary Work

Energy can be both added to the system or converted to useful work through the compression or expansion of the control volume. During the compression stroke, the piston moves upwards, compressing the mixture and increasing its temperature and pressure. During the expansion stroke, the hot combustion products expand and push the piston down, providing useful work from the engine. The rate at which boundary work is being done these processes is described using:

$$\dot{W}_{boundary} = P \frac{dV}{dt} \quad (3.7)$$

where  $\frac{dV}{dt}$  is the rate of change of volume of the combustion chamber. The cylinder pressure,  $P$ , can be determined using the ideal gas law:

$$P = \frac{N_m \cdot R_u \cdot T_m}{V} \quad (3.8)$$

where the subscript  $m$  refers to mixture properties,  $R_u$  is the universal gas constant, and  $V$  is the instantaneous cylinder volume and is determined from the slider crank mechanism (Heywood 1988):

$$V = V_c \left[ 1 + \frac{1}{2} (CR - 1) \left( \frac{l}{r_c} + 1 - \cos \theta - \left( \left( \frac{l}{r_c} \right)^2 - \sin^2 \theta \right)^{\frac{1}{2}} \right) \right] \quad (3.9)$$

where  $V_c$  is the clearance volume,  $CR$  is the compression ratio,  $r_c$  is the crank throw radius,  $l$  is the connecting rod length, and  $\theta$  is the crank angle relative to Top Dead Center (TDC).

### 3.2.3 Internal Energy

Changes in the internal energy are used to determine the effect of chemical reactions on the thermodynamic state. As the reactions progress, converting the fresh air and fuel to combustion products, the composition and the thermodynamic state also change. For example, consider an adiabatic and constant volume system (i.e.  $\frac{dU}{dt} = 0$ , by equation 3.1), a change in the composition requires a change in temperature to maintain a constant internal energy, as the internal energy is a function of both the mixture composition and temperature. By using the assumptions outlined on page 36 the change in temperature is determined as follows.

The molar internal energy,  $\bar{U}_m$ , of a mixture is defined as:

$$\bar{U}_m = \sum_i N_i \bar{u}_i \quad (3.10)$$

where  $N_i$  is the number of moles of the  $i^{th}$  specie, and  $\bar{u}_i$  is the molar specific internal energy of the  $i^{th}$  specie. The rate form of equation 3.10 is found by taking the derivative with respect to time using the chain rule:

$$\frac{d\bar{U}_m}{dt} = \frac{d}{dt} \left( \sum_i N_i \bar{u}_i \right) = \sum_i \frac{dN_i}{dt} \bar{u}_i + \sum_i N_i \frac{d\bar{u}_i}{dt} \quad (3.11)$$

Combustion modeling is generally discussed in terms of *enthalpy* rather than in-

ternal energy, which are related by:

$$\bar{u}_i = \bar{h}_i - Pv = \bar{h}_i - R_u T \quad (3.12)$$

Where  $\bar{h}_i$  is the specific molar enthalpy of the  $i^{th}$  specie. Substituting equation 3.12 into 3.11 and differentiating gives:

$$\frac{d\bar{U}_m}{dt} = \sum_i \frac{dN_i}{dt} \bar{h}_i - R_u T \sum_i \frac{dN_i}{dt} + \sum_i N_i \frac{d\bar{h}_i}{dt} - R_u \frac{dT}{dt} \sum_i N_i \quad (3.13)$$

which is further simplified through the definition of  $\bar{h}_i$ :

$$\left( \frac{\partial \bar{h}_i}{\partial T} \right)_p = \bar{c}_{p,i}(T) \quad (3.14)$$

At each time step the pressure is assumed to remain constant, then

$$\frac{d\bar{h}_i}{dt} = \frac{d\bar{h}_i}{dT} \frac{dT}{dt} = \bar{c}_{p,i} \frac{dT}{dt} \quad (3.15)$$

Combining equations 3.15 and 3.13 the differential form of the internal energy (in terms of enthalpy) is given as:

$$\frac{d\bar{U}_m}{dt} = \sum_i \frac{dN_i}{dt} \bar{h}_i - R_u T \sum_i \frac{dN_i}{dt} + \frac{dT}{dt} (N_i \bar{c}_{p,i} - N_{mix} R_u) \quad (3.16)$$

### 3.2.4 Energy Balance - Revisited

The thermodynamic state of the system can be described by substituting equations 3.7 and 3.16 into equation 3.1

$$\boxed{\frac{dT}{dt} = \frac{-P \frac{dV}{dt} + \frac{dQ_{wall}}{dt} - \sum_i \frac{dN_i}{dt} \bar{h}_i + RT \sum_i \frac{dN_i}{dt}}{\sum_i N_i \bar{c}_{p,i} - N_{mix} R}} \quad (3.17)$$

The temporal variation of the mixture composition,  $\frac{dN_i}{dt}$ , and thermodynamic properties of each specie,  $\bar{h}_i$  and  $\bar{c}_{p,i}$ , are needed to solve equation 3.17. The thermodynamic properties are determined from existing databases of polynomial approximations, or estimated when existing data is not available. The mixture composition is determined using chemical kinetics.

### 3.3 Thermodynamic Properties

Solution of the differential temperature through equation 3.17 requires the knowledge of both the specific heat and the absolute enthalpy of each specie. Typically in combustion modeling the thermodynamic properties are represented by a set of polynomials rather than being tabulated in look-up tables. The most common of these polynomials are the “Old NASA Polynomials”, introduced by NASA (Mcbride et al. 1993). The thermodynamic properties of each specie are represented using two 7<sup>th</sup> order polynomials, one polynomial for temperatures above 1000K and one for below 1000K. Two sets of coefficients are required due to the characteristic “knee” of the specific heat (Burcat 1984). There are several compilations of these polynomials available, the most comprehensive being the Burcat Database (Burcat 2001) which was used for the majority of the chemical species in this investigation.

Given a set of NASA polynomials, the specific heat, absolute enthalpy, absolute entropy, and Gibbs energy are determined as follows (Burcat 2001):

$$\frac{C_p^\circ}{R} = a_1 + a_2T + a_3T^2 + a_4T^3 + a_5T^4 \quad (3.18)$$

$$\frac{H_T^\circ}{RT} = a_1 + \frac{a_2T}{2} + \frac{a_3T^2}{3} + \frac{a_4T^3}{4} + \frac{a_5T^4}{5} + \frac{a_6}{T} \quad (3.19)$$

$$\frac{S_T^\circ}{R} = a_1 \ln T + a_2T + \frac{a_3T^2}{2} + \frac{a_4T^3}{3} + \frac{a_5T^4}{4} + a_7 \quad (3.20)$$

$$\frac{G_T^\circ}{RT} = \frac{H_T^\circ}{RT} - \frac{S_T^\circ}{R} \quad (3.21)$$

Where equation 3.19 represents the absolute enthalpy, which includes the enthalpy of formation:

$$H_T^o = \Delta H_{f,298K}^o + \int_{298K}^T C_p^o dT \quad (3.22)$$

where  $\Delta H_{f,298}^o$  is the enthalpy of formation at 298K. It should be noted that the absolute enthalpy is not the same as tabulated values which typically do not include the enthalpy of formation.

For some species, such as short lived radicals, existing thermodynamic data is not available and the properties are estimated based on additivity rules and statistical thermodynamics.

### 3.3.1 Estimating the Specific Heat

Thermodynamic properties which are not available from tables or polynomial databases are estimated based on additivity rules and statistical thermodynamics. Three sets of additivity rules, each of different orders, can be used to predict the specific heat of a given chemical specie (Benson 1976, Benson & Buss 1958):

**Additivity of Atomic Properties** The simplest, zeroth order approximation states that the specific heat of a compound can be estimated as being the sum of the specific heat of each of it's composing atoms. This implies that for a chemical reaction, the specific heat of the mixture will not change. As this is not the case, this approximation is rarely used.

**Additivity of Bond Properties** This first order approximation states that each bond will have a characteristic contribution to the specific heat of the compound. In practice, this method incurs large errors for heavily branched molecules and provides no accommodation for isomers, both of which are important aspects in combustion chemistry.

**Additivity of Group Properties** This second order approximation states that the specific heat of a molecule can be approximated as the sum of the contributions of each of its constituent groups. A group is defined as a polyvalent atom bonded to one or more mono- or polyvalent atoms. This approximation takes into account both which molecules are in the group, and how they are arranged.

The method of additivity of group properties was used in this investigation, as the former two methods do not provide accurate enough estimates for combustion modeling.

The specific heat of a molecule can be estimated by considering the contribution of all its constituent groups. Each group has a characteristic contribution that is tabulated for temperatures ranging from 300K to 1500K. An example of using the Benson additivity rules to determine the specific heat of iso-octane is given in appendix A.1.

If a molecule cannot be described using the available groups, statistical thermodynamics are used to estimate the specific heat. In general, the specific heat of a molecule is attributed to molecular motion through rotation, translation, and vibration. Rotational motion refers to the molecule rotating as a whole in space, and similarly translational motion refers to the molecule moving through space in any one of three directions. Standard approximations are used to determine the specific heat contributions of the rotational and translational motions:

$$C_{v,trans} = \frac{3}{2}R \quad (3.23)$$

$$C_{v,rot} = \begin{cases} R & \text{For linear molecules} \\ \frac{3}{2}R & \text{For non-linear molecules} \end{cases} \quad (3.24)$$

Where  $C_{v,trans}$  is the specific heat contribution from translation, and  $C_{v,rot}$  is the contribution from rotation.

Vibrational motion is more complex and is composed of the motions of the separate atoms within a molecule relative to each other. There are five fundamental types of vibration:

**Internal Rotation** The free rotation of one or more atoms about a single bond.

**Torsion** Similar to internal rotation except it involves a double bond which inhibits the free rotation.

**Bending** The change in the relative angle between two bonds in a molecule.

**Group Movement of Atoms** Similar to bending except that the motion now involves two or more atoms moving, rather than just one moving relative to the other. This motion is further classified depending how the atoms move relative to each other and the rest of the molecule. For example, two atoms could twist or shift.

**Stretch** The bonds within a molecule expand and contract causing motion of one or more atoms relative to each other.

The contributions of each of these internal motions to the specific heat of the molecule are defined by the frequency of the vibration.

### Radicals

Estimating the properties of radicals poses a unique problem in that radicals contain groups for which contributions are not tabulated. It is assumed that the specific heat of a radical R· can be estimated by determining the specific heat of the parent molecule, RH, and then compensating for the effects of the hydrogen

abstraction:

$$C_p(\text{R}\cdot) = C_p(\text{RH}) + \delta C_p \quad (3.25)$$

Where the correction  $\delta C_p$  is the change in specific heat due to changes in the internal rotation and fundamental vibrations:

$$\delta C_p = \delta C_{p,int.rot.} + \delta C_{p,vib.} \quad (3.26)$$

Values for  $\delta C_{p,vib.}$  are determined by considering the vibrational modes due to the abstracted H atom, using the techniques discussed above. The rotational contribution,  $\delta C_{p,int.rot.}$  is calculated based on the symmetry of the molecule.

Using the above techniques to estimate thermodynamic properties is simplified by using existing software packages, some of which also provide the properties in the form of NASA polynomials. Among these is the National Institute of Standards and Technology's (NIST) on-line implementation (Stein & Brown 2003), which requires a sketch of the molecule and determines the specific heat from  $T = 300$  to  $T \sim 1000K$ . It also provides the absolute entropy and enthalpy at 298K, but not the NASA polynomials. Other packages such as THERGAS (Muller et al. 1995) and THERM (Ritter & Bozzelli 1991) also extrapolate the specific heat to 5000K and determine a set of NASA polynomials.

### 3.3.2 Determination of NASA Polynomials

The NIST program is used in this investigation to determine the specific heats, which were subsequently extrapolated and fit to the NASA polynomials. Several methods exist to extrapolate relatively few low temperature specific heat values to the higher temperatures required for combustion modeling. The Harmonic Oscillator Equation (HOE) presented by (Ritter & Bozzelli 1991) takes into account

statistical thermodynamics to predict the specific heat at higher temperatures. This is the more accurate method when only a few low temperature specific heat values are known. If sufficient low temperature points are known it is simpler to use the Wilhoit polynomials to extrapolate to higher temperatures (Burcat 1984). The Wilhoit polynomial is fitted to the known low temperature points using a least squares regression, while the high temperature properties are predicted using the theoretical high temperature specific heat,  $C_p(\infty)$ , and a parameter,  $B$ , describing how fast the limit is approached:

$$C_p(T) = C_p(0) + [C_p(\infty) - C_p(0)] y^2 \left[ 1 + (y - 1) \sum_{i=0}^n a_i y^i \right] \quad (3.27)$$

where:

$$y = \frac{T}{T + B} \quad (3.28)$$

$$C_p(0) = \begin{cases} \frac{7}{2}R & \text{For linear molecules} \\ 4R & \text{For non-linear molecules} \end{cases} \quad (3.29)$$

$$C_p(\infty) = \begin{cases} \frac{3N-3}{2}R & \text{For linear molecules} \\ \frac{3N-2}{2}R & \text{For non-linear molecules} \end{cases} \quad (3.30)$$

The values of  $B$  depend on the molecule for which the extrapolation is being done. In general it ranges from 300-1000K, with larger molecules having values in the range of 300-500K.

Once the specific heats are known for the full temperature range, the NASA polynomial coefficients (for equations 3.18-3.20) are determined. A least squares fit of the specific heat values to equation 3.18 is used to determine  $a_1 \rightarrow a_5$ . The coefficients  $a_6$  and  $a_7$  are determined by solving equations 3.19 and 3.20,

respectively with known enthalpy and entropy values (from NIST) as follows:

$$a_6 = \frac{H_T^\circ}{R} - \left( \sum_{i=1}^5 a_i \frac{T^i}{i} \right) \quad (3.31)$$

$$a_7 = \frac{S_T^\circ}{R} - \left( a_1 \ln T + \sum_{i=2}^5 a_i \frac{T^i}{i-1} \right) \quad (3.32)$$

Recall that there are two sets of coefficients to improve the fit of the polynomials over the full temperature range. The polynomials are split at  $T = 1000\text{K}$  and the coefficients are determined such that each polynomial returns the same value at  $1000\text{K}$ .

## 3.4 Chemical Kinetics

The change in the composition of the mixture with respect to time,  $\frac{dN_i}{dt}$ , is described using a chemical kinetic mechanism. The following discussion first focusses on the solution methodology for a given chemical kinetic mechanism, while the chemical kinetic mechanism itself will be discussed in section 3.4.2. Only topics directly relevant to this investigation are discussed and the interested reader is referred to Gardiner & Burcat (1984) or Côme (2001) for a more comprehensive discussion of chemical kinetics.

### 3.4.1 Kinetic Modeling

Given a set of  $J$  elementary<sup>1</sup> reactions describing the chemical processes involving  $I$  species, the concentration of each specie in a constant mass system is

---

<sup>1</sup>An elementary reaction is one which describes an individual molecular event. For example, reaction 1 in Table 3.2 is an elementary reaction, while the general combustion equation given in equation 3.60 is an overall reaction describing multiple elementary reactions.

determined using the Law of Mass action:

$$\frac{d[M_i]}{dt} = \sum_{j=1}^J \left[ (\nu''_{i,j} - \nu'_{i,j}) k_{f,j} \prod_{i=1}^I [M_i]^{\nu'_{i,j}} \right] \quad (3.33)$$

where  $[M_i]$  is the concentration of the  $i^{\text{th}}$  specie,  $\frac{d[M_i]}{dt}$  is the rate of change of the concentration of the  $i^{\text{th}}$  specie,  $\nu''_{i,j}$  is the stoichiometric coefficient of the  $i^{\text{th}}$  specie on the product side of the  $j^{\text{th}}$  chemical reaction, and  $\nu'_{i,j}$  is the stoichiometric coefficient of the  $i^{\text{th}}$  specie on the reactant side of the  $j^{\text{th}}$  chemical reaction. The forward reaction rate constant of the  $j^{\text{th}}$  reaction,  $k_{f,j}$  is defined by:

$$k = AT^n \exp\left(\frac{-E_a}{RT}\right) \quad (3.34)$$

Where  $A$  is the pre-exponential constant,  $E_a$  is the activation energy, and the exponent  $n = 0$  for Arrhenius behavior. The change in molar composition can be related to the change in concentration as follows:

$$\frac{d}{dt} \left( \frac{N_i}{V} \right) = \frac{d[M_i]}{dt} \quad (3.35)$$

then

$$\frac{dN_i}{dt} = V \frac{d[M_i]}{dt} + [M_i] \frac{dV}{dt} \quad (3.36)$$

As an example of the application of the law of mass action, consider the arbitrary, elementary reaction:



Where  $a$ ,  $b$ ,  $c$ , and  $d$  are the stoichiometric coefficients of the chemical species A, B, C, and D. In equation 3.37 both a forward and a reverse rate constant are

specified, as the reaction can occur in either direction. The rate of change of the concentration of A can be described using equation 3.33 as follows:

$$\frac{d[A]}{dt} = (0 - a)k_f[A]^a[B]^b + (a - 0)k_b[C]^c[D]^d \quad (3.38)$$

The first term on the right hand side describes the consumption of A by the forward reaction, while the second term describes the formation of A by the reverse reaction. If more than one reaction affects A, equation 3.33 would be applied to the other reactions as well.

### Equilibrium

It is often difficult to measure the reverse rate constant,  $k_b$  and instead it is determined using the equilibrium constant. The forward and reverse reaction rate constants for an elementary reaction are related through the equilibrium constant by:

$$K_c = \frac{k_f}{k_b} \quad (3.39)$$

Where the subscript  $c$  denotes that the equilibrium constant is based on concentrations, as opposed to  $K_p$  which is based on the partial pressures of the species. The two forms are related using:

$$K_c = RT^{-\Delta\nu} K_p \quad (3.40)$$

where  $\Delta\nu$  is the change in number of moles from reactants to products.

The condition that must be satisfied for equilibrium is the minimization of Gibbs Free Energy, or

$$(dG)_{T,P} = 0 \quad (3.41)$$

## CHAPTER 3: BACKGROUND THEORY

---

As the Gibbs free energy is an intrinsic property and can be determined for each specie, it is then possible to determine the equilibrium constant for a reaction by ensuring that equation 3.41 is satisfied. For an arbitrary reaction, the equilibrium constant can be defined as:

$$K_p = e^{\frac{-\Delta G}{RT}} \quad (3.42)$$

or by equation 3.40,

$$K_c = RT^{-\Delta\nu} e^{\frac{-\Delta G}{RT}} \quad (3.43)$$

In terms of the NASA polynomials, this is given as (Burcat 2001):

$$K_c = RT^{-\Delta\nu} \exp \left[ -\Delta a_1 (1 - \ln(T)) + \Delta a_2 \frac{T}{2} + \Delta a_3 \frac{T^2}{6} + \dots \right. \\ \left. \Delta a_4 \frac{T^3}{12} + \Delta a_5 \frac{T^4}{20} - \frac{\Delta a_6}{T} + \Delta a_7 - 0.0136 \right] \quad (3.44)$$

where  $\Delta a_i$  refers to the sum of the changes in the mole numbers of each specific specie multiplied by its polynomial coefficients. That is,

$$\Delta a_i = \sum_{k=1}^K \Delta \nu_k a_{k,i} \quad i = 1 \dots 7 \quad (3.45)$$

where there are  $K$  species in the chemical reaction.

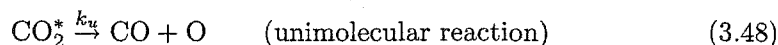
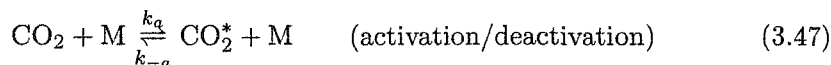
### Non-Arrhenius Behavior

In some cases, namely unimolecular reactions, the rate constant,  $k$ , does not follow a pure Arrhenius relationship that is only dependant on the temperature. Rather, the rate constant is also dependant on the mixture pressure. Consider the

dissociation of  $\text{CO}_2$ ,



where M is any inert<sup>2</sup> collision partner. According to the Lindemann model (Lindemann 1922), this reaction represents three fundamental steps.  $\text{CO}_2$  must collide with any inert specie to increase its vibrational energy level such that it is activated. Once this happens, the activated  $\text{CO}_2$  molecule can either decompose to its dissociation products, or be involved in another collision which will deactivate it.



By assuming that the activated molecule,  $\text{CO}_2^*$ , is in equilibrium (i.e.  $\frac{d[\text{CO}_2^*]}{dt} = 0$ ), the rate of formation of CO is given by:

$$\frac{d[\text{CO}]}{dt} = \frac{k_u k_a [\text{CO}_2][\text{M}]}{k_{-a}[\text{M}] + k_u} \quad (3.49)$$

The inert collision partner, M, is any specie in the mixture (except for the  $\text{CO}_2$  molecule being considered) and its concentration is thus proportional to mixture pressure. At low pressures when  $[\text{M}] \rightarrow 0$  and  $k_{-a}[\text{M}] \ll k_u$ , equation 3.49 becomes  $k_a[\text{CO}_2][\text{M}]$  and the overall rate of the reaction is defined by the mixture pressure. At higher pressures  $k_{-a}[\text{M}] \gg k_u$ , equation 3.49 is defined by

$$\frac{d[\text{CO}]}{dt} = \frac{k_u k_a}{k_{-a}} [\text{CO}_2] = k_\infty [\text{CO}_2] \quad (3.50)$$

<sup>2</sup>M is only inert in the sense that it is not affected by the reaction being considered. It is possible that M may react in other reactions with other species.

Where  $k_\infty$  is defined as the high pressure Arrhenius rate constant. In order to describe the effect of both pressure and temperature on the rate constant, the rate of change of  $\text{CO}_2$  in the example is specified as

$$\frac{d[\text{CO}_2]}{dt} = k_{eff}[\text{CO}_2] \quad (3.51)$$

where  $k_{eff}$  is an effective rate constant defined by the Lindemann form

$$k_{eff} = k_\infty \left( \frac{P_r}{1 + P_r} \right) \quad (3.52)$$

where  $P_r$ , the reduced pressure can be found using:

$$P_r = \frac{k_o[M]}{k_\infty} \quad (3.53)$$

The low pressure rate constant,  $k_o$  is determined using equation 3.34 with parameters specific to the low pressure reaction:

$$k_o = A_o T^{n_o} e^{-\frac{E_o}{RT}} \quad (3.54)$$

### 3.4.2 Hydrocarbon Ignition and Combustion

The chemical kinetics governing hydrocarbon autoignition and combustion in an HCCI engine are similar to those in SI engine knock. In chapter 2 the development of chemical kinetic mechanisms suited to HCCI was reviewed, while the following discussion focusses on the physical processes which these mechanisms describe. Hydrocarbon ignition is a complex process including phenomena such as relatively long induction periods followed by rapid temperature and pressure increases, cool flames, two stage ignition, and Negative Temperature Coefficient

(NTC) regions. Two stage ignition refers to an induction period during which radicals are produced, followed by a small increase in temperature (the cool flame) and then another slightly exothermic induction period prior to the main combustion event. NTC regions are those in which increases in the mixture temperature actually increases the ignition delay. These phenomena are explained by the effect that temperature has on various chain reactions.

In combustion systems, the presence of radicals (i.e. chemical species with free valences) greatly increases the reaction rates due to their higher reactivities compared to stable non-radical species. The ignition of hydrocarbons occurs when sufficient radicals are produced, and reaction rates are sufficiently high that the energy released by the chemical activity is greater than that lost to the surroundings. The formation and destruction of radical species is described using the following different classes of chain reactions:

**Chain Initiation** A reaction in which stable (non-radical) reactants produce one or more radicals.

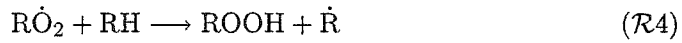
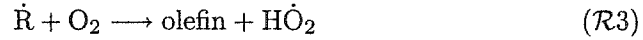
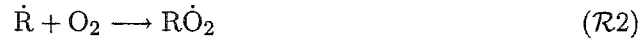
**Chain Propagation** A reaction in which an equal number of radicals are consumed and produced. There is no net change in the number of radicals by such a reaction.

**Chain Branching** A reaction in which there is a net increase in the number of radicals. Even a reaction that is only slightly branching can drastically increase the overall reaction rate of a system.

**Chain Termination** A reaction in which there is a net decrease in the number of radicals.

The critical condition for ignition is that chain branching occurs and increases the number of radicals. A general mechanism for the ignition of hydrocarbons is

(Glassman 1996):



Where  $\mathcal{R}1$  is a chain initiating reaction;  $\mathcal{R}2$ ,  $\mathcal{R}3$ ,  $\mathcal{R}4$ ,  $\mathcal{R}5$ , and  $\mathcal{R}11$  are chain propagating reactions;  $\mathcal{R}7$ ,  $\mathcal{R}8$ , and  $\mathcal{R}10$  are chain branching reactions; and  $\mathcal{R}9$  is a chain terminating reaction. In this general mechanism, RH corresponds to the complete hydrocarbon,  $\dot{\text{R}}$  is the radical formed by removing one of the hydrogens from the base hydrocarbon, and  $\text{R}'$  and  $\text{R}''$  are hydrocarbon radicals with one and two free sites, respectively.

After radicals are formed by the hydrogen abstraction reaction ( $\mathcal{R}1$ ),  $\dot{\text{R}}$  is consumed to either produce a peroxy radical ( $\text{R}\dot{\text{O}}_2$ ) through  $\mathcal{R}2$ , or an olefin and a hydroperoxy radical ( $\text{H}\dot{\text{O}}_2$ ) through  $\mathcal{R}3$ . At low temperatures, the  $\text{H}\dot{\text{O}}_2$  radical eventually forms water and oxygen, inhibiting ignition.  $\text{R}\dot{\text{O}}_2$  on the other hand will form  $\dot{\text{R}}\text{OOH}$  which then decomposes in a chain branching manner through

$\mathcal{R}7$ . This competition for the  $\dot{R}$  radical between  $\mathcal{R}2$  and  $\mathcal{R}3$  is responsible for the cool flame and NTC behaviors. At low temperatures,  $\mathcal{R}2$  is considerably faster than  $\mathcal{R}3$  and thus leads to chain branching and subsequently to ignition. As the temperature increases however, the equilibrium of  $\mathcal{R}2$  shifts towards the reactants reducing the formation of  $R\dot{O}_2$  and subsequent chain branching (as the temperature is still too low for  $H\dot{O}_2$  to play an important role), thereby increasing the ignition delays. As the temperature increases further,  $\mathcal{R}3$  becomes faster and the  $H\dot{O}_2$  is decomposed through the chain branching reaction  $\mathcal{R}10$ . This process in which either chain branching or chain propagation takes place is referred to as *degenerate chain branching* and is the basis for representing hydrocarbon ignition phenomena. For larger hydrocarbons, the isomerization reaction  $\mathcal{R}11$  is the rate controlling reaction for  $\dot{R}OOH$  formation, though the degenerate chain branching will still cause the cool flame and NTC behavior.

Shown in Figure 3.2 is a representative temperature history for the autoignition of a hydrocarbon/air mixture, to illustrate the various ignition phenomena. The induction period during which chain initiation takes place, is shown in region A. A small increase in temperature in region B is due to the formation of  $R\dot{O}_2$  through  $\mathcal{R}2$ . As the temperature increases, the equilibrium of  $\mathcal{R}2$  shifts towards the reactants and the exothermicity decreases (region C). This process is luminous but causes relatively little temperature increases and is referred to as the cool flame<sup>3</sup>. Here the slightly endothermic reactions  $\mathcal{R}3$  and  $\mathcal{R}11$  are rate determining for intermediate and large hydrocarbons, respectively. Before the chain branching

---

<sup>3</sup>In systems in which heat transfer decreases the temperature after the cool flame, it is possible to observe multiple cool flames. As the heat transfer decreases the temperature, the equilibrium shifts back towards the products and more fuel is consumed. The associated heat release once again increases the temperature and shifts the equilibrium towards the products. This cycle continues until either all of the fuel is consumed or sustainable conditions for chain branching are reached

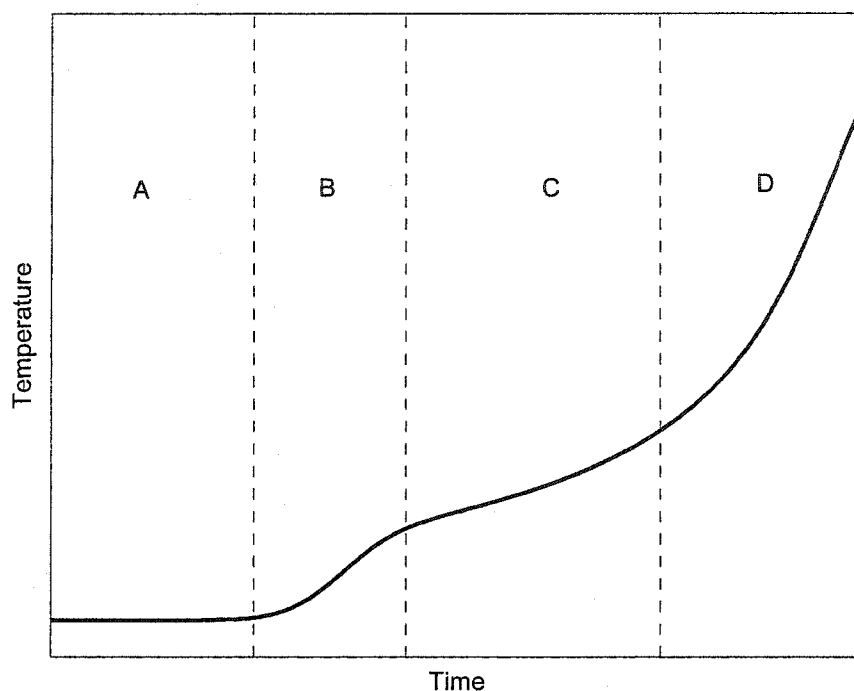


Figure 3.2: A characteristic temperature history of the two-stage autoignition of a hydrocarbon. Region A: Induction period, Region B: Cool flame, Region C:  $\dot{R}OOH$  and  $R'CHO$  formation, Region D: Hot ignition.

reactions have a notable impact, the concentrations of  $\dot{R}OOH$  and  $R'CHO$  must be sufficiently high. Once reactions  $\mathcal{R}7$  and  $\mathcal{R}8$  become important, the exothermicity increases and the chain branching decomposition of  $H_2O_2$  occurs further increasing the exothermicity. This generally occurs at a temperature of 1100K and is referred to as the hot ignition (region D).

The NTC behavior is also explained using the degenerate chain branching mechanism. Figure 3.3 shows the characteristic dependence of the ignition delay on the initial mixture temperature. In region 1, as the temperature initially increases, the ignition delays decrease due to the strongly temperature dependant rate of  $\mathcal{R}2$ . As the temperature further increases into region 2, the equilibrium of  $\mathcal{R}2$  shifts towards the reactants, increasing the ignition delays. Further increases

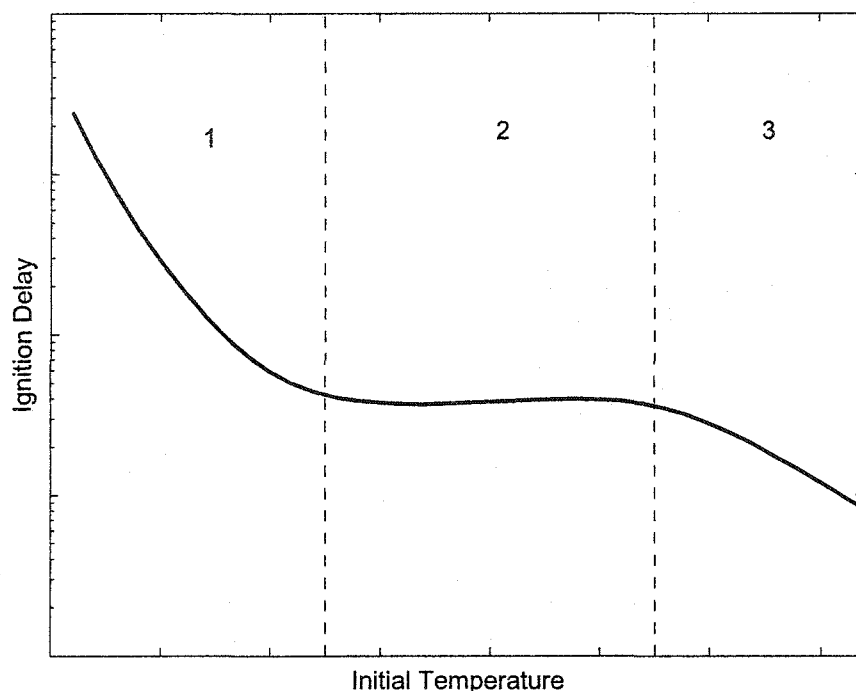


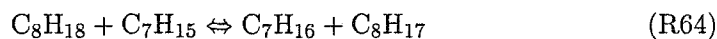
Figure 3.3: A characteristic dependence of the autoignition delay of hydrocarbon air mixtures, as a function of the initial mixture temperature. The middle region bounded by the vertical lines is the negative temperature coefficient region.

in temperature into region 3, cause the  $\dot{\text{H}}\text{O}_2$  from  $\mathcal{R}3$  to be increasingly converted to  $\text{H}_2\text{O}_2$  and subsequently decomposed through the chain branching reaction  $\mathcal{R}10$ , once again decreasing the ignition delays (region 3). The location of the NTC region is sensitive to the system pressure as the decomposition of  $\dot{\text{R}}\text{OOH}$  ( $\mathcal{R}7$ ) is a unimolecular, pressure sensitive reaction. For a given temperature, an increase in pressure will result in higher rates for  $\mathcal{R}7$  and hence move the NTC region to lower temperatures.

### 3.4.3 A Skeletal Kinetic Mechanism

In this investigation, a skeletal kinetic mechanism representing the ignition and combustion of an arbitrary PRF blend was formed by modifying the mechanism

presented by Zheng et al. (2002). Their mechanism is a skeletal mechanism for 20PRF based on the ignition chemistry of Li et al. (1996) and the high temperature mechanism presented by Griffiths et al. (1994). A schematic of the new mechanism is shown in Figure 3.4 and the complete mechanism, consisting of 58 species and 120 reactions, is given in Table 3.2 at the end of this chapter. The ignition chemistry was modified to include fuel specific ignition reactions for iso-octane and n-heptane, rather than just one fuel blend so arbitrary PRF blends can be used without having to first determine fuel specific rate constants. The interaction between the fuels is described using the reaction presented by Tanaka et al. (2003), as it was found to improve the prediction of ignition delays (the equation number refers to the reaction number in Table 3.2):



Although not required for this investigation, a more comprehensive  $\text{H}_2/\text{O}_2$  sub-mechanism from Marinov et al. (1995) replaced that used by Zheng et al. (2002) (20 reactions versus the previous 9), as future investigations will use hydrogen as a fuel. The more comprehensive high temperature sub-mechanism used by Zheng et al. (2002) was chosen in preference to global reactions (as done by Tanaka et al. (2003), for example), as it represents the high temperature process more accurately. Global reactions have the advantage of reduced computational requirements, but the conditions for which they are valid must be well known and they are not well suited to extrapolative purposes. The high temperature mechanism was modified to use a more comprehensive  $\text{CO}/\text{CO}_2$  sub mechanism from

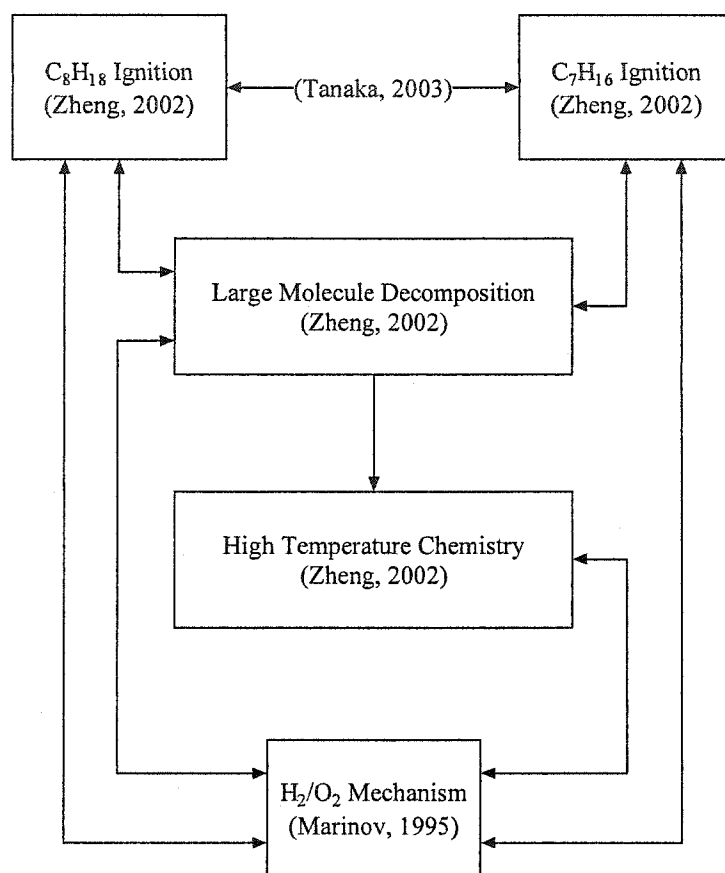
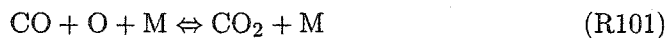


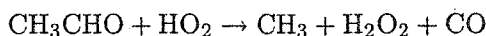
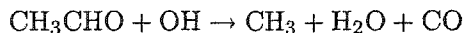
Figure 3.4: Schematic of the reduced chemical kinetics model of n-heptane and iso-octane mixtures

Smith et al. (2004) including the following reactions:



The following reactions which were originally included in the high temperature

mechanism by Zheng et al. (2002) were not included as  $\text{CH}_3\text{CHO}$  was not considered in the mechanism (Zheng 2002).



### 3.5 The Complete Thermokinetic Model

The thermokinetic model described in this chapter results in 59 ordinary differential equations requiring integration, 58 describing the specie concentrations and one describing the mixture temperature. As only the temporal variation of the concentrations and temperature are of interest, the solution is only in terms of time and the system of Ordinary Differential Equations (ODEs) can be classified as an Initial Value Problem (IVP). A schematic of the solution methodology used is shown in Figure 3.5. The input parameters are specified to the thermokinetic model and used to determine the initial conditions for each of the differential equations, using methods which are discussed in section 3.5.1.

Using these initial conditions, the differential equations are numerically integrated to obtain the temperature history for the given conditions. At each time step the pressure is determined using the ideal gas law, the reaction rates are calculated according to equations 3.34, 3.39, and 3.52, and the thermodynamic properties are determined from the database using equations 3.18, 3.19, and 3.44. The temperature, pressure, and complete mixture composition are calculated at each time step.

One goal of this research is to provide a model which can be used to evaluate different HCCI control strategies numerically. The thermokinetic model is implemented directly in Matlab (The Mathworks Inc. 2002) as it is a useful tool

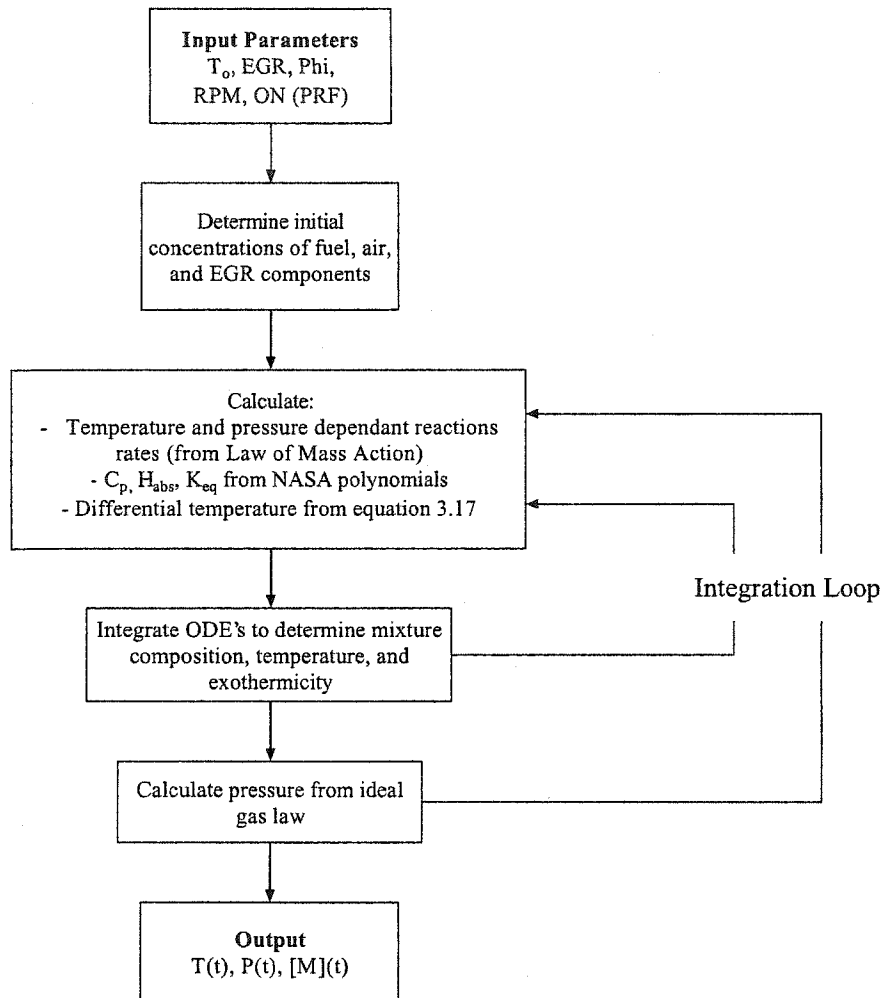


Figure 3.5: Schematic of the thermokinetic model

for control system development (Lee et al. 2003). Matlab has an abundance of built in functions and toolboxes which expedited the development time of the thermokinetic model. Commercial software packages capable of determining the thermokinetic history of an HCCI engine cycle, such as CHEMKIN (Reaction Design Inc. 2004), are available but are not easily integrated with Matlab for control system development.

### 3.5.1 Initial Conditions

To ensure the modularity of the thermokinetic model, it accepts standard engine operating parameters as inputs and uses them to determine initial conditions for the differential equations. The following parameters were used to determine the initial conditions:

- The temperature at the beginning of compression (or IVC) was estimated from the intake temperature.
- The air fuel equivalence ratio,  $\Phi$ , defined by

$$\Phi = \frac{A/F_{stoich}}{A/F_{actual}} \quad (3.55)$$

where  $A/F_{actual}$  is the operating air to fuel ratio (mass basis) and  $A/F_{stoich}$  is the stoichiometric air to fuel ratio.

- Fuel Octane Number, ON. This is equivalent to PRF number and is defined by the volume fraction of iso-octane.
- The initial pressure,  $P_o$ , taken to be the cylinder pressure at the beginning of compression or IVC.
- Recirculated exhaust gas fraction (EGR). This is defined as:

$$EGR = \frac{[CO_2]_{intake}}{[CO_2]_{exhaust}} \quad (3.56)$$

where  $[CO_2]_{intake}$  is the dry  $CO_2$  concentration in the intake manifold after the EGR has been introduced, and  $[CO_2]_{exhaust}$  is the dry  $CO_2$  concentration in the exhaust.

- The engine speed,  $N$

- Chamber volume,  $V$ , taken to be the volume at the beginning of compression or IVC.

Initial conditions must be specified for each of the differential equations describing the mixture temperature and specie concentrations. The temperature is measured or correlated to a measured value. The concentrations of each specie are more difficult to determine as they depend on the chamber volume, mixture pressure and temperature,  $\Phi$ , EGR fraction, and octane number. As the reaction rate parameters are specified for concentrations in units of  $[\text{mol}/\text{cm}^3]$ , the concentrations are defined as

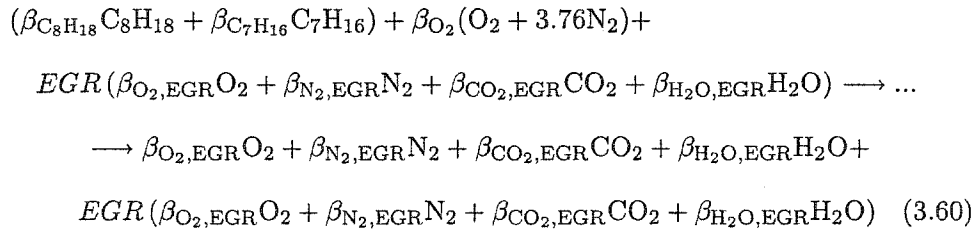
$$[M_i] = \frac{N_i}{V} \quad (3.57)$$

where  $[M_i]$  is the concentration of the  $i^{\text{th}}$  specie,  $N_i$  is the number of moles of the  $i^{\text{th}}$  specie, and  $V$  is the combustion chamber volume in  $\text{cm}^3$ . The total number of moles defined by the ideal gas law (equation 3.58) can be used to determine the number of moles of each specie, given that the mole fractions of each specie are known.

$$PV = N_{mix}R_uT \quad (3.58)$$

$$N_i = Y_i N_{mix} \quad (3.59)$$

where  $Y_i$  is the mole fraction of the  $i^{\text{th}}$  specie and is determined from the general combustion equation:



where  $EGR$  is the EGR rate and the stoichiometric coefficients,  $\beta_i$ , are defined as follows:

$$\beta_{C_8H_{18}} = \frac{ON}{100} \quad (3.61)$$

$$\beta_{C_7H_{16}} = 1 - \frac{ON}{100} \quad (3.62)$$

$$\beta_{O_2} = \frac{11 + 1.5 \frac{ON}{100}}{\Phi} \quad (3.63)$$

$$\beta_{O_2,EGR} = \beta_{O_2} (1 - \Phi) \quad (3.64)$$

$$\beta_{N_2,EGR} = 3.76\beta_{O_2} \quad (3.65)$$

$$\beta_{CO_2,EGR} = \frac{ON}{100} + 7 \quad (3.66)$$

$$\beta_{H_2O,EGR} = \frac{ON}{100} + 8 \quad (3.67)$$

It should be noted in the combustion equation that the exhaust fraction appears on both the reactant and product sides to maintain conservation of matter. The mole fraction of the  $i^{th}$  specie,  $Y_i$ , is determined from

$$Y_i = \frac{\beta_i}{\sum \beta_i} \quad (3.68)$$

where

$$\sum \beta_i = \beta_{C_8H_{18}} + \beta_{C_7H_{16}} + 4.76\beta_{O_2} + \dots$$

$$EGR(\beta_{O_2,EGR} + \beta_{N_2,EGR} + \beta_{CO_2,EGR} + \beta_{H_2O,EGR}) \quad (3.69)$$

### 3.5.2 Solution Methodology

Using the initial conditions determined in the preceding section, the system of differential equations was integrated using solvers included in Matlab. The two solvers, `ode15s` and `ode23tb` are summarized in Table 3.1. The `ode23tb` algorithm

was used for the development of the model as it is more robust to errors in the differential equations, while `ode15s` was used with the finished model as it is more computationally efficient when finer tolerances are used. The difference between the two solvers is that `ode23tb` is based on the implicit Runge Kutta method (i.e. an iterative single step solver), while `ode15s` is a multi-step solver based on the numerical differentiation formulas. The heuristically determined tolerances, given in Table 3.1, provide a compromise between calculation speed and solution convergence.

Table 3.1: Summary of the Matlab differential equation integrators used.

Solver	Type	Rel. Tol.	Abs. Tol.	Step Size
<code>ode15s</code>	Backward Numerical Differentiation	1E-7	1E-11	Variable
<code>ode23tb</code>	Implicit Runge Kutta	1E-5	1E-9	Variable

### 3.6 Summary

A thermokinetic model of the HCCI engine is developed in this chapter. A new chemical kinetic mechanism describing the ignition and combustion of iso-octane and n-heptane blends is developed and coupled to a single zone thermodynamic model. A single zone approximation neglects any spatial variations in the thermodynamic state of the mixture. In addition to the single zone assumption, it is assumed that all species are in the gaseous phase and can be treated as ideal gases, and that the mass of the cylinder contents is constant. Using these assumptions the change in mixture temperature with respect to time is described using equation 3.17:

$$\frac{dT}{dt} = \frac{-P \frac{dV}{dt} + \frac{dQ_{wall}}{dt} - \sum_i \frac{dN_i}{dt} \bar{h}_i + RT \sum_i \frac{dN_i}{dt}}{\sum_i N_i \bar{c}_{p,i} - N_{mix} R} \quad (3.17)$$

Equation 3.17 requires the knowledge of both the composition and thermodynamic properties of the mixture. To describe the composition of the mixture, a chemical kinetic mechanism, capable of describing the ignition and combustion of iso-octane and n-heptane, was developed based on existing sub-mechanisms. This mechanism includes the reactions responsible for ignition phenomena such as induction periods, cool flames, hot ignition, and negative temperature coefficient regions, as well as a high temperature sub-mechanism. The change in mixture composition as a function of time is described using 58 differential equations in the form of equation 3.33. The thermodynamic properties of the mixture are determined using existing databases suitable for computer programs, or estimated based on the Benson (1976) additivity rules. The complete chemical kinetic mechanism is given below in Table 3.2.

Table 3.2: Reactions of the kinetic mechanism shown in Figure 3.4. Equilibrium is only considered in reactions where " $\leftrightarrow$ " is used as the separator between the reactants and products. References: [1](Zheng et al. 2002), [2] (Li et al. 1996), [3] (Tanaka et al. 2003), [4] (Marinov et al. 1995), [5] (Smith et al. 2004). Units: kcal, mol, cm<sup>3</sup>, s

#	Reaction	log(A)	n	E <sub>a</sub>	Source
1	C <sub>8</sub> H <sub>18</sub> + O <sub>2</sub> → C <sub>8</sub> H <sub>17</sub> + HO <sub>2</sub>	16	0	46	[1]
2	C <sub>8</sub> H <sub>17</sub> + HO <sub>2</sub> → C <sub>8</sub> H <sub>18</sub> + O <sub>2</sub>	12	0	0	[1]
3	C <sub>8</sub> H <sub>17</sub> + O <sub>2</sub> → C <sub>8</sub> H <sub>17</sub> OO	12	0	0	[1]
4	C <sub>8</sub> H <sub>17</sub> OO → C <sub>8</sub> H <sub>17</sub> + O <sub>2</sub>	13.4	0	27.4	[1]
5	C <sub>8</sub> H <sub>17</sub> OO → C <sub>8</sub> H <sub>16</sub> OOH	11	0	22.4	[2]
6	C <sub>8</sub> H <sub>16</sub> OOH → C <sub>8</sub> H <sub>17</sub> OO	11	0	11	[2]
7	C <sub>8</sub> H <sub>16</sub> OOH + O <sub>2</sub> → OOC <sub>8</sub> H <sub>16</sub> OOH	11.5	0	0	[1]
8	OOC <sub>8</sub> H <sub>16</sub> OOH → C <sub>8</sub> H <sub>16</sub> OOH + O <sub>2</sub>	13.4	0	27.4	[1]
9	OOC <sub>8</sub> H <sub>16</sub> OOH → OC <sub>8</sub> H <sub>15</sub> OOH + OH	11.3	0	17	[1]
10	OH + C <sub>8</sub> H <sub>18</sub> → H <sub>2</sub> O + C <sub>8</sub> H <sub>17</sub>	13.3	0	3	[1]

*continued on next page...*

CHAPTER 3: BACKGROUND THEORY

References: [1](Zheng et al. 2002), [2] (Li et al. 1996), [3] (Tanaka et al. 2003), [4] (Marinov et al. 1995), [5] (Smith et al. 2004). Units: kcal, mol, cm<sup>3</sup>, s

11	$\text{OC}_8\text{H}_{15}\text{OOH} \rightarrow \text{OC}_8\text{H}_{15}\text{O} + \text{OH}$	15.6	0	40	[1]
12	$\text{OC}_8\text{H}_{15}\text{O} \rightarrow \text{HCHO} + \text{C}_3\text{H}_7\text{CHO} + \text{C}_3\text{H}_5$	14	0	15	[1]
13	$\text{C}_8\text{H}_{16}\text{OOH} \rightarrow \text{C}_3\text{H}_7\text{CHO} + \text{OH} + \text{C}_4\text{H}_8$	14.4	0	31	[1]
14	$\text{C}_8\text{H}_{17}\text{OO} + \text{C}_3\text{H}_7\text{CHO} \rightarrow \text{C}_8\text{H}_{17}\text{OOH} + \text{C}_3\text{H}_7\text{CO}$	11.4	0	8.6	[1]
15	$\text{HO}_2 + \text{C}_8\text{H}_{18} \rightarrow \text{C}_8\text{H}_{17} + \text{H}_2\text{O}_2$	11.7	0	16	[1]
16	$\text{C}_8\text{H}_{17} + \text{H}_2\text{O}_2 \rightarrow \text{HO}_2 + \text{C}_8\text{H}_{18}$	10.8	0	8	[1]
17	$\text{C}_8\text{H}_{17}\text{OO} + \text{C}_8\text{H}_{18} \rightarrow \text{C}_8\text{H}_{17}\text{OOH} + \text{C}_8\text{H}_{17}$	11.2	0	16	[1]
18	$\text{C}_8\text{H}_{17}\text{OOH} + \text{C}_8\text{H}_{17} \rightarrow \text{C}_8\text{H}_{17}\text{OO} + \text{C}_8\text{H}_{18}$	10.1	0	8	[1]
19	$\text{C}_8\text{H}_{18} + \text{C}_3\text{H}_7\text{O}_2 \rightarrow \text{C}_3\text{H}_7\text{OOH} + \text{C}_8\text{H}_{17}$	11.3	0	16	[1]
20	$\text{C}_3\text{H}_7\text{OOH} + \text{C}_8\text{H}_{17} \rightarrow \text{C}_8\text{H}_{18} + \text{C}_3\text{H}_7\text{O}_2$	10.1	0	8	[1]
21	$\text{C}_8\text{H}_{16} + \text{OH} \rightarrow \text{OH} + 2\text{C}_3\text{H}_7\text{CHO}$	12.8	0	-1.04	[1]
22	$\text{C}_8\text{H}_{17}\text{OOH} \rightarrow \text{C}_8\text{H}_{17}\text{O} + \text{OH}$	15.6	0	43	[1]
23	$\text{C}_8\text{H}_{17}\text{O} \rightarrow \text{C}_4\text{H}_9 + \text{C}_3\text{H}_7\text{CHO}$	13.3	0	15	[1]
24	$\text{C}_8\text{H}_{17}\text{OO} \rightarrow \text{C}_8\text{H}_{16} + \text{HO}_2$	9.85	0	23	[1]
25	$\text{C}_8\text{H}_{17}\text{OO} \rightarrow \text{C}_8\text{H}_{16}\text{O} + \text{OH}$	8.78	0	18	[2]
26	$\text{C}_8\text{H}_{16}\text{O} \rightarrow \text{CH}_3\text{O} + \text{C}_7\text{H}_{13}$	14.7	0	24.8	[1]
27	$\text{C}_7\text{H}_{16} + \text{O}_2 \rightarrow \text{C}_7\text{H}_{15} + \text{HO}_2$	16	0	46	[1]
28	$\text{C}_7\text{H}_{15} + \text{HO}_2 \rightarrow \text{C}_7\text{H}_{16} + \text{O}_2$	12	0	0	[1]
29	$\text{C}_7\text{H}_{15} + \text{O}_2 \rightarrow \text{C}_7\text{H}_{15}\text{OO}$	12	0	0	[1]
30	$\text{C}_7\text{H}_{15}\text{OO} \rightarrow \text{C}_7\text{H}_{15} + \text{O}_2$	13.4	0	27.4	[1]
31	$\text{C}_7\text{H}_{15}\text{OO} \rightarrow \text{C}_7\text{H}_{14}\text{OOH}$	11.9	0	19	[2]
32	$\text{C}_7\text{H}_{14}\text{OOH} \rightarrow \text{C}_7\text{H}_{15}\text{OO}$	11	0	11	[2]
33	$\text{C}_7\text{H}_{14}\text{OOH} + \text{O}_2 \rightarrow \text{OOC}_7\text{H}_{14}\text{OOH}$	11.5	0	0	[1]
34	$\text{OOC}_7\text{H}_{14}\text{OOH} \rightarrow \text{C}_7\text{H}_{14}\text{OOH} + \text{O}_2$	13.4	0	27.4	[1]
35	$\text{OOC}_7\text{H}_{14}\text{OOH} \rightarrow \text{OC}_7\text{H}_{13}\text{OOH} + \text{OH}$	11.3	0	17	[1]
36	$\text{OH} + \text{C}_7\text{H}_{16} \rightarrow \text{H}_2\text{O} + \text{C}_7\text{H}_{15}$	13	0	3	[1]
37	$\text{OC}_7\text{H}_{13}\text{OOH} \rightarrow \text{OC}_7\text{H}_{13}\text{O} + \text{OH}$	15.6	0	40	[1]
38	$\text{OC}_7\text{H}_{13}\text{O} \rightarrow \text{HCHO} + \text{C}_3\text{H}_7\text{CHO} + \text{C}_2\text{H}_3$	14	0	15	[1]
39	$\text{C}_7\text{H}_{14}\text{OOH} \rightarrow \text{C}_3\text{H}_7\text{CHO} + \text{OH} + \text{C}_3\text{H}_6$	14.4	0	31	[1]
40	$\text{C}_7\text{H}_{15}\text{OO} + \text{C}_3\text{H}_7\text{CHO} \rightarrow \text{C}_7\text{H}_{15}\text{OOH} + \text{C}_3\text{H}_7\text{CO}$	11.4	0	8.6	[1]
41	$\text{HO}_2 + \text{C}_7\text{H}_{16} \rightarrow \text{C}_7\text{H}_{15} + \text{H}_2\text{O}_2$	11.7	0	16	[1]
42	$\text{C}_7\text{H}_{15} + \text{H}_2\text{O}_2 \rightarrow \text{HO}_2 + \text{C}_7\text{H}_{16}$	10.8	0	8	[1]
43	$\text{C}_7\text{H}_{15}\text{OO} + \text{C}_7\text{H}_{16} \rightarrow \text{C}_7\text{H}_{15}\text{OOH} + \text{C}_7\text{H}_{15}$	11.2	0	16	[1]
44	$\text{C}_7\text{H}_{15}\text{OOH} + \text{C}_7\text{H}_{15} \rightarrow \text{C}_7\text{H}_{15}\text{OO} + \text{C}_7\text{H}_{16}$	10.1	0	8	[1]
45	$\text{C}_7\text{H}_{16} + \text{C}_3\text{H}_7\text{O}_2 \rightarrow \text{C}_3\text{H}_7\text{OOH} + \text{C}_7\text{H}_{15}$	11.3	0	16	[1]
46	$\text{C}_3\text{H}_7\text{OOH} + \text{C}_7\text{H}_{15} \rightarrow \text{C}_7\text{H}_{16} + \text{C}_3\text{H}_7\text{O}_2$	10.1	0	8	[1]
47	$\text{C}_7\text{H}_{15}\text{OOH} \rightarrow \text{C}_7\text{H}_{15}\text{O} + \text{OH}$	15.6	0	43	[1]
48	$\text{C}_7\text{H}_{15}\text{O} \rightarrow \text{C}_3\text{H}_7 + \text{C}_3\text{H}_7\text{CHO}$	13.3	0	15	[1]

continued on next page...

CHAPTER 3: BACKGROUND THEORY

References: [1](Zheng et al. 2002), [2] (Li et al. 1996), [3] (Tanaka et al. 2003), [4] (Marinov et al. 1995), [5] (Smith et al. 2004). Units: kcal, mol, cm<sup>3</sup>, s

49	$C_7H_{15}OO \rightarrow C_7H_{14} + HO_2$	9.85	0	23	[1]
50	$C_7H_{15}OO \rightarrow C_7H_{14}O + OH$	9.48	0	18	[2]
51	$C_7H_{14} + OH \rightarrow OH + C_3H_7CHO + C_2H_5CHO$	12.7	0	-1.04	[1]
52	$C_7H_{14}O \rightarrow CH_3O + C_6H_{11}$	14.7	0	24.8	[1]
53	$HO_2 + C_3H_7CHO \rightarrow H_2O_2 + C_3H_7CO$	11.7	0	8.64	[1]
54	$C_3H_6 + HO_2 \rightarrow C_3H_6O + OH$	10.9	0	10	[1]
55	$C_4H_8 + HO_2 \rightarrow C_4H_8O + OH$	10.9	0	10	[1]
56	$C_3H_7CHO + OH \rightarrow C_3H_7CO + H_2O$	13.3	0	0	[1]
57	$C_3H_7CO + M \rightarrow M + CO + C_3H_7$	16.8	0	15	[1]
58	$C_3H_7 + O_2 \rightarrow C_3H_7O_2$	12	0	0	[1]
59	$C_3H_7O_2 \rightarrow C_3H_7 + O_2$	13.4	0	27.4	[1]
60	$C_3H_7O_2 \rightarrow C_3H_6 + HO_2$	11.8	0	28.9	[1]
61	$C_3H_7CHO + C_3H_7O_2 \rightarrow C_3H_7OOH + C_3H_7CO$	11.5	0	8.6	[1]
62	$C_3H_7OOH \rightarrow C_3H_7O + OH$	15.6	0	43	[1]
63	$C_3H_7O + O_2 \rightarrow C_3H_6O + HO_2$	10.6	0	2.14	[1]
64	$C_8H_{18} + C_7H_{15} \leftrightarrow C_7H_{16} + C_8H_{17}$	12.7	0	0	[3]
65	$C_3H_6O \rightarrow C_2H_5 + HCO$	13.3	0	57.2	[1]
66	$C_4H_8O \rightarrow C_3H_7 + HCO$	13.3	0	57.2	[1]
67	$C_3H_7CHO + M \rightarrow M + C_3H_7 + HCO$	15.9	0	81.8	[1]
68	$C_4H_9 \rightarrow CH_3 + C_3H_6$	13.4	0	31.9	[1]
69	$C_6H_{11} \rightarrow C_2H_4 + C_4H_7$	11	0	37.1	[1]
70	$C_7H_{13} \rightarrow C_3H_4 + C_4H_9$	11	0	37.1	[1]
71	$C_4H_7 \rightarrow C_2H_4 + C_2H_3$	11	0	37.1	[1]
72	$C_2H_5CHO + M \rightarrow M + C_2H_5 + HCO$	15.9	0	81.8	[1]
73	$OH + H_2 \leftrightarrow H + H_2O$	8.33	1.52	3.45	[4]
74	$O + OH \leftrightarrow O_2 + H$	14.3	-0.4	0	[4]
75	$O + H_2 \leftrightarrow OH + H$	4.7	2.67	6.29	[4]
76 <sup>4</sup>	$H + O_2 \leftrightarrow HO_2$	13.7	0	0	[4]
	low pressure...	19	-1.26	0	
77	$H + O_2 + N_2 \leftrightarrow N_2 + HO_2$	13.7	0	0	[4]
	low pressure...	20.3	-1.59	0	
78	$H + O_2 + H_2 \leftrightarrow H_2 + HO_2$	13.7	0	0	[4]
	low pressure...	19.2	-1.13	0	
79	$H + O_2 + H_2O \leftrightarrow H_2O + HO_2$	13.7	0	0	[4]
	low pressure...	23.3	-2.44	0	
80	$OH + HO_2 \leftrightarrow H_2O + O_2$	13.5	0	-0.5	[4]

continued on next page...

<sup>4</sup>Third body efficiencies: H<sub>2</sub>O, 0; H<sub>2</sub>, 0; N<sub>2</sub>, 0;

CHAPTER 3: BACKGROUND THEORY

References: [1](Zheng et al. 2002), [2] (Li et al. 1996), [3] (Tanaka et al. 2003), [4] (Marinov et al. 1995), [5] (Smith et al. 2004). Units: kcal, mol, cm<sup>3</sup>, s

81	$H + HO_2 \leftrightarrow 2OH$	14.2	0	1	[4]
82	$H + HO_2 \leftrightarrow H_2 + O_2$	11.9	0.65	1.24	[4]
83	$H + HO_2 \leftrightarrow O + H_2O$	13.5	0	1.72	[4]
84	$O + HO_2 \leftrightarrow O_2 + OH$	13.5	0	0	[4]
85	$2OH \leftrightarrow O + H_2O$	4.55	2.4	-2.11	[4]
86 <sup>5</sup>	$2H + M \leftrightarrow M + H_2$	18	-1	0	[4]
87	$2H + H_2 \leftrightarrow 2H_2$	17	-0.6	0	[4]
88	$2H + H_2O \leftrightarrow H_2O + H_2$	19.8	-1.25	0	[4]
89 <sup>6</sup>	$H + OH + M \leftrightarrow M + H_2O$	22.3	-1.25	0	[4]
90	$H + O + M \leftrightarrow M + OH$	18.7	-1	0	[4]
91	$2O + M \leftrightarrow M + O_2$	13.3	0	-1.79	[4]
92	$2HO_2 \leftrightarrow H_2O_2 + O_2$	14.6	0	12	[4]
93	$2HO_2 \leftrightarrow H_2O_2 + O_2$	11.1	0	-1.63	[4]
94	$2OH \leftrightarrow H_2O_2$	14.1	-0.37	0	[4]
	low pressure...	30.5	-4.63	2.05	
95	$H_2O_2 + H \leftrightarrow OH + H_2O$	13.5	0	4.22	[4]
96	$H_2O_2 + H \leftrightarrow HO_2 + H_2$	6.3	2	2.44	[4]
97	$H_2O_2 + O \leftrightarrow OH + HO_2$	6.98	2	3.97	[4]
98	$H_2O_2 + OH \leftrightarrow H_2O + HO_2$	0.38	4.04	-2.16	[4]
99	$CO + OH \leftrightarrow CO_2 + H$	7.68	1.23	0.07	[5]
100	$CO + HO_2 \leftrightarrow CO_2 + OH$	14.2	0	23.6	[5]
101 <sup>7</sup>	$CO + O \leftrightarrow CO_2$	10.3	0	2.39	[5]
	low pressure...	14.8	0	3	
102	$CO + O_2 \leftrightarrow CO_2 + O$	12.4	0	47.8	[5]
103	$HCO + O_2 \rightarrow CO + HO_2$	13.1	0	0.4	[1]
104	$HCO + M \rightarrow M + CO + H$	17.3	-1	17	[1]
105	$HCHO + O \rightarrow HCO + OH$	13.6	0	3.54	[1]
106	$HCHO + OH \rightarrow HCO + H_2O$	9.54	1.2	-0.45	[1]
107	$HCHO + HO_2 \rightarrow HCO + H_2O_2$	6.75	2	12	[1]
108	$HCHO + O_2 \rightarrow HCO + HO_2$	14	0	40	[1]
109	$CH_3 + O_2 \rightarrow HCHO + OH$	12.4	0	20.3	[1]
110	$C_2H_3 + O_2 \rightarrow HCHO + HCO$	12.6	0	-0.25	[1]
111	$C_2H_4 + OH \rightarrow C_2H_3 + H_2O$	6.56	2	2.5	[1]
112	$C_2H_4 + O \rightarrow CH_3 + HCO$	7.1	1.8	0.22	[1]

continued on next page...

<sup>5</sup>Third body efficiencies: H<sub>2</sub>O, 0; H<sub>2</sub>, 0;

<sup>6</sup>Third body efficiencies: H<sub>2</sub>O, 6.3;

<sup>7</sup>Third body efficiencies: H<sub>2</sub>, 2; O<sub>2</sub>, 6; H<sub>2</sub>O, 6; CO, 1.5; CO<sub>2</sub>, 3.5;

## CHAPTER 3: BACKGROUND THEORY

---

References: [1](Zheng et al. 2002), [2] (Li et al. 1996), [3] (Tanaka et al. 2003), [4] (Marinov et al. 1995), [5] (Smith et al. 2004). Units: kcal, mol,  $\text{cm}^3$ , s

113	$\text{C}_2\text{H}_5 + \text{O}_2 \rightarrow \text{C}_2\text{H}_4 + \text{HO}_2$	11.9	0	3.88	[1]
114	$\text{C}_3\text{H}_5 + \text{O}_2 \rightarrow \text{C}_3\text{H}_4 + \text{HO}_2$	11.8	0	10	[1]
115	$\text{C}_3\text{H}_4 + \text{OH} \rightarrow \text{HCHO} + \text{C}_2\text{H}_3$	12	0	0	[1]
116	$\text{C}_3\text{H}_6 + \text{OH} \rightarrow \text{C}_3\text{H}_5 + \text{H}_2\text{O}$	6.49	2	-0.3	[1]
117	$\text{C}_3\text{H}_6 + \text{O}_2 \rightarrow \text{C}_3\text{H}_5 + \text{HO}_2$	12.3	0	39	[1]
118	$\text{C}_3\text{H}_6 + \text{HO}_2 \rightarrow \text{C}_3\text{H}_5 + \text{H}_2\text{O}_2$	11.5	0	14.9	[1]
119	$\text{C}_3\text{H}_7 \rightarrow \text{C}_2\text{H}_4 + \text{CH}_3$	10.3	0	29.5	[1]
120	$\text{CH}_3\text{O} + \text{O}_2 \rightarrow \text{HCHO} + \text{HO}_2$	10.9	0	2.7	[1]

## Chapter 4

# Validation of the Thermokinetic Model

### 4.1 Introduction

The suitability of the thermokinetic model for predicting ignition processes was validated through a comparison with theoretical and experimental results. Through such validations, various components of the thermokinetic model and the model as a whole were evaluated so that it could be used for predictive calculations. The validation of the thermokinetic model was carried out in several steps, each validating an increasingly complex aspect of the model. The ability of the thermokinetic model to describe the equilibrium conditions after combustion in an adiabatic, constant volume combustion chamber was validated through comparison with theoretically determined results. This primarily validated the thermodynamic model (conservation of energy) and the routines used to determine unknown thermodynamic properties, but did little to validate the temporal performance of the model. One of the primary reasons for using a chemical kinetic

mechanism when modeling the HCCI engine is the ability to predict the ignition timing. Thus, the ability of model to predict the ignition delays was validated using measurements from a Rapid Compression Machine (RCM) and a shock tube, both of which were approximated as constant volume, adiabatic systems by considering only the system after compression. While the equilibrium and ignition delay investigations validated the thermodynamic model and kinetic mechanism separately, they did nothing to validate the performance of the complete model for variable volume systems in which heat transfer is relevant. The final validation was a comparison with experimental HCCI engine pressure traces.

Each of these validations are discussed in this chapter, with a focus on the applicability of the validation to HCCI engines, the assumptions made in each case, and a discussion of the results.

## 4.2 Equilibrium Validation

To validate the ability of the model to describe the combustion event from a thermodynamic stand point, the equilibrium temperature and composition of an adiabatic, constant volume combustion event were compared with those obtained from a minimization of Gibbs energy analysis (see section 3.4.1). The computer program STANJAN (Reynolds 1987) was used to carry out the minimization of Gibbs energy analysis. STANJAN, given the initial thermodynamic state of a mixture (i.e. the mixture composition, temperature and pressure) and the species present in the equilibrium state, calculates the thermodynamic state at equilibrium. This validation is intended as a means of determining whether or not the equations presented in chapter 3 are properly implemented. The equilibrium state predicted by minimization of Gibbs energy analysis will be the same as that predicted by a thermokinetic model, given that the following conditions are met

(Côme 2001):

1. All pertinent reactions describing the interactions of the species in the equilibrium mixture must be included in the mechanism. The equilibrium validation will only validate the parts of the mechanism directly affecting the composition of the products, and not the intermediate chemistry.
2. Both the forward and the reverse reaction rates must be accurately specified by the mechanism. The reverse rates may be determined from the equilibrium constant through equation 3.39.
3. The chemical kinetic simulation must be solved for a sufficiently long time such that steady state (i.e. equilibrium) conditions are attained.

Agreement between the equilibrium thermodynamic state calculated by the thermokinetic model and STANJAN, subject to the above three conditions, validates the ability of the model to predict the equilibrium conditions.

### 4.2.1 Equilibrium Calculations

Equilibrium composition, temperature and pressure were calculated using the thermokinetic model for a constant volume, adiabatic combustion event using various 20PRF mixtures. In particular,  $\Phi$  was varied from 0.5 to 1.0, with an initial temperature and pressure of 800K and 30bar, respectively. These values were chosen as they are representative of typical TDC conditions in an HCCI engine. Heat transfer was neglected for these calculations so that the chemical kinetic mechanism and thermodynamic model could be evaluated independent of the heat transfer correlation. To ensure that the results from the thermokinetic model were representative of equilibrium, the system was solved until steady state was reached (1 second).

The STANJAN calculations were carried out using the mixture compositions specified in Table 4.1. After specifying these initial conditions, the equilibrium conditions were determined for a system with the same internal energy and volume as the initial mixture. The equilibrium mixture was assumed to be composed of  $\text{CO}_2$ ,  $\text{CO}$ ,  $\text{O}$ ,  $\text{O}_2$ ,  $\text{N}_2$ ,  $\text{H}_2\text{O}$ ,  $\text{H}$ ,  $\text{OH}$ , and  $\text{H}_2$ . This is analogous to solving for the adiabatic flame temperature in a constant pressure system, where the enthalpy is constant.

Table 4.1: Initial mixture compositions used for STANJAN equilibrium calculations.  $T_o = 800\text{K}$ ,  $P_o = 30\text{bar}$ .

$\Phi$	Number of moles			
	$\text{C}_8\text{H}_{18}$	$\text{C}_7\text{H}_{16}$	$\text{O}_2$	$\text{N}_2$
1.0	0.2	0.8	11.3	42.5
0.7	0.2	0.8	16.1	60.7
0.5	0.2	0.8	22.6	85.0

#### 4.2.2 Results

A comparison of the adiabatic combustion temperatures as calculated by STANJAN and the thermokinetic model is shown in Figure 4.1. As time progresses, the combustion temperatures calculated by the thermokinetic model approach those calculated by STANJAN. As the mixture composition approaches stoichiometric, the thermokinetic model under-predicts the combustion temperature by 8.5%, due to incomplete conversion of  $\text{CO}$  to  $\text{CO}_2$ . The conversion of  $\text{CO}$  to  $\text{CO}_2$  accounts for the majority of the exothermicity in the combustion of hydrocarbons (Dryer & Glassman 1977) and incomplete combustion leads to lower combustion temperatures.

The thermokinetic model was capable of predicting the temperature of the equilibrium mixture to within 8.5%. Recalling the three conditions outlined ear-

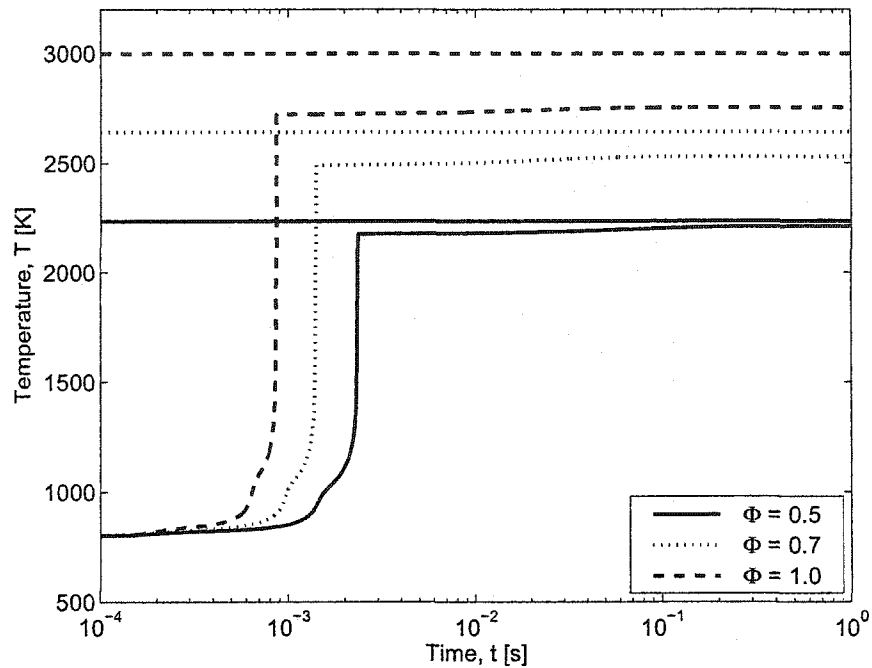


Figure 4.1: Comparison of the adiabatic combustion temperatures determined using the thermokinetic model, and STANJAN. The horizontal lines indicate the combustion temperatures calculated using STANJAN, while the curves represent the results from the thermokinetic model. Initial mixture composition given in Table 4.1,  $T_o = 800\text{K}$ ,  $P_o = 30\text{bar}$ , 20PRF.

lier, this indicates that the chemical kinetic mechanism contains sufficient detail to describe the net combustion process. An investigation of equilibrium conditions provides no insight of the thermokinetic model's ability to predict temporal variations of the thermodynamic state.

### 4.3 Ignition Delay Validation

The timing of the combustion event relative to TDC in an internal combustion engine strongly influences the thermodynamic efficiency and exhaust gas composition, regardless of the cycle being considered. If the combustion event is advanced

(i.e. earlier in the cycle) then the moving piston will compress the already hot combustion products, leading to higher temperatures and  $\text{NO}_x$  emissions. In addition, the increased compression work will reduce the thermodynamic efficiency of the cycle. If the combustion event is retarded (i.e. later in the cycle) the downward motion of the piston will decrease the temperature and pressure of the mixture, inhibiting combustion and increasing unburned hydrocarbon emissions. Furthermore, the reduced temperature and pressure may lead to incomplete combustion and unused chemical potential energy in the fuel. Due to the sensitivity of the engine performance on the ignition timing, it is crucial that the thermokinetic model is capable of predicting ignition delays. The ability of the thermokinetic model to predict the qualitative effects of mixture parameters on ignition delays in practical combustion systems was therefore thoroughly validated.

#### 4.3.1 Rapid Compression Machine Validation

Ignition delay measurements from an RCM were compared to those calculated using the thermokinetic model. An RCM is a device in which a piston rapidly compresses a fuel air mixture and then holds the piston stationary at the end of its stroke (TDC position). Depending on the thermodynamic state of the mixture after compression a variety of combustion phenomena, such as single or two stage ignition, are possible. The temperature and pressure at TDC are varied by altering the compression ratio, the initial temperature, pressure, or the specific heat ratio of the inert gas fraction (usually a mixture of nitrogen and argon). By neglecting the compression stroke and beginning the thermokinetic simulations at TDC, it is assumed that only negligible kinetic activity is taking place during the compression stroke. In this investigation, the compression stroke was not considered in order to simplify the analysis. In a similar analysis Minetti

et al. (1995) obtained acceptable agreement between calculated and experimental ignition delays while neglecting the compression process.

### Thermokinetic Modeling of the Rapid Compression Machine

The experimental RCM ignition delays used for this validation are taken from Park & Keck (1990), for 5 different stoichiometric PRF mixtures with various initial temperatures and pressures. The assumption of a sufficiently fast compression process with negligible kinetic activity results in a constant volume system, with the initial conditions given in Table 4.2. Table 4.2 list the the end of compression temperatures and pressures, which were determined based on the mixture conditions at the beginning of compression and by assuming isentropic compression.

The experimental ignition delay is defined as being the time from the inflection point in the pressure trace just prior to TDC, to the point at which the core temperature exceeds  $1100\text{K}^1$  (Park & Keck 1990). As the compression process was not included in the simulations, the calculated ignition delay was defined as being the time from the beginning of the simulation, to the point at which the temperature exceeds  $1100\text{K}$ .

Due to the design of the RCM, it was possible to neglect the effects of heat transfer for the simulations. The RCM piston used by Park & Keck (1990) has a wedge shaped crevice volume on it's circumference, which captures the roll-up vortex typically formed during the compression process. A comparison of a regular piston and one with crevice volumes to capture the vortices is shown in Figure 4.2. It is this vortex which is responsible for the bulk of the fluid motion and hence convective heat transfer prior to combustion in an engine. Without

---

<sup>1</sup>Section 3.4.2 - This temperature corresponds to the high temperature, or second stage ignition.

Table 4.2: Compression conditions used for Rapid Compression Machine validation. For each of the conditions the ignition delay is determined for stoichiometric mixtures of 0, 50, 75, 90, and 100 PRF blends. Taken from Park & Keck (1990).

Temperature [K]	Pressure [kPa]	$k$ [-]
760	5770	1.365
752	2940	1.372
732	5580	1.353
720	2830	1.358
686	5170	1.325
672	2570	1.323

this vortex the fluid motion and heat transfer to the cylinder walls are reduced. Furthermore, Griffiths et al. (1993) found, through a CFD investigation, that the core temperature is relatively unchanged prior to ignition in a RCM without the aforementioned crevice volumes. With these crevice volumes the heat transfer is even further reduced, making it a valid assumption to neglect heat transfer. By validating the thermokinetic model with results from a system with negligible heat transfer, only the ability of the kinetic mechanism to predict ignition delays is evaluated, rather than the validity of the heat transfer correlation.

#### Comparison of the RCM and Calculated Ignition Delays

Shown in Figure 4.3 is a comparison of the experimental (markers) and calculated (lines) RCM ignition delays. This indicates that the thermokinetic model is capable of predicting the ignition delays (shown on the ordinate) for various PRF's (denoted by different marker styles), temperatures (shown in the Arrhenius form along the abscissa), and pressures (denoted by the hollow and solid markers). In all cases the thermokinetic model was able to predict the qualitative dependence of the ignition delay on these parameters. The quantitative ignition delay agreement is better for the higher octane number mixtures than for the lower octane number

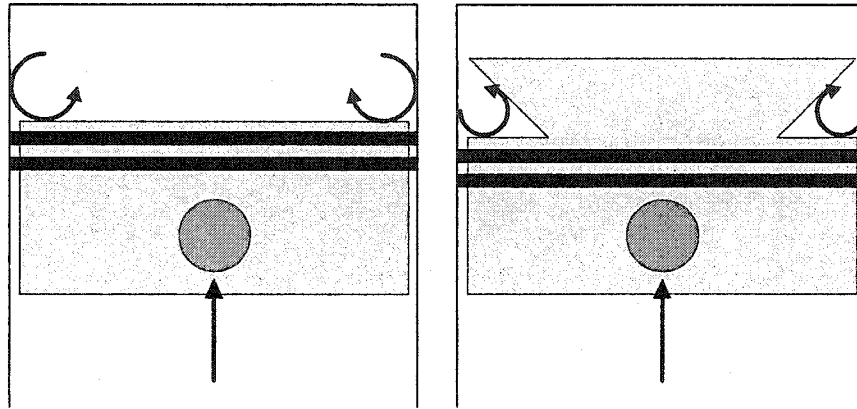


Figure 4.2: Comparison of a regular piston (left) with a piston containing crevice volumes to capture the roll-up vortices (right). Such a piston is used by Park & Keck (1990) to reduce the fluid motion and convective heat transfer in a rapid compression machine.

mixtures. For pure n-heptane, which has an octane number of zero, the qualitative behavior is captured but the ignition delays are consistently under-predicted. To verify whether this indicated an error with the mechanism, or an experimental uncertainty, further ignition delay validation was necessary for n-heptane.

### 4.3.2 Shock Tube Validation

To further evaluate the ability of the mechanism to predict ignition delays for n-heptane, experimental shock tube ignition delay measurements were used. Figure 4.4 shows a general schematic of a shock tube. A high pressure driving chamber (chamber one) and a low pressure driven chamber (chamber two) are separated by a burst diaphragm (Côme 2001). Chamber one is filled with an inert gas, such as nitrogen, until the diaphragm bursts, sending a shock wave through chamber two which is filled with the mixture of combustion reactants. As the incident shock wave propagates through chamber two, the temperature and pressure of the mixture are rapidly (in  $\sim 1\mu\text{s}$ ) increased. At the end of the tube, the shock wave

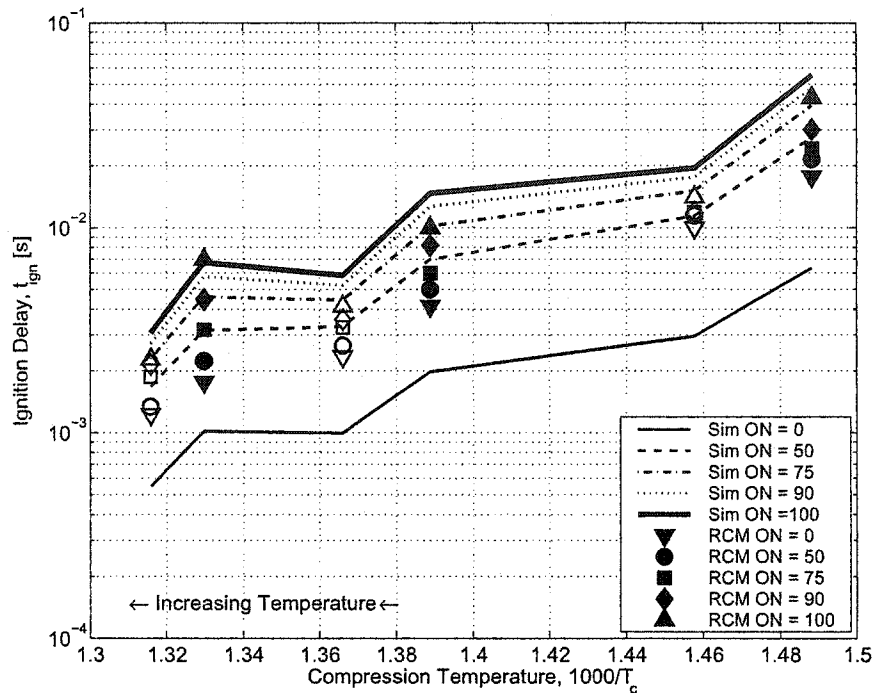


Figure 4.3: Comparison of measured (Park & Keck 1990) and calculated RCM ignition delays for various stoichiometric PRF blends. Hollow markers indicate initial pressure of  $\sim 5$ MPa and solid markers indicate initial pressures of  $\sim 2$ MPa.

is reflected and once again increases the mixture temperature and pressure as it propagates back through chamber two. By measuring the speed of the incident and reflected shock waves with either pressure or heat flux transducers, it is possible to determine the initial reaction conditions. Shock tubes compress the mixture more rapidly than an RCM, increasing the validity of the assumption that there is negligible chemical kinetic activity during compression.

#### Calculation of Shock Tube Ignition Delays

Shock tube ignition delay measurements taken from Fieweger et al. (1997) for n-heptane were compared to the ignition delays predicted by the thermokinetic model. As in the RCM validation, the system was modeled as a constant volume,

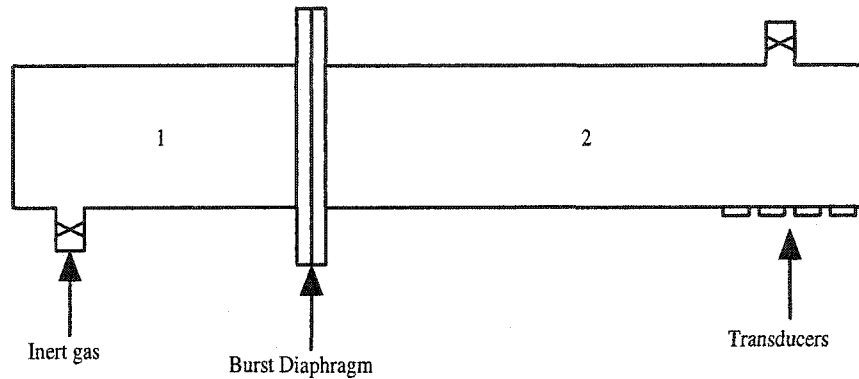


Figure 4.4: Schematic of a shock tube used to determine ignition delays, based on Côme (2001). Chamber one: high pressure driving chamber, chamber two: low pressure sample chamber.

adiabatic system. For this validation, stoichiometric mixtures of n-heptane and air with an initial pressure of 40bar were considered. The initial temperature was varied between 600K and 1200K in 20K increments and included the NTC region. The “compression” and subsequent ignition processes were assumed to be sufficiently fast that heat transfer is negligible (Westbrook & Dryer 1984). The experimental ignition delay was defined as being the time from when the reflected shock wave passed through the mixture, to the point at which the pressure sharply increases (i.e. maximum  $\frac{dP}{dt}$ ). The numerical ignition delay was similarly defined as being the time from the beginning of the simulation to the maximum rate of pressure rise.

### Comparison of the Shock Tube and Calculated Ignition Delays

Shown in Figure 4.5 is a comparison of the measured and calculated shock tube ignition delays. The solid line represents the simulation results and the points represent the experimental ignition delays from Fieweger et al. (1997). Good qualitative and quantitative agreement is obtained for temperatures below the

NTC region (i.e.  $\frac{1000}{T_c} > 1.3$ ). As the temperature is further increased, the location of the NTC region is reproduced, though the ignition delays within this region are increasingly under predicted as the temperature is increased. Once the upper temperature limit of the NTC region is reached (i.e.  $\frac{1000}{T_c} < 1$ ), the agreement once again improves. The thermokinetic model is thus capable of predicting ignition delays and capturing the NTC ignition phenomena for n-heptane.

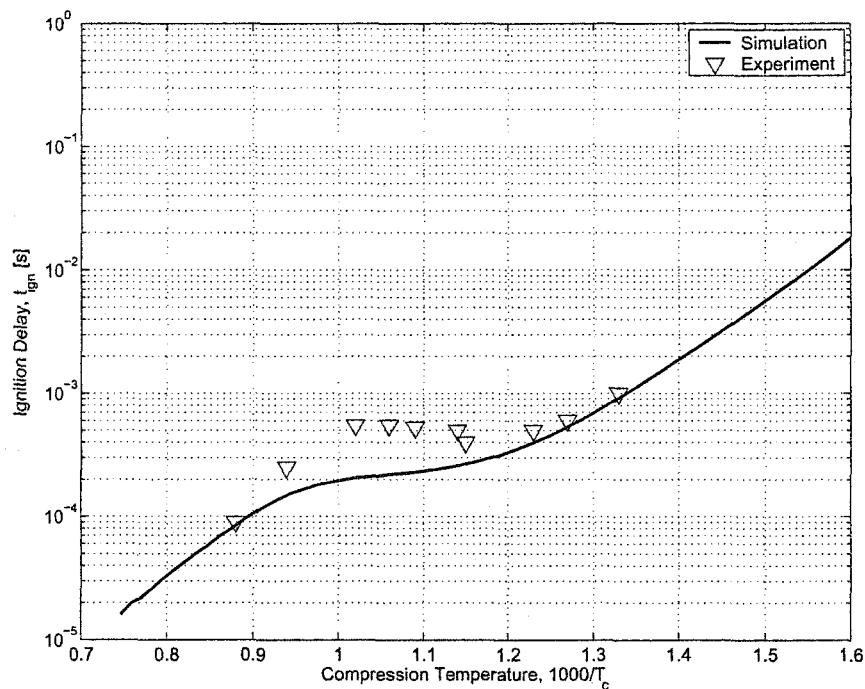


Figure 4.5: Comparison of calculated and experimental shock tube ignition delays taken from Fieweger et al. (1997).  $P = 40\text{bar}$ , stoichiometric n-heptane/air mixture. Simulations were carried out from 600K to 1200K in 20K increments.

#### 4.4 HCCI Validation

The preceding validations of the thermokinetic model indicates that it is able to predict equilibrium conditions and ignition delays of various practical combus-

tion systems. This section investigates the ability of the thermokinetic model to predict the ignition timing in an experimental HCCI engine. In the previous investigations, the ignition *delay* in seconds was of interest. For this validation the ignition *timing*, which is the timing of the combustion event relative to TDC, is of interest. Both the RCM and shock tube are simplified systems in which the compression process occurs rapidly enough that it can be neglected. In addition, the short compression times and limited fluid motion allowed the effects of heat transfer to be neglected. Both the compression process and heat transfer must be accounted for in modeling of the HCCI cycle and are included in this validation.

Experimental pressure traces taken from a Cooperative Fuels Research (CFR) engine running in HCCI mode by Atkins (2004) are compared to those determined using the thermokinetic model. A schematic of the engine test bench used by Atkins (2004) is shown in Figure 4.6, with the engine geometry outlined in Table 4.3. The intake port temperature was held constant using an intake air heater. Recirculated exhaust gases were introduced into the intake manifold using an insulated return line from the exhaust manifold. The amount of EGR used was controlled by means of a gate valve in the return line and quantified using equation 3.56. By maintaining a constant intake port temperature, the charge heating effect of the EGR was decoupled from the thermal, chemical, and dilution effects (see section 2.2.7). The fuel/air equivalence ratio was determined using a broadband lambda sensor, with corrections for the different carbon hydrogen ratios of the different PRF blends. The cylinder pressure was recorded every 0.1 CAD.

#### 4.4.1 Calculating the HCCI Ignition Timing

For each of the conditions outlined in Table 4.4, the simulations were carried out starting at IVC and finishing 180 CAD later. Each of the points listed in Table

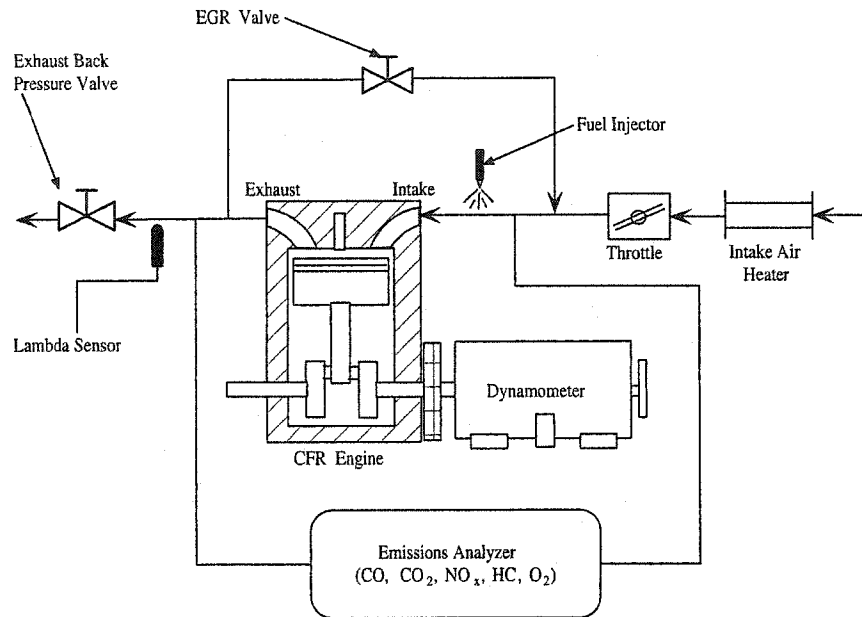


Figure 4.6: Schematic of the single cylinder CFR engine test bench (Atkins 2004)

Table 4.3: CFR engine configuration. IVC - Intake Valve Closing, EVO - Exhaust Valve Opening

Bore	83mm
Stroke	114mm
Compression Ratio	12:1
Displacement	0.622L
IVC	-146° aTDC
EVO	140° aTDC

4.4 correspond to an IMEP of approximately 5 bar for different PRF blends. To achieve this, different EGR rates and equivalence ratios were required for each of the fuels, allowing the ability of the model to predict their effects on ignition timing to be evaluated. Heat transfer was included in this investigation using the Woschni (1967) correlation (see equation 3.4), with  $C_2 = 0$  for all phases of the engine cycle (from equation 3.6).

The thermodynamic state of the mixture must be known at the beginning of

Table 4.4: Single cylinder HCCI engine operating conditions used for validation. All runs were at  $N = 700\text{rpm}$ ,  $IMEP \approx 5\text{bar}$  (Atkins 2004).

PRF (-)	$\Phi$ (-)	$EGR$ (-)	$T_{in}$ (K)	$P_{IVC}$ (kPa)
20	0.983	0.305	360	94.1
40	0.808	0.189	360	90.0
60	0.662	0.0142	360	90.2

compression in order to provide the thermokinetic model with initial conditions. These initial conditions were determined using the methods discussed in section 3.5.1. The initial mixture temperature was taken as being the mean mixture temperature (over 50 cycles) measured at the intake port. Similarly, the initial mixture pressure was taken as being the mean cylinder pressure (over 50 cycles) at IVC. To account for the piston ring blow-by in the engine, the compression ratio specified in the thermokinetic model was adjusted such that the compression pressures matched those of the experimental results. An effective compression ratio of 11:1, rather than the geometric ratio of 12:1, was used for all subsequent calculations and was not changed.

### Ignition Timing

In order to compare the calculated and experimental ignition timing, the point of ignition for both the experimental and calculated engine cycles should be determined in the same fashion. A standard definition of ignition is the point at which the exothermicity of chemical reactions is greater than the energy lost to the environment (Glassman 1996). This definition could be used to determine the ignition timing from the simulation results as the heat transfer rate and reaction exothermicity were known quantities, but not for the experimental data as only the cylinder pressure was measured.

A method was developed in which the ignition timing can be determined directly from both the calculated and measured cylinder pressure histories. In particular, a method designed to detect engine knock from an SI engine pressure trace was adapted to detect autoignition in an HCCI engine. Checkel & Dale (1986) presented a method in which the onset of knock is characterized by a decrease in the third derivative of the pressure trace. This decrease corresponds to the rapid change of concavity of the pressure history from positive to negative during knocking. In HCCI engines it is the point at which the reaction exothermicity becomes substantial and begins to increase the cylinder pressure which must be detected. In the crank angle region near TDC during compression, the pressure history has a negative concavity, which becomes positive during ignition (i.e. a positive third derivative). By detecting this transition from negative to positive concavity, the point of ignition can be determined. In this investigation, ignition is defined as being the point at which the third derivative of the pressure trace with respect to the crank angle,  $\theta$ , exceeds a heuristically determined limit:

$$\frac{d^3 P}{d\theta^3} > \frac{d^3 P}{d\theta^3} \Big|_{lim} = 0.003 \left[ \frac{\text{kPa}}{\text{CAD}^3} \right] \quad (4.1)$$

By monitoring the rate of change of the concavity, the ignition event is detected when the ignition process causes the concavity of the pressure to change at a rate greater than the threshold. It was found that if the ignition process is so slow that this algorithm does not detect it, the mixture does not go through the second ignition stage and is therefore not of interest. The limit was selected such that the point of ignition represented the change in concavity and was not effected by noise in the differentiated signal.

As Checkel & Dale (1986) note, the third derivative is not the only method which detects autoignition, but it is the most robust. Using the first derivative of

the pressure trace to characterize ignition (for example, by stating that ignition occurs when the rate of pressure rise exceeds a certain limit), has the disadvantage that the rate of pressure increase during ignition varies with engine operating parameters.

A major concern when differentiating numerically is the amplification of noise, as successive differentiation of the signal amplifies high frequency noise components. Both the experimental and simulated pressure traces were filtered using a fourth order Butterworth low pass filter to attenuate the high frequency noise which would have been amplified during differentiation. A heuristically determined cutoff frequency of  $f_c = 0.278\text{CAD}^{-1}$  provided sufficient suppression of high frequency noise, without undue distortion of the pressure trace. As the pressure history was discretized at a constant angular rate (every 0.1CAD), the signal was filtered in the crank angle domain to avoid having to change  $f_c$  for different engine speeds. For example, at an engine speed of 700rpm the crank angle based cutoff frequency corresponds to a time based frequency of 1.17kHz, while at 2000rpm it corresponds to a frequency of 3.34kHz. In order to remove any phase shift incurred by the filtering process, the filter was applied in both the forward and reverse directions during postprocessing. Both the experimental and calculated pressure traces were filtered in the same manner to ensure that the ignition timings were indicative of the same phenomena.

#### 4.4.2 Results

Each of the calculated pressure histories were compared to the average pressure history of 50 cycles taken from the CFR engine with the operating conditions outlined in Table 4.4. The individual experimental pressure traces were averaged every 0.1 CAD to account for slight variations in engine parameters, and hence

ignition timing, during the data acquisition. By assuming that the variation between each cycle is independent, the mean pressure trace is indeed representative of pressure history. The goal is to gain a pressure history which is representative of the operation with the conditions given in Table 4.4. Shown in Figure 4.7 is a comparison of the pressure traces of each of the 50 cycles and the mean pressure trace. The mean pressure trace does not capture the knock-like pressure fluctuations at the end of combustion, but does capture the overall trend of the pressure history of each of the individual cycles.

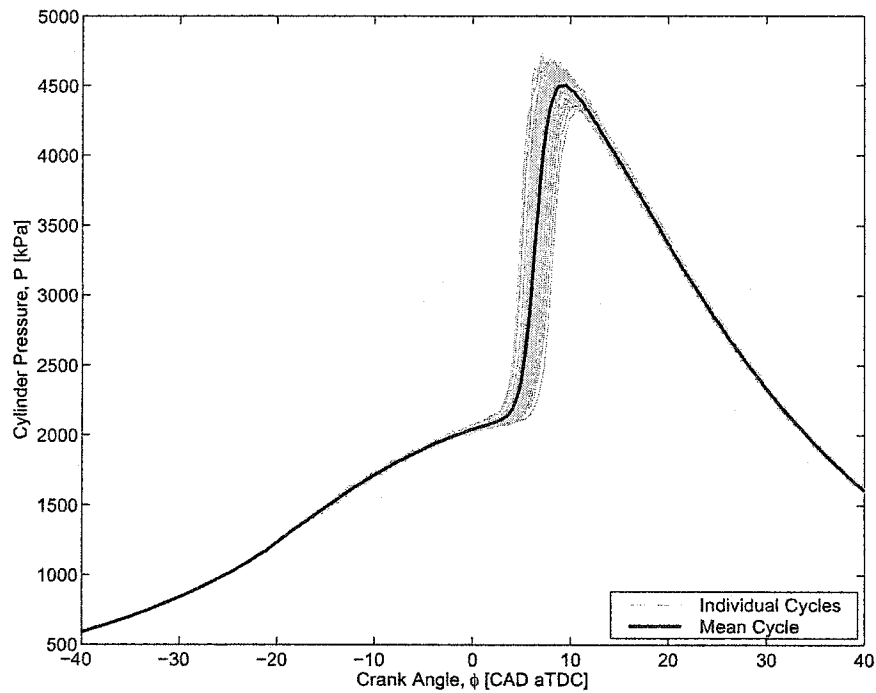


Figure 4.7: Comparison of the individual experimental pressure traces (Atkins 2004) and their mean. Conditions are outlined in Table 4.4 for the 20PRF case

A comparison of the experimental and calculated pressure traces is shown in figures 4.8, 4.9, and 4.10 for 20PRF, 40PRF, and 60PRF, respectively. The ignition timing was predicted to within the experimental variability for both the 40 and 60PRF cases, while for the 20PRF case the predicted ignition timing was

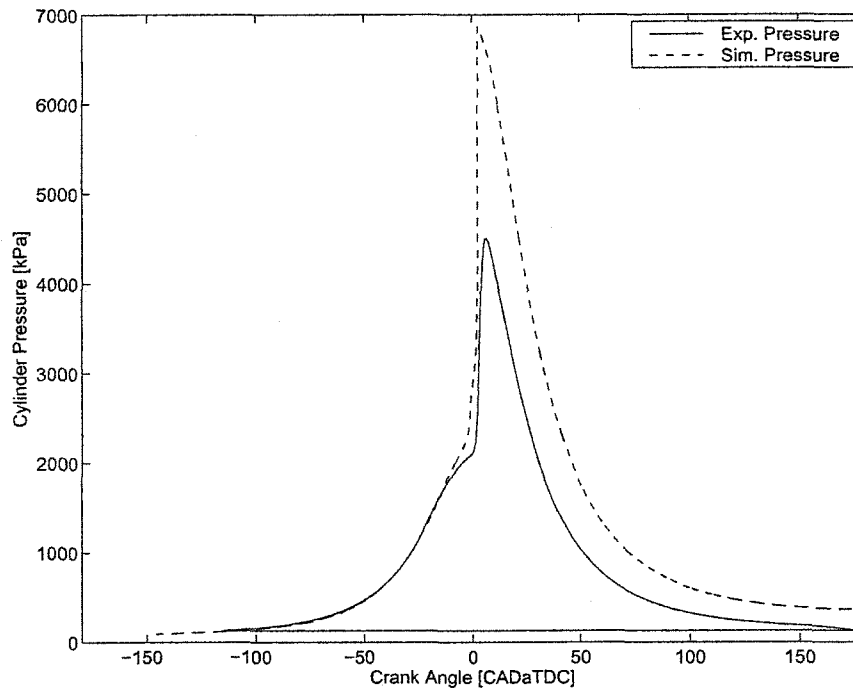


Figure 4.8: Comparison of calculated and experimental pressure histories using 20PRF fuel. Experimental pressure history from Atkins (2004).  $T_{o,sim} = 360\text{K}$ ,  $\theta_{ign,exp} = 1.1 \pm 1.7 \text{ CAD}$ ,  $\theta_{ign,sim} = -2.3\text{CAD}$ ,  $T_{wall} = 390\text{K}$

slightly advanced. The sensitivity of the ignition process to the initial temperature is such that if the specified initial temperature had been decreased by  $2^\circ$ , the predicted ignition timing would be within the experimental observed range. The high sensitivity of the ignition process on the initial conditions implies that any model, including this one, must be provided with accurate initial conditions in order to predict the pressure history.

In all three cases, the combustion process predicted by the thermokinetic model was considerably faster than those observed experimentally. As discussed in section 2.3, this is due to the single zone approximation used to describe the system. The increased reaction rate also results in the two stage ignition process being more apparent in the calculated pressure traces than in the experimental pressure

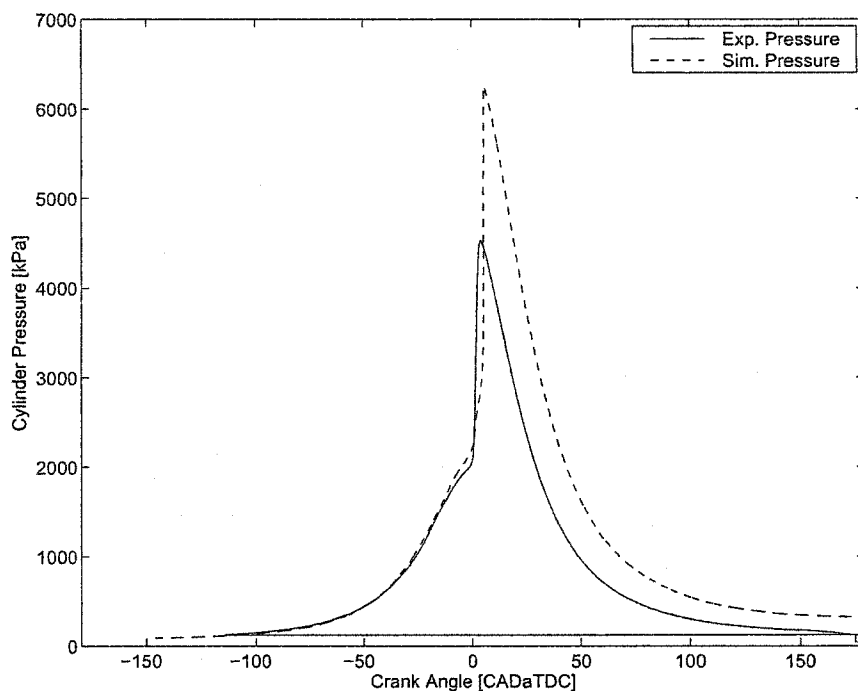


Figure 4.9: Comparison of calculated and experimental pressure histories using 40PRF fuel. Experimental pressure history from Atkins (2004).  $T_{o,sim} = 360\text{K}$ ,  $\theta_{ign,exp} = 0.4 \pm 1.4\text{CAD}$ ,  $\theta_{ign,sim} = 0.5\text{CAD}$ ,  $T_{wall} = 390\text{K}$

traces, as shown in Figure 4.11. Figure 4.11 shows a comparison of the experimental and calculated heat releases determined using the method presented by Rassweiler & Withrow (1938). The low temperature ignition process as calculated by the thermokinetic model, over-predicts the reaction rate (due to the one zone assumption) and the temperature increases much more rapidly than in the experimental case. The rapid temperature increase causes the equilibrium of R29 ( $\dot{\text{R}} + \text{O}_2 \rightarrow \text{R}\dot{\text{O}}_2$ ) to shift towards the reactants and causes a cool flame. In the experimental case, the reaction rates are slower and by the time that the equilibrium of R29 would shift, a substantial concentration of  $\dot{\text{R}}\text{OOH}$  is present, leading to chain branching and high temperature ignition.

These results show that the thermokinetic model is capable of predicting the

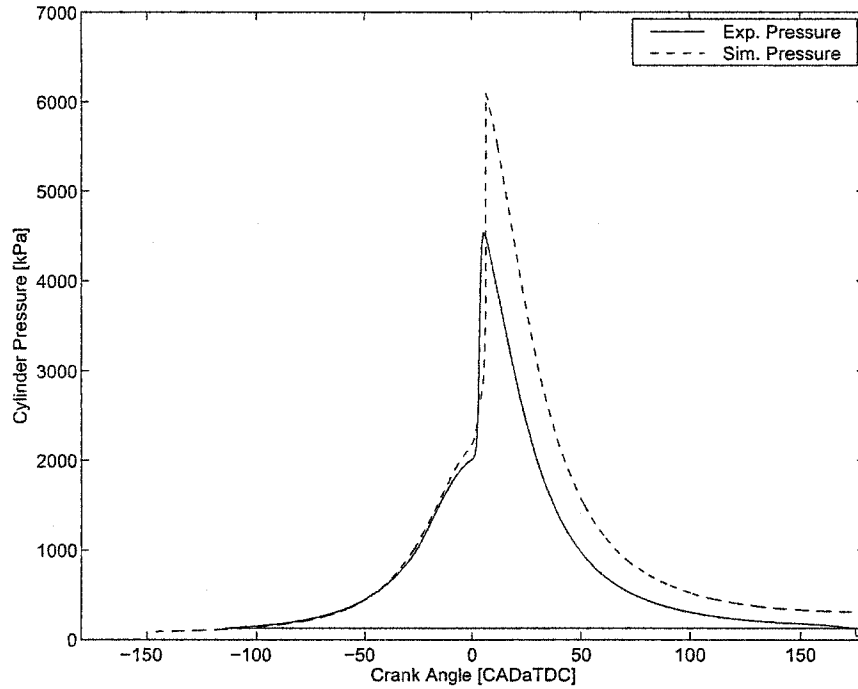


Figure 4.10: Comparison of calculated and experimental pressure histories using 60PRF fuel. Experimental pressure history from Atkins (2004).  $T_{o,sim} = 360\text{K}$ ,  $\phi_{ign,exp} = 1.8 \pm 1.9\text{CAD}$ ,  $\phi_{ign,sim} = 1.3\text{CAD}$ ,  $T_{wall} = 390\text{K}$

ignition timing in an HCCI engine, for widely ranging conditions. Each of the three points considered used a different fuel blend requiring that different EGR rates and equivalence ratios be used to maintain acceptable ignition timing. In all cases the model was able to predict the qualitative dependence of the ignition delay on the engine operating parameters, to within experimental uncertainty.

In order to the predict combustion duration or exhaust gas composition using this model, it is necessary to extend it to use a multi-zone approximation which accounts for the boundary layer and crevice regions.

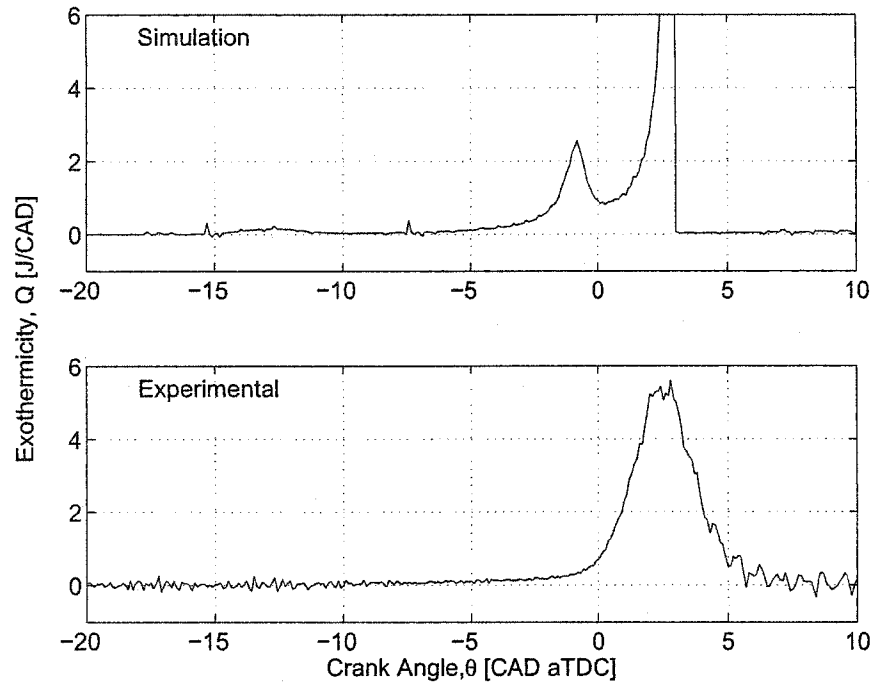


Figure 4.11: Comparison of the exothermicity during combustion for the experimental and calculated engine cycles for the 20PRF case.

## 4.5 Summary

So that the thermokinetic model may be used with confidence to further explore the HCCI cycle, its ability to predict equilibrium thermodynamic state, RCM and shock tube ignition delays, and HCCI ignition timing was validated. These validations compared both theoretical calculations and experimental measurements from independent sources to provide confidence that the model does indeed capture the underlying physics. These comparisons showed that thermokinetic model does achieve the purpose for which it was developed - to predict the ignition timing in a HCCI engine.

The ability of the thermokinetic model to determine the thermodynamic state of the combustion products was validated through a comparison with the equilib-

rium temperature and mixture composition determined using STANJAN. It was found that, as the temperature and mixture compositions agreed, the thermokinetic model described the thermodynamic process adequately, and the chemical kinetic mechanism described the interaction of the equilibrium species.

To evaluate the ability of the thermokinetic model to predict temporal variations of the thermodynamic state, experimental ignition delays were compared those calculated using the thermokinetic model. The thermokinetic model predicted the qualitative effects of the mixture temperature, pressure, and octane number on RCM ignition delays (from Park & Keck (1990)). In the RCM validation it was found that the ignition delays of n-heptane were under-predicted by the thermokinetic model and a subsequent shock tube ignition delay validation was carried out for n-heptane. The thermokinetic model was able to predict the shock tube ignition delays (from Fieweger et al. (1997)) for n-heptane, including the negative temperature coefficient region.

The pressure histories determined using the thermokinetic model were compared to pressure histories from an experimental HCCI engine (Atkins 2004). In particular, the ignition timings of three HCCI operation points, each with different equivalence ratios, EGR rates, and octane numbers, were compared. The thermokinetic model was able to predict the ignition of all three points, capturing the qualitative effects of the engine parameters. The thermokinetic model successfully predicted the ignition timing in an HCCI engine, which was the objective of the model. The model is not suitable for predicting combustion durations and distorts the two stage ignition phenomena due the single zone approximation. By extending the thermodynamic model to use a multi-zone approximation and include spatial variations in the thermodynamic state, the model would be better able to predict combustion duration and exhaust gas compositions.

## Chapter 5

# Applications of the Thermokinetic Model

### 5.1 Introduction

Control of the HCCI engine relies largely on the ability to control the ignition timing. Ignition timing is affected by not only the thermodynamic state at the beginning of compression, but also the engine speed. To control the ignition timing, insight as to the influences of these factors on the ignition process is required. For example, if the engine speed is changed, how must the intake temperature be changed to maintain a constant ignition timing? In order to have the same ignition timing relative to TDC for two different engine speeds, a different initial thermodynamic state is required such that the time dependent ignition delay is changed accordingly<sup>1</sup>.

---

<sup>1</sup>Recall that ignition *timing* refers to the timing of the ignition relative to some crank angle based reference point. Ignition *delay* refers to the absolute time required, for a given thermodynamic state, for the mixture to autoignite. At different engine speeds different ignition *delays* are required to ensure a constant ignition *timing* as the time available for ignition varies with engine speed.

This chapter focusses on determining the net effect of the various engine parameters on the ignition timing and how they are interrelated. The thermokinetic model was used to independently vary parameters so that their effect on the ignition timing may be determined. A dimensional analysis was used to form a functional relationship between the engine parameters, based on the results of the parameter variations. Using this functional form, it was possible to determine the conditions required for a given ignition timing.

### 5.2 Parameter Variations

To observe the effects of various parameters on HCCI ignition timing, they were varied independently through a series of simulations. The initial temperature and pressure, engine speed, EGR rate, and equivalence ratio were varied over ranges typical of practical HCCI operation and are given in Table 5.1. For each set of conditions, a simulation was carried out using the thermokinetic model for 180 CAD, starting at IVC. The same engine configuration was used as in the HCCI ignition timing validation (see Table 4.3). Since each parameter was varied independently a total of 270 simulations were performed.

The simulations were carried out using the Westgrid High Performance Computing Network to reduce the computation times. Each simulation was run on a single 400MHz processor and required approximately 20 minutes to complete. As multiple simulations were run simultaneously, the computation times were reduced considerably when compared to running the simulations in serial. The number of simulations that could be run simultaneously was limited by the number of software licenses available.

The ignition timing for each of the simulations was determined using the third

Table 5.1: Ranges of the HCCI parameters varied in the simulations carried out using the thermokinetic model.

Parameter	Range
Initial Pressure	50, 100 kPa
Initial Temperature	300, 325, 350, 375, 400 K
EGR Rate	0, 25, 50%
Equivalence Ratio	0.5, 0.7, 0.9
Octane Number	0
Engine Speed	1000, 3000, 5000 rpm

derivative method outlined in section 4.4.1 with a modified limit:

$$\frac{d^3P}{dt^3} \geq 0.05 \left[ \frac{kPa}{CAD^3} \right] \quad (5.1)$$

This limit represents the second stage ignition process and the timing of the majority of the exothermicity. Second stage ignition occurred in only 53 of the 270 simulations.

The individual effects of each of the parameters have been extensively studied in the literature, as discussed in section 2.2. The effects of the five variables ( $T_o$ ,  $P_o$ ,  $N$ , EGR, and  $\Phi$ ) on the ignition timing are interrelated, making it difficult to determine the net effect of each parameter. A dimensional analysis was used to determine a relationship between the various parameters and correlate the results of the 53 simulations.

### 5.3 Dimensional Analysis

A dimensional analysis provides a combination of selected variables, such that the product is dimensionless. If the selected variables capture all of the relevant physical processes in a given system, the resulting dimensionless parameter or parameters may be able to characterize the system. While dimensional analysis

does provide a dimensionally homogeneous equation, it does not guarantee that the resulting equation is representative of the physical process. A detailed discussion of dimensional analysis is available in either the original paper by Buckingham (1914) or in texts devoted to subject such as that by Isaacson & Isaacson (1975).

If a system can be described using  $n$  physical variables, in a total of  $r$  dimensions, the system can be potentially reduced to  $n - r$  dimensionless parameters (IIs). Once the IIs are determined, it is necessary to determine a relationship between them which describes the characteristic behavior of the system. The fundamental dimensions ( $r$ ) used to describe this system are mass [M], length [L], time [T], and temperature [ $\Theta$ ]. The dimensions of the parameters are represented in terms of these fundamental dimensions. Pressure, for example, has units of force per unit area which is represented using the fundamental dimensions as  $[ML^{-1}T^{-2}]$ . Determining each II requires solving a system of  $r$  equations with  $r$  unknowns.

To use a dimensional analysis, it is necessary to select  $n$  variables which are relevant to the problem being considered. In the case of HCCI autoignition, these variables are the intake temperature and pressure, engine speed, EGR rate, and equivalence ratio (see, for example, Zhao et al. (2001)). While the octane number and compression ratio do indeed affect the ignition timing, they were not included in this investigation in order to simplify the analysis.

These variables often do not directly represent the physical process responsible for the observed behavior. For example, the equivalence ratio is a measure of the air-fuel ratio relative to the stoichiometric air-fuel ratio. While this is a widely used tool for characterizing combustion systems, it is difficult to use in a dimensional analysis as it is already dimensionless. To perform a dimensional analysis, it is not enough to simply identify the relevant parameters, rather it is also necessary

to determine the underlying physical processes by which they affect the system. Each of the parameters are discussed below with respect to how they affect the ignition timing and how they are represented in the dimensional analysis.

### 5.3.1 Initial Pressure

The initial pressure changes the overall concentration of the mixture, thereby increasing the rate of kinetic activity (equation 3.38). For this investigation, the intake pressure was represented using the cylinder pressure at IVC, with dimensions of pressure ( $[ML^{-1}T^{-2}]$ ).

### 5.3.2 Initial Temperature

The mixture temperature at the Beginning Of Compression (BOC) influences the Arrhenius rate constant and hence affects the ignition timing. Recall that the reaction rate is proportional to the Arrhenius rate constant:

$$k = Ae^{-E_a/R_uT} \quad (3.34)$$

The dimensions of which are governed by the pre-exponential constant  $A$ , which is not temperature dependant. Noting that  $A$ ,  $E_a$ , and  $R$  are all constants, the rate constant is then only proportional to the exponential of the inverse of the temperature:

$$k \propto e^{-C/T} \quad \rightarrow \quad k \propto T \quad (5.2)$$

where  $C$  is a constant with dimensions of [K]. The ignition delay is of the interest in this investigation, not the reaction rate. The ignition delay is inversely proportional to the reaction rate, which leads to the relationship:

$$t_{ign} \propto \frac{1}{T} \quad (5.3)$$

Thus, the effect of the mixture temperature is included in the dimensional analysis using the inverse of the fundamental dimension of temperature.

The end of compression temperature is more relevant to the ignition process than the BOC temperature, as the mixture is essentially inert at BOC. The end of compression temperature was estimated from the isentropic compression relationship:

$$\frac{T_2}{T_1} = \left( \frac{v_1}{v_2} \right)^{k-1} \quad (5.4)$$

where  $T_2$  and  $v_2$  are the end of compression temperature and specific volume, respectively,  $T_1$  and  $v_1$  are the BOC temperature and specific volume, respectively, and  $k$  is the ratio of specific heats,  $c_p/c_v$ . The compression temperature,  $T_c$ , can be expressed in terms of the geometric compression ratio,  $CR$ , as:

$$T_c = T_o CR^{k-1} \quad (5.5)$$

To determine the compression temperature, a representative value of  $k$  at the beginning of compression was used ( $k = 1.36$ ).

### 5.3.3 Engine Speed

The engine speed changes the time available for the ignition process to take place. At low engine speeds the mixture is exposed to high temperatures and pressures for longer periods of time than at higher engine speeds. The ignition delay (in seconds) required in order to maintain a constant ignition timing (in CAD) varies as the engine speed is changed. Rather than simply representing the engine speed with dimensions of time, the mean piston speed,  $\bar{S}_p$ , with units of speed ( $[LT^{-1}]$ ) is used:

$$\bar{S}_p = \frac{LN}{30} \quad (5.6)$$

Where  $L$  is the stroke length in centimeters and  $N$  is the engine speed in rpm. Not only does this represent changes in the engine speed, but also accounts for changes in the stroke length.

### 5.3.4 EGR Rate

EGR affects the ignition timing through predominantly the charge heating and thermal effects, as discussed in section 2.2.7. The charge heating effect, which is the more substantial of the two, changes the initial temperature of the mixture when sufficiently hot exhaust gases are used. The lesser, though still significant, thermal effect changes the specific heat capacity of the mixture and hence changes the thermodynamic behavior of the mixture during compression and ignition. The charge heating effect is accounted for by the initial temperature as this temperature represents that of the mixture at IVC, regardless of the EGR rate. This allows the investigation of the effects of *isothermal* EGR, where different EGR rates are considered, but the mixture temperature at BOC is the same.

In order to represent isothermal EGR in the dimensional analysis, it was necessary to clarify the mechanism by which it affects the ignition timing. As the isothermal EGR fraction increases, the ratio of specific heats increases slightly (sample calculations are provided in appendix A.3), leading to higher compression temperatures. Figure 5.1 shows a comparison of motored and fired<sup>2</sup> temperature histories for HCCI operation with different EGR fractions. Indeed, when the chemical kinetic activity is neglected the compression temperatures are higher with increasing EGR fraction. When the chemical kinetic activity is considered,

---

<sup>2</sup>Motored engine operation refers to when the piston moves up and down without a combustion event occurring. In an SI engine this is accomplished by not firing the spark plug, while in these HCCI simulations it was achieved by setting all the reaction rates to zero. Fired operation refers to standard engine operation in which combustion takes place.

the ignition timing is retarded, as seen in the fired temperature histories in Figure 5.1. The retarded ignition timing has been noted in other investigations both experimentally (Atkins 2004), and numerically (Zhao et al. 2001). Thus there are factors other than a change in the ratio of specific heats which cause the ignition timing to be retarded.

Table 5.2: A comparison of the effect of the EGR rate on the compression temperatures (for motored operation), ignition timing (for fired operation), ratio of specific heat capacities ( $k$ ), and the specific heat capacity ( $c_v$ ).

	$T_{comp}$ [K]	$\theta_{ign}$ CAD aTDC	$k$ [-]	$c_v$ kJ/kg/K
0% EGR	855	-19.2	1.353	0.789
25% EGR	858	-15.4	1.354	0.792
50% EGR	860	-11.3	1.355	0.795

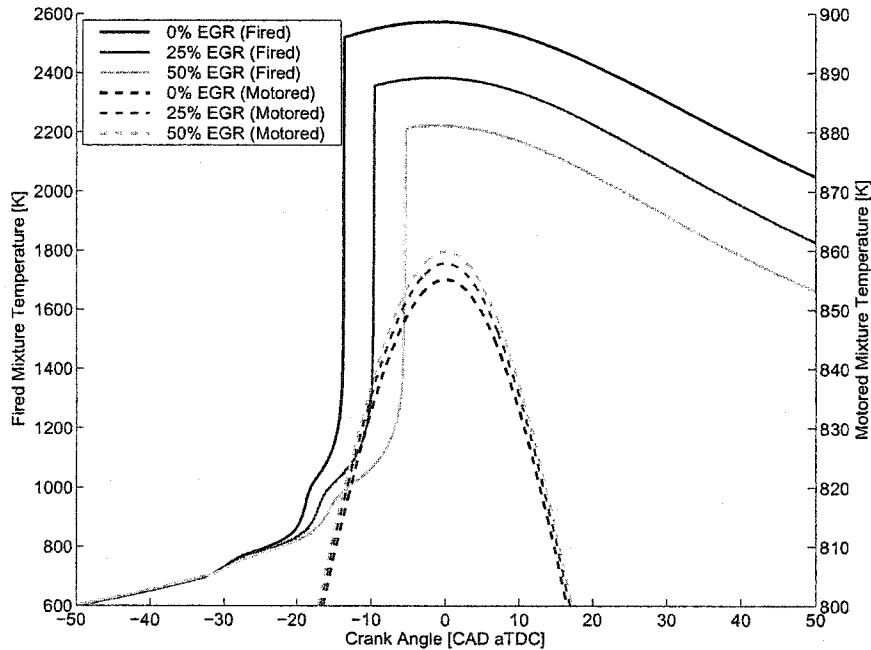


Figure 5.1: The effect of EGR addition on the compression temperature for motored operation and ignition timing for fired operation. Motored temperature histories were determined by setting all reaction rates to zero.  $ON=0$ ,  $N = 1000\text{rpm}$ ,  $T_o = 400\text{K}$ ,  $\Phi = 0.7$ ,  $P_o = 100\text{kPa}$ .

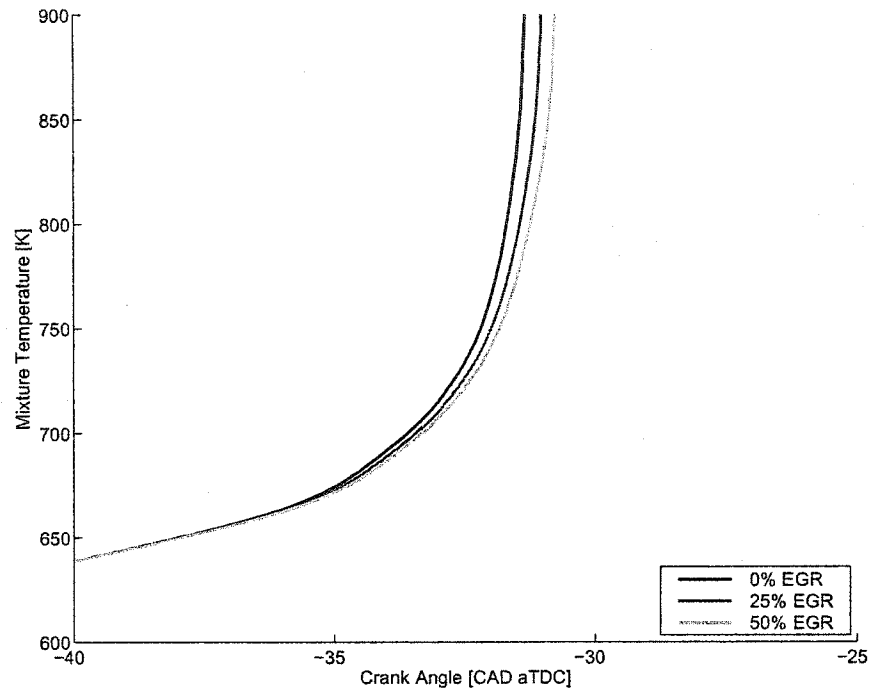


Figure 5.2: The effect of EGR addition on the ignition timing for fired HCCI operation, for mixtures with a constant specific heat capacity.  $ON=0$ ,  $N = 1000\text{rpm}$ ,  $T_o = 400\text{K}$ ,  $\Phi = 0.7$ ,  $P_o = 100\text{kPa}$ .

An increase in the EGR fraction increases both the specific heat capacity and the ratio of specific heats as shown in Table 5.2. To determine if the change in specific heat capacity is responsible for the retarded ignition timing, simulations were carried out in which the isothermal EGR rate was varied while setting the specific heat to be that of the fresh mixture. The results of this variation are shown in Figure 5.2 and indicate that if the temperature and specific heat capacity of the mixture are constant, the ignition timing does not change significantly with EGR. The change in ignition timing for different rates of isothermal EGR can thus be attributed to a change in the specific heat capacity of the mixture. As the EGR rate, and hence specific heat capacity, increases, the temperature increase prior to ignition is decreased slowing the self-accelerating ignition process. The change in

temperature can be represented by:

$$\Delta T = \frac{q}{c_v} \quad (5.7)$$

Where  $q$  is the energy released by the chemical reactions per unit mass, which is a function of the fuel being used and remains constant for different EGR rates. An increase in  $c_v$  causes  $\Delta T$  to decrease and the ignition to be retarded. This effect is apparent in Figure 5.1 in which the temperatures begin to increase at approximately -32 CAD aTDC for all EGR rates, but those mixtures with lower EGR rates and specific heat capacities, have higher rates of temperature rise. The slight retardation of the ignition timing with increasing EGR fraction seen in Figure 5.2 was attributed to the decreasing  $O_2$  concentration with higher EGR rates (the dilution effect).

The effects of EGR are summarized in Figure 5.3. An increase in EGR will increase the mixture temperature, specific heat capacity, ratio of specific heat capacities, and will decrease the  $O_2$  concentration. The increase in temperature increases the reaction rates and leads to an advancement of the ignition timing. The increase in ratio of specific heat capacities leads to slightly higher compression temperatures, but the increase in the heat capacity itself, reduces the exothermicity. The net effect on the ignition timing by the change in the specific heat capacity is that the ignition timing is retarded. Finally, the reduction of the  $O_2$  concentration reduces the overall reaction rate and retards the ignition timing.

For the dimensional analysis, the effect of isothermal EGR was represented as an increase in the specific heat capacity due to the addition of EGR:

$$\Delta c_{v,EGR} = \frac{\partial c_v}{\partial EGR} \propto (1 + EGR) \left[ \frac{J}{kgK} \right] \quad (5.8)$$

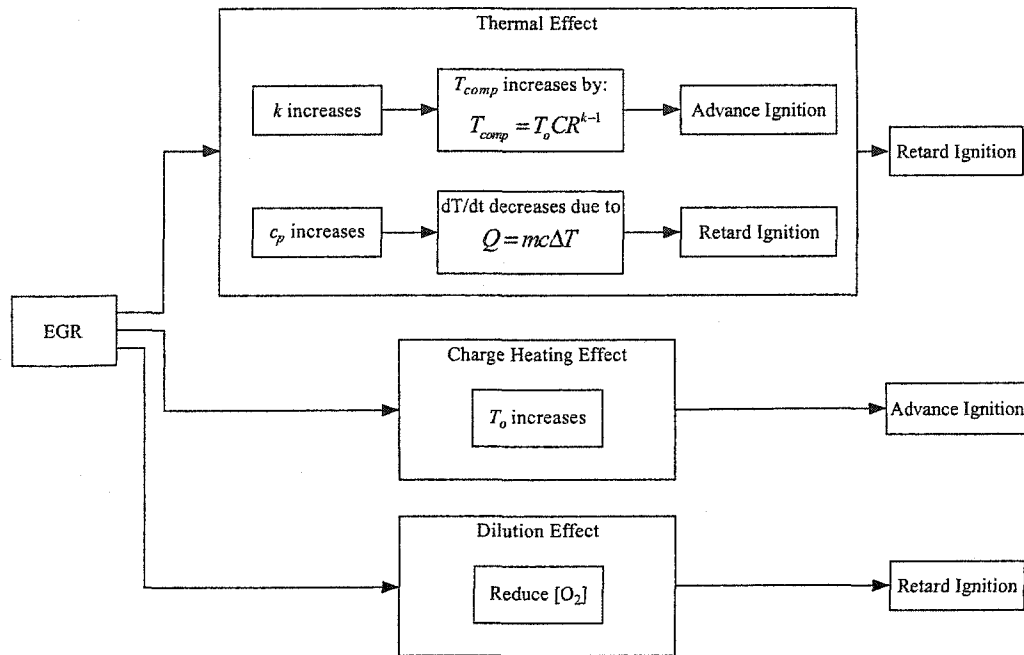


Figure 5.3: Schematic of EGR effects on the ignition timing. Note that the chemical effect is not included as it was found by Zhao et al. (2001) not to affect the ignition timing.

A partial derivative is used to determine the effect of only EGR on the specific heat capacity, although it is also affected by the equivalence ratio.

### 5.3.5 Equivalence Ratio

The equivalence ratio represents the relative fuel/air quantity (see equation 3.55) and is dimensionless. To reduce the number of dimensionless parameters for which a functional form must be determined, it is desirable to represent the equivalence ratio in a manner such that it has dimensions (Isaacson & Isaacson 1975). Changes in the equivalence ratio affect the ignition timing by changing the relative number of fuel and air molecules, and hence the kinetic activity. As the mixture is enriched, there is a greater possibility of the molecules colliding and reacting, and the ignition is advanced. To represent the mass of the fuel relative

to the mass of the air,  $\Delta m$ , the following relationship is used:

$$\Delta m = m_{O_2} - m_{fuel} \quad (5.9)$$

where  $m_{O_2}$  and  $m_{fuel}$  are the mass of oxygen and fuel, respectively. The equivalence ratio was included in the dimensional analysis using the dimension of [M].

### 5.3.6 Ignition Delay

The ignition process is governed by the Law of Mass Action (equation 3.38) in the time domain (seconds) and not in the crank angle domain (CAD). Thus, for the purpose of the dimensional analysis, the ignition timing is defined as being the time in seconds from the beginning of compression (i.e. IVC) to the time at which the mixture autoignites. The ignition timing,  $\theta_{ign}$ , in CAD after IVC is determined from the time domain ignition delay using the engine speed,  $N$ , in rpm:

$$\theta_{ign} = 6Nt_{ign} \quad (5.10)$$

where  $t_{ign}$  is the ignition delay in seconds after IVC.

Although this investigation is concerned with the crank angle ignition timing rather than the time based ignition delay, the kinetics of the ignition process are defined in terms of time. Therefore, the time based ignition process is considered in the dimensional analysis and is converted later to the CAD domain using equation 5.10.

### 5.3.7 Evaluation of Dimensionless Parameters

Using the representations of the engine parameters discussed above, a dimensional analysis was carried out to determine two dimensionless parameters repre-

## CHAPTER 5: APPLICATIONS OF THE THERMOKINETIC MODEL

---

senting the ignition process. The following parameters were considered:

$t_{ign}$  Ignition time in seconds ( $[T]$ )

$T_c$  Compression temperature ( $[\Theta^{-1}]$ )

$S_p$  Mean piston speed ( $[LT^{-1}]$ )

$P_o$  Initial mixture pressure ( $[ML^{-1}T^{-2}]$ )

$\Delta m$  Relative fuel/air mass ( $[M]$ )

$\Delta c_v$  Change in specific heat capacity due EGR ( $[L^2T^{-2}\Theta^{-1}]$ )

Choosing  $t_{ign}$  and  $S_p$  as the independent variables, the indicial matrix given in equation 5.11 is solved for the two right hand sides.

$$\begin{matrix} M \\ L \\ T \\ \Theta \end{matrix} \begin{bmatrix} T_c & P_o & \Delta m & \Delta c_v \\ 0 & 1 & 1 & 0 \\ 0 & -1 & 0 & 2 \\ 0 & -2 & 0 & -2 \\ -1 & 0 & 0 & -1 \end{bmatrix} = \begin{bmatrix} t_{ign} \\ 0 \\ 0 \\ 1 \\ 0 \end{bmatrix} = \begin{bmatrix} S_p \\ 0 \\ 1 \\ -1 \\ 0 \end{bmatrix} \quad (5.11)$$

The solution of the two systems gives the two parameters:

$$\Pi_1 = t_{ign} \frac{\Delta c_v^{1/6} P_o^{1/3}}{T_c^{1/6} (\Delta m)^{1/3}} \quad \Pi_2 = S_p \frac{T_c^{1/2}}{\Delta c_v^{1/2}} \quad (5.12)$$

The first parameter,  $\Pi_1$ , is a measure of energy which must be added to the system for a given ignition delay. The second parameter,  $\Pi_2$ , is the rate at which the energy is being added to the system. Values of  $\Pi_1$  and  $\Pi_2$  were calculated for each of the 53 simulations in which combustion took place and are shown in Figure 5.4. The markers in Figure 5.4 represent the simulation results from the

parameter variations given in Table 5.1 using n-heptane as a fuel, while the line represents a least squares fit of  $\Pi_2$  as a function of  $\Pi_1$ .

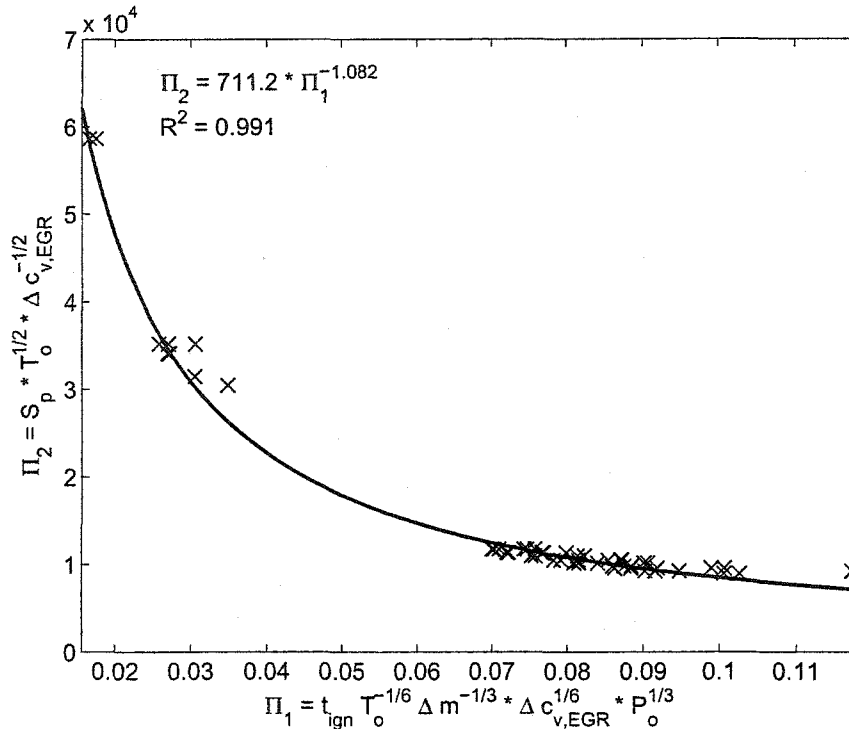


Figure 5.4: Relationship between the parameters  $\Pi_1$   $\Pi_2$ , for all fired cases in the parameter variations (see Table 5.1).

The least squares correlation given in Figure 5.4 can be rearranged such that the ignition delay is given in terms of the of the mixture state:

$$t_{ign} = 432.4 \frac{\Delta c_v^{0.295} (\Delta m)^{1/3}}{T_o^{0.295} P_o^{1/3} S_p^{0.924}} \quad (5.13)$$

As the engine speed varies, so too does the ignition delay required for constant ignition timing. For example, if TDC ignition timing is desired for all engine

speeds, the required ignition delay,  $t_{TDC}$ , is determined from:

$$t_{TDC} = \frac{\theta_{TDC} - \theta_{IVC}}{6N} = 432.4 \frac{\Delta c_v^{0.295} (\Delta m)^{1/3}}{T_o^{0.295} P_o^{1/3} S_p^{0.924}} \quad (5.14)$$

Where  $\theta_{TDC}$  is the ignition angle, in this case TDC (0 CAD aTDC), and  $\theta_{IVC}$  is the IVC crank angle (-146 CAD aTDC).

The ignition delays required for TDC and  $\pm 10$  degree (advanced and retarded) ignition timing as function of engine speed are shown as lines in Figure 5.5, along with the results from the 53 simulations (markers). For an arbitrary engine speed,  $t_{ign}$  can be evaluated using equation 5.14 and used to determine the parameters required to realize the appropriate ignition delay. Figure 5.5 lends insight to the sensitivity of the ignition process to the engine speed and what the implications are when utilizing equation 5.14. At lower engine speeds, relatively large variations in the engine parameters, and hence in  $t_{ign}$  can be tolerated while still remaining within the  $\pm 10$  CAD ignition timing interval. At higher engine speeds the engine parameters must be more accurately controlled to ensure that ignition timing is within the same interval.

## 5.4 Predicting the Ignition Timing Parametrically

To evaluate the ability of the new correlation to predict the conditions required for ignition, equation 5.14 was used to predict the engine parameters required for TDC ignition at engine speeds other than those used in the preceding parameter variations. In particular, the required initial temperature was estimated using equation 5.14 for TDC ignition with the operation conditions outlined in Table 5.3. The details of calculation of the initial temperature using equation 5.14 are given in appendix A.2.

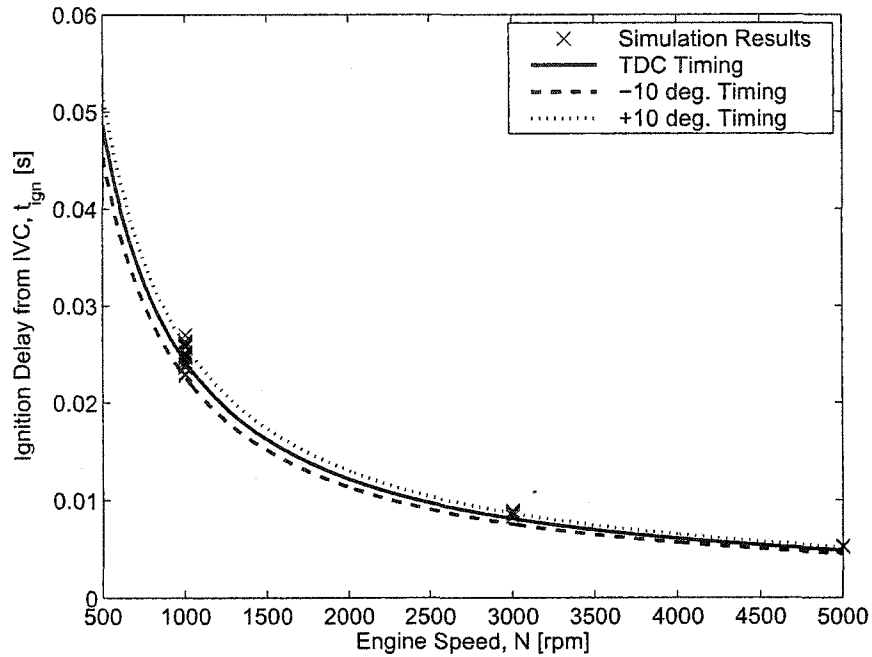


Figure 5.5: A correlation describing the initial conditions required for a given ignition timing at different engine speeds.

Table 5.3: Summary of the engine parameters used in validating the ignition correlation. Note the estimated initial temperature refers to that from the ignition correlation, while the actual temperature refers to the temperature required for TDC ignition as determined using the thermokinetic model.

	Engine Speed	
	2000rpm	4000rpm
Equivalence Ratio	0.7	0.7
EGR Fraction	0	0
Octane Number	0	0
Initial Pressure	100kPa	100kPa
Est. Initial Temp.	416K	454K
Act. Initial Temp.	375K	422K
Difference	11%	7.6%

The actual temperature required for TDC ignition timing was determined using the thermokinetic model by carrying out a temperature sweep from 340K to

430K in steps of 10K, for each of the two engine speeds. The initial temperature required for TDC ignition was interpolated from the results of the temperature sweep. The engine configuration was the same as that used in the HCCI validation and parameter variations (see Table 4.3). As shown in Table 5.3, the ignition correlation predicted the required temperature to within 11% of the actual temperature determined by the thermokinetic model. In this test of the correlation it should be noted that although the temperature was predicted for the system from which the correlation was developed, the two engine speeds at which the correlation was tested were not part of the original parameter variations. This indicates that the correlation is able to interpolate between the data to which it was fitted, illustrating that the dimensional analysis describes the physics of the ignition process.

Using the ignition correlation determined in the preceding section it is not necessary to carry out comprehensive thermokinetic simulations or experiments to determine the required engine parameters for every engine load/speed combination. Instead, values of the required conditions can be quickly estimated. This has several implications in the implementation of the HCCI cycle:

- When performing experimental investigations, it is possible to predict the approximate conditions required not only to ensure combustion at a given load/speed point, but also to have acceptable ignition timing. Furthermore, rather than exploring the entire operating regime, it is possible to only investigate several points, use this data to fit the dimensionless parameters, and subsequently “fill in” the rest of the map using the parameters.
- For the purpose of engine control in realtime, it is possible estimate the engine conditions required for a given ignition timing, and then rely on some sort of feedback (such as an ionization sensor (Herweg et al. 2003)) to

finely adjust the ignition timing.

The ignition correlation determined by the dimensional analysis will certainly not replace standard thermodynamic or chemical kinetic modelling of the HCCI engine, however it does provide a relatively simple means of estimating the required engine parameters for a given ignition timing.

#### 5.4.1 Implementing the Ignition Correlation

The ignition correlation presented in equation 5.14 is a least squares fit of the parameters  $\Pi_1$  and  $\Pi_2$ , to the results of the 53 parameter variations obtained using the thermokinetic model. This version of ignition correlation is only suitable for predicting the conditions required for ignition in the virtual engine being approximated by the thermokinetic model. How well this correlation predicts the ignition timing in a real engine has not yet been evaluated. To obtain an ignition correlation for a real engine, a similar parameter variation can be carried out on the real engine so that an engine specific relationship between  $\Pi_1$  and  $\Pi_2$  can be determined.

From this investigation it was determined that, in general,  $\Pi_1$  and  $\Pi_2$  are related through an equation of the form:

$$\Pi_2 = a\Pi_1^{-b} \quad (5.15)$$

where  $a$  and  $b$  are coefficients which were determined through a least squares fit of the parameters to the simulation results. Rather than carrying out such a comprehensive variation, future calibrations of the ignition correlation can be done by considering the operating conditions required for the same ignition timing at various engine speeds. This is in contrast to independently varying all of the

parameters at relatively few engine speeds as was done in this investigation.

## 5.5 Summary

To implement the HCCI cycle, it is necessary to be able to control the ignition timing. The effects of various engine parameters on the ignition timing were determined using the thermokinetic model by independently varying the initial mixture temperature and pressure, EGR rate, equivalence ratio and engine speed. The results of this parameter variation were used in conjunction with a dimensional analysis to form a correlation describing the conditions required to achieve a given ignition timing.

To carry out the dimensional analysis, it was necessary to determine how each of the engine parameters affected the ignition timing and how they should be represented in the dimensional analysis:

**Temperature** The mixture temperature influences the ignition timing by changing the overall reaction rate. An increase in the temperature increases the reaction rate, which decreases the ignition delay (i.e. advances the ignition timing). Therefore, the effect of the temperature was included in the dimensional analysis using *dimensions of the inverse of temperature*.

**Pressure** The mixture pressure changes the mixture concentration and hence the likelihood of molecular collisions occurring. This effect was included in the dimensional analysis using units of pressure.

**EGR Rate** From this investigation it was found that the EGR rate affects the ignition timing through changes in the specific heat capacity of the mixture. Thus the EGR rate was represented in the dimensional analysis using the *dimensions of specific heat capacity*.

**Equivalence Ratio** The equivalence ratio is a measure of the relative fuel and air quantities and was represented as the difference in the oxygen and fuel masses.

**Engine Speed** Different engine speeds change the amount of time during which ignition occurs. To account for changes in the engine speed and the engine geometry, the engine speed was represented using the mean piston speed.

Two parameters were determined from the dimensional analysis and were correlated using the results from the parameter variation. This correlation specified the relative parameter values required for a given ignition timing and was used to predict the temperatures required for TDC ignition timing at two different engine speeds. The ignition correlation was able to predict the required temperatures to within 11% of the temperatures determined using the thermokinetic model.

## Chapter 6

# Conclusions and Future Work

### 6.1 Conclusions

The focus of this thesis was to determine the effects of various engine parameters on the ignition timing of an HCCI engine, with goal of simplifying the development of HCCI control systems. To do this a thermokinetic model using a new chemical kinetic mechanism was developed and validated. 270 simulations, each with different engine operating parameters, were carried out using the thermokinetic model to determine the effect of the parameters on the ignition timing. The results of these simulations were correlated using a dimensional analysis to describe the net effect of the parameters on the ignition timing. This correlation was used to predict the required initial conditions for a specified ignition timing at different engine speeds.

The major contributions of this work are the development of a chemical kinetic mechanism capable of describing both the ignition and combustion of arbitrary PRF blends, and the correlation of engine parameters to the ignition timing. Each of these contributions are concluded in the following sections.

### 6.1.1 Thermokinetic Model

A thermokinetic model was developed by coupling a single zone thermodynamic model with a skeletal chemical kinetic mechanism. The single zone assumption implies that the thermodynamic state of the mixture is spatially uniform. This work developed a new chemical kinetic mechanism by combining existing sub-mechanisms for iso-octane and n-heptane ignition, large molecule decomposition, and CO and H<sub>2</sub> oxidation from the literature. The complete mechanism consists of 58 chemical species and 120 reactions and describes the ignition and combustion of an arbitrary PRF blend. The thermodynamic properties of each of the chemical species were either taken from existing databases or estimated based on additivity rules.

Simulation results from the thermokinetic model were compared with known results for several different combustion systems to validate the model. Combustion temperatures for an adiabatic, constant volume combustion event determined using the thermokinetic model were compared with those determined using STANJAN. The thermokinetic model was able to predict the combustion temperatures to within 8.5% of those calculated using STANJAN. To validate the ability of the thermokinetic model to predict ignition delays, experimental results from a rapid compression machine (Park & Keck 1990) and a shock tube (Fieweger et al. 1997) were compared to those predicted by the thermokinetic model. From these validations, it was shown that the model is capable of predicting the qualitative effects of the temperature, pressure, and octane number on the ignition delay. A comparison of pressure histories calculated by the thermokinetic model with pressure histories obtained experimentally from an HCCI engine (Atkins 2004) was used to determine the model's applicability to HCCI. Three different engine operating points, each with a different fuel octane number, EGR rate and equivalence ratio were simu-

lated and compared to the experimental results. The thermokinetic model was able to predict the ignition timing of each of the points to within 1 CAD of the range observed experimentally.

The thermokinetic model was not capable of predicting the combustion duration and exhaust gas composition in an HCCI engine due to the single zone approximation which was used. This limitation of the single zone model has been noted by other researchers (Aceves et al. 1999) and was known at the onset of this work. The goal of this investigation, which has been accomplished, was to develop a model capable of confidently predicting the ignition timing in an HCCI engine.

### 6.1.2 Parameter Variations

While the thermokinetic model is capable of predicting the effect of engine parameters on the ignition timing, it does not directly indicate what conditions are required to ensure combustion at a given ignition timing. In order to develop such a criteria, the mixture temperature, pressure, equivalence ratio, EGR rate and engine speed were varied independently using the thermokinetic model and the effect on the ignition timing was noted. Two parameters were determined using a dimensional analysis, one representing the rate at which energy is added to the system, and the other representing the thermodynamic state required for ignition. By determining a relationship between these two parameters based on the results of the parameter variations, it was possible to determine a correlation which specifies the conditions required for a given ignition timing.

The applicability of such a correlation was illustrated when it was used to determine the initial temperature required to maintain a given ignition timing for two engine speeds, given the same equivalence ratio, initial pressure, EGR rate and fuel composition. The initial temperature predicted using the ignition correlation

was within 11% of the actual temperature as determined using the thermokinetic model. This ignition correlation can be implemented in a control application and used as a simple model to predict the conditions required for ignition. Furthermore, it can be used to expedite experimental investigations. Rather than having to iteratively determine the conditions required for ignition, the correlation can predict them relatively quickly. It is not necessary to investigate the entire engine speed/load regime, as it is possible to determine only several points experimentally and use the relationship between the two dimensionless parameters to determine the conditions at the interim points.

## 6.2 Future Work

The thermokinetic model and ignition correlation presented in this work are useful tools in gaining insight to the HCCI cycle. There are, however, still improvements and further refinements that can be made.

### 6.2.1 Thermokinetic Model

#### Extend to Multi-zone Model

The focus of this investigation was the determination of the effects of various parameters on the ignition timing in an HCCI engine. A single zone model is well suited to this, but by the inclusion of the effects of spatial variations in temperature and mixture composition, it would also become possible to more accurately predict the exhaust gas composition and combustion duration. Viable HCCI operation requires not only appropriate ignition timing, but an acceptable combustion duration as well. Too rapid of a combustion event can damage the engine and too slow of a combustion event can lead to incomplete combustion. The exhaust

gas composition should also be considered to ensure that excess pollutants, such as CO, NO<sub>x</sub>, or uHC, are not being formed. Methods of increasing the number of thermodynamic zones to include spatial variations in the thermodynamic state are discussed in section 2.3.

### **Reduce the Chemical Kinetic Mechanism**

The number of differential equations requiring solution in a multi-zone model increase linearly with the number of thermodynamic zones. For example, a two zone model will have twice as many differential equations to solve than a single zone model. To decrease the number of computations for a multi-zone model, the chemical kinetic mechanism can be reduced. Reduction methods such as those described in section 2.3.1 can be used to reduce the chemical kinetic mechanism.

The H<sub>2</sub>/O<sub>2</sub> sub-mechanism in particular could be the focus of such a reduction investigation. A comprehensive H<sub>2</sub>/O<sub>2</sub> sub-mechanism was included in this investigation as there was a possibility of using hydrogen as a supplemental fuel. If this is not done, this sub-mechanism could be reduced. For such a reduction analysis, the ignition timing, combustion duration, and exhaust gas compositions must all be considered in order to ensure the validity of the resulting mechanism and comparison with experimental data from an HCCI engine would be required.

### **Incorporate Thermokinetic Model into a Full Cycle Simulation**

This investigation focusses only on the closed portion of the engine cycle (i.e. from IVC to EVO) and determines the initial mixture composition from a set of general equations. Instead, the thermokinetic model can be incorporated into a model describing the entire engine cycle, including the gas exchange process (i.e. the intake and exhaust strokes). The mixture composition at the beginning of

compression can then be determined based on the inducted charge, which may be a mixture of fresh air, fuel and exhaust gases from the preceding cycle. Furthermore, it becomes possible to investigate different Variable Valve Train (VVT) applications such as internal EGR or changes in the effective compression ratio by changing the timing of IVC (Law et al. 2002, Agrell et al. 2003).

A thermokinetic model describing the complete engine cycle can also be used to investigate different change over strategies between SI and HCCI. As HCCI is not well suited to high load operation (due to the high rates of pressure rise), SI operation can be used at higher engine loads. Switching between HCCI and SI operation requires that engine parameters, such as the EGR rate and equivalence ratio are changed in sequential cycles. A complete engine simulation could be used to determine what the changes should be, and how to implement them.

### **Extend the Ignition Correlation**

Currently, the ignition correlation only indicates the conditions required for a given ignition timing, but gives no insight to the subsequent combustion process. It does not indicate whether or not the combustion duration is appropriate, or if the exhaust gas composition is acceptable from an emissions standpoint. A multi-zone thermokinetic model could be used to carry out parameter variations, similar to those in this investigation, to determine the effect of the engine parameters on the exhaust gas composition and combustion duration. By incorporating these variables as well, it would be possible to not only determine the conditions required for a particular ignition timing, but also to achieve an acceptable combustion event from an engine durability and emissions standpoint. This would then provide an overall HCCI operation criteria, specifying the conditions for desired ignition timing and appropriate combustion duration and acceptable emissions.

# Bibliography

- Aceves, S. M., Flowers, D., Martinez-Frias, J., Smith, J. R., Dibble, R., Au, M. & Girard, J. (2001), 'HCCI combustion: analysis and experiments'. SAE 2001-01-2077.
- Aceves, S. M., Smith, J. R., Westbrook, C. K. & Pitz, W. J. (1999), 'Compression ratio effect on methane HCCI combustion', *Journal of Engineering for Gas Turbines and Power Transactions of the Asme* **121**(3), 569–574.
- Agrell, F., Ångström, H. E., Eriksson, B., Wikander, J. & Linderyd, J. (2003), 'Integrated simulation and engine test of closed-loop HCCI control by aid of variable valve timings'. SAE 2003-01-0748.
- Assanis, D. N. & Heywood, J. B. (1986), 'Development and use of a computer simulation of the turbocompounded diesel system for engine performance and component heat transfer studies'. SAE 860329.
- Atkins, M. (2004), Experimental Examination of the effects of Fuel Octane and Diluent on HCCI Combustion, M.Sc. Thesis, University of Alberta.
- Benson, S. W. (1976), *Thermochemical Kinetics*, 2nd edn, Wiley, New York.

## BIBLIOGRAPHY

---

- Benson, S. W. (1981), 'The kinetics and thermochemistry of chemical oxidation with application to combustion and flames', *Progress in Energy and Combustion Science* **7**, 125–134.
- Benson, S. W. & Buss, J. H. (1958), 'Additivity Rules for the Estimation of Molecular Properties. Thermodynamic Properties', *The Journal of Chemical Physics* **29**(3), 546–572.
- Borman, G. & Nishiwaki, K. (1987), 'A Review of Internal Combustion Engine Heat Transfer', *Progress in Energy and Combustion Science* **13**(1), 1–46.
- Buckingham, E. (1914), 'On Physically Similar Systems; Illustrations of the use of Dimensional Equations', *Physical Review* **4**(4), 345–376.
- Bulaty, T. & Glanzmann, W. (1984), 'Bestimmung Der Wiebe-Verbrennungsparameter', *MTZ Motortech Z. v 45 n 7 8 Jul Aug 1984*, p 299 303 .
- Burcat, A. (1984), Thermochemical Data for Combustion Calculations, in W. C. Gardiner, ed., 'Combustion Chemistry', Springer-Verlag, New York, pp. 455–473.
- Burcat, A. (2001), Third Millenium Ideal Gas and Condensed Phase Thermochemical Database for Combustion, Technical Report TAE 867, Faculty of Aerospace Engineering, Israel Institute of Technology. <ftp.technion.ac.il/pub/supported/aetdd/thermodynamics>.
- Cengel, Y. A. & Boles, M. A. (1998), *Thermodynamics: An Engineering Approach*, 3rd edn, McGraw Hill.
- Checkel, M. D. & Dale, J. D. (1986), 'Computerized knock detection from engine pressure records'. SAE 860028.

## BIBLIOGRAPHY

---

- Chen, R., Milovanovic, N., Turner, J. & Blundell, D. (2003), 'The thermal effect of internal exhaust gas recirculation on controlled auto-ignition'. SAE 2003-01-0751.
- Côme, G.-M. (2001), *Gas-Phase Thermal Reactions : Chemical Engineering Kinetics*, Kluwer Academic Publishers, Boston.
- Curran, H. J., Gaffuri, P., Pitz, W. J. & Westbrook, C. K. (1998), 'A comprehensive modeling study of n-heptane oxidation', *Combustion and Flame* **114**(1-2), 149-177.
- Curran, H. J., Gaffuri, P., Pitz, W. J. & Westbrook, C. K. (2002), 'A comprehensive modeling study of iso-octane oxidation', *Combustion and Flame* **129**(3), 253-280.
- Dryer, F. L. & Glassman, I. (1977), Combustion Chemistry of Chain Hydrocarbons, in C. Bowmann & J. Birkeland, eds, 'Alternative Hydrocarbon Fuels: Combustion and Chemical Kinetics', Vol. 62 of *Progress in Astronautics and Aeronautics*, American Institute of Aeronautics and Astronautics, Columbia, Maryland.
- Eng, J. (2003), Kinetics of HCCI Combustion, in F. Zhao, T. Asmus, D. N. Assanis, J. E. Dec, J. Eng & P. Najt, eds, 'Homogeneous Charge Compression Ignition (HCCI) Engines: Key Research and Development Issues', Society of Automotive Engineers.
- Fieweger, K., Blumenthal, R. & Adomeit, G. (1997), 'Self-ignition of SI engine model fuels: A shock tube investigation at high pressure', *Combustion and Flame* **109**(4), 599-619.

## BIBLIOGRAPHY

---

- Fiveland, S. B. & Assanis, D. N. (2001), 'Development of a two-zone HCCI combustion model accounting for boundary layer effects'. SAE 2001-01-1028.
- Flowers, D. L., Aceves, S. M., Martinez-Frias, J. & Dibble, R. W. (2003), 'Prediction of carbon monoxide and hydrocarbon emissions in iso-octane HCCI engine combustion using multizone simulations', *Proceedings of the Combustion Institute* **29**, 687–694.
- Gardiner, W. C. & Burcat, A. (1984), *Combustion chemistry*, Springer-Verlag, New York.
- Glassman, I. (1996), *Combustion*, 3rd edn, Academic Press, San Diego, Calif.
- Griffiths, J. F., Hughes, K. J., Schreiber, M. & Poppe, C. (1994), 'A Unified Approach to the Reduced Kinetic Modeling of Alkane Combustion', *Combustion and Flame* **99**(3-4), 533–540.
- Griffiths, J. F., Jiao, Q., Kordylewski, W., Schreiber, M., Meyer, J. & Knoche, K. F. (1993), 'Experimental and Numerical-Studies of Ditertiary Butyl Peroxide Combustion at High-Pressures in a Rapid Compression Machine', *Combustion and Flame* **93**(3), 303–315.
- Halstead, M. P., Kirsch, L. J. & Quinn, C. P. (1977), 'Autoignition of Hydrocarbon Fuels at High Temperatures and Pressures - Fitting of a Mathematical Model', *Combustion and Flame* **30**(1), 45–60.
- Haraldsson, G., Tunestål, P., Johansson, B. & Hyvönen, J. (2003), 'HCCI combustion phasing with closed-loop combustion control using variable compression ratio in a multi-cylinder engine'. SAE 2003-01-1830.

## BIBLIOGRAPHY

---

- Haraldsson, G., Tunestål, P., Johansson, B. & Hyvönen, J. (2004), 'HCCI Closed-Loop Combustion Control Using Fast Thermal Management'. SAE 2004-01-0943.
- Herweg, R., Kessler, M., Kirchen, P., Pfeffer, V. & Schäflein, J. (2003), 'Method for Operating an Internal Combustion Engine'. Patent Application Number WO 002003085244 A1.
- Heywood, J. B. (1988), *Internal combustion engine fundamentals*, McGraw-Hill, New York.
- Hu, H. & Keck, J. (1987), 'Autoignition of adiabatically compressed combustible gas mixtures'. SAE 872110.
- Hyvönen, J., Haraldsson, G. & Johansson, B. (2003), 'Supercharging HCCI to Extend the Operating Range in a Multi-Cylinder VCR HCCI Engine'. SAE 2003-01-3214.
- Isaacson, E. & Isaacson, M. (1975), *Dimensional methods in engineering and physics: reference sets and the possibilities of their extension*, Edward Arnold, London.
- Kong, S. C. & Reitz, R. D. (2003), 'Application of detailed chemistry and CFD for predicting direct injection HCCI engine combustion and emissions', *Proceedings of the Combustion Institute* **29**, 663–669.
- Law, D., Allen, J. & Chen, R. (2002), 'On the mechanism of controlled auto ignition'. SAE 2002-01-0421.
- Lee, W., Yoon, M. & Sunwoo, M. (2003), 'A cost- and time-effective hardware-in-the-loop simulation platform for automotive engine control systems', *Proceed-*

## BIBLIOGRAPHY

---

- ings of the Institution of Mechanical Engineers Part D- Journal of Automobile Engineering* **217**(D1), 41-52.
- Li, H., Miller, D. & Cernansky, N. P. (1992), 'A Study on the Application of a Reduced Chemical Reaction Model to Motored Engines for Heat Release Prediction'. SAE 922328.
- Li, H., Miller, David, L. & Cernansky, N. P. (1996), 'Development of a reduced chemical kinetic model for prediction of preignition reactivity and autoignition of primary reference fuels'. SAE 960498.
- Lindemann, F. A. (1922), 'The radiation theory of chemical action', *Transactions of the Faraday Society* **17**, 599.
- Marinov, N. M., Westbrook, C. K. & Pitz, W. J. (1995), Detailed and Global Chemical Kinetics Model for Hydrogen, *in* 'Transport Phenomena in Combustion: Proceeding of the Eighth International Symposium on Transport Phenomena', Taylor and Francis, San Francisco, California, USA, pp. 118-130.
- Martinez-Frias, J., Aceves, S. M., Flowers, D., Smith, J. R. & Dibble, R. (2001), 'Equivalence ratio-EGR control of HCCI engine operation and the potential for transition to spark-ignited operation'. SAE 2001-01-3613.
- Mcbride, B. J., Gordon, S. & Reno, M. A. (1993), Coefficients for calculating thermodynamic and transport properties of individual species, Technical Report NASA-TM-4513 E-7981 NAS 1.15:4513, NASA Lewis Research Center.
- Minetti, R., Carlier, M., Ribaucour, M., Therssen, E. & Sochet, L. R. (1995), 'A rapid compression machine investigation of oxidation and auto-ignition of n-

## BIBLIOGRAPHY

---

- heptane: Measurements and modeling', *Combustion and Flame* **102**(3), 298–309.
- Muller, C., Michel, V., Scacchi, G. & Come, G. (1995), 'THERGAS: a computer program for the evaluation of thermochemical data of molecules and free radical in the gas phase', *Journal de Chimie Physique et de Physico-Chimie Biologique* **92**(5), 1154–1178.
- Najt, P. M. & Foster, D. E. (1983), 'Compression-ignited homogeneous charge combustion'. SAE 830264.
- Olsson, J.-O., Tunestål, P. & Johansson, B. (2004), 'Boosting for High Load HCCI'. SAE-2004-01-0940.
- Onishi, S., Jo, S. H., Shoda, K., Jo, P. D. & Kato, S. (1979), 'Active Thermo-Atmosphere Combustion (ATAC) a new combustion process for internal combustion engines'. SAE 790501.
- Park, P. & Keck, J. C. (1990), 'Rapid compression machine measurements of ignition delays for primary reference fuels'. SAE 900027.
- Rassweiler, G. M. & Withrow, L. (1938), 'Motion Pictures of Engine Flames Correlated with Pressure Cards', *SAE* **42**(5), 185–204.
- Reaction Design Inc. (2004), 'CHEMKIN'. Version 4.0.
- Reynolds, W. (1987), 'STANJAN Chemical equilibrium solver'. v3.91, IBM-PC.
- Ritter, E. R. & Bozzelli, J. W. (1991), 'Therm - Thermodynamic Property Estimation for Gas-Phase Radicals and Molecules', *International Journal of Chemical Kinetics* **23**(9), 767–778.

## BIBLIOGRAPHY

---

- Scott, D. (1974), *Chemical Thermodynamic Properties of Hydrocarbons and Related Substances. Properties of the Alkane Hydrocarbons, C1 through C10 in the Ideal Gas State from 0 to 1500K.*, Technical Report Bulletin 666, U.S. Bureau of Mines.
- Semenov, N. N. (1935), *Chemical Kinetics and Chain Reactions*, Oxford.
- Sjöberg, M. & Dec, J. E. (2003), 'A parametric study of HCCI combustion The sources of emissions at low loads and the effects of GDI fuel injection'. SAE 2003-01-3173.
- Slavinskaya, N. A. & Haidn, O. J. (2003), 'Modeling of n-heptane and iso-octane oxidation in air', *Journal of Propulsion and Power* **19**(6), 1200–1216.
- Smith, G., Golden, D., Frenklach, M., Moriarty, N., Eiteneer, B., Goldenberg, M., Bowman, C., Hanson, R., Song, S., Gardiner, W. C., Lissianski, V. V. & Qin, Z. (2004), 'GRI-Mech 3.0'. <http://www.me.berkeley.edu/gri-mech/version30/text30.html>.
- Soyhan, H. S., Mauss, F. & Sorousbay, C. (2002), 'Chemical kinetic modeling of combustion in internal combustion engines using reduced chemistry', *Combustion Science and Technology* **174**(11-2), 73–91.
- Stein, S. E. & Brown, R. L. (2003), Structures and Properties Group Additivity Model, in P. J. Linstrom & W. G. Mallard, eds, 'NIST Chemistry WebBook, NIST Standard Reference Database Number 69', National Institute of Standards and Technology, Gaithersburg MD, 20899. <http://webbook.nist.gov>.
- Sun, R., Thomas, R. & Gray, C. L. (2004), 'An HCCI Engine: Power Plant for a Hybrid Vehicle'. SAE 2004-01-0933.

## BIBLIOGRAPHY

---

- Tanaka, S., Ayala, F. & Keck, J. C. (2003), 'A Reduced chemical kinetic model for HCCI combustion of primary reference fuels in a rapid compression machine', *Combustion and Flame* **133**(4), 467–481.
- The Mathworks Inc. (2002), 'Matlab'. Version 6.5, Release 13.
- Thring, R. H. (1989), 'Homogeneous Charge Compression Ignition (HCCI) engines'. SAE 892068.
- Tunestål, P., Olsson, J. & Johansson, B. (2002), Closed Loop Control of HCCI Engines, *in* R. Johansson & A. Rantzer, eds, 'Nonlinear and Hybrid Systems in Automotive Control', Springer-Verlag, Lund.
- Vibe, I. (1970), *Brennverlauf und Kreisprozess von Verbrennungsmotoren*, VEB Verlag Technik, Berlin.
- Warnatz, J., Maas, U. & Dibble, R. W. (2001), *Combustion : physical and chemical fundamentals, modeling and simulation, experiments, pollutant formation*, 3rd edn, Springer, New York.
- Westbrook, C. E. & Dryer, F. L. (1984), 'Chemical Kinetic Modeling of Hydrocarbon Combustion', *Progress in Energy and Combustion Science* **10**, 1–57.
- Westbrook, C. K. (2000), 'Chemical kinetics of hydrocarbon ignition in practical combustion systems', *Proceedings of the Combustion Institute* **28**, 1563–1577.
- Woschni, G. (1967), 'Universally applicable equation for the instantaneous heat transfer coefficient in the internal combustion engine'. SAE 670931.
- Zhao, H., Peng, Z. & Ladommatos, N. (2001), 'Understanding of controlled autoignition combustion in a four-stroke gasoline engine', *Proceedings of the*

## BIBLIOGRAPHY

---

*Institution of Mechanical Engineers Part D Journal of Automobile Engineering* **215**(D12), 1297–1310. 2001.

Zheng, J. (2002). Personal communication.

Zheng, J., Yang, W., Miller, D. L. & Cernansky, N. P. (2001), 'Prediction of pre-ignition reactivity and ignition delay for HCCI using a reduced chemical kinetic model'. SAE 2001-01-1025.

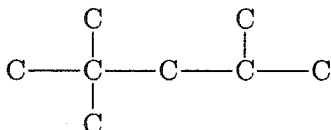
Zheng, J., Yang, W., Miller, D. L. & Cernansky, N. P. (2002), 'A skeletal chemical kinetic model for the HCCI combustion process'. SAE 2002-01-0423.

## Appendix A

# Sample Calculations

### A.1 Estimation of the Specific Heat of Iso-Octane

Given that a molecule consists of two or more polyvalent atoms, it can be decomposed into its constituent groups and the thermodynamic properties can be determined. For example, iso-octane (2,2,4-trimethyl-pentane) has the structure:



Note that hydrogen atoms are not indicated in this diagram, however their location and number can be determined from the number of free valences on each carbon atom. This structure can then be decomposed into its constituent polyvalent atomic groups as follows:

$(\text{C}-(\text{H})_3\text{C}) \times 5$  Five groups consisting of one carbon atom singly bonded to one other carbon atom and three hydrogen atoms.

## APPENDIX A: SAMPLE CALCULATIONS

---

$(\text{C}-(\text{C})_4) \times 1$  One group consisting of one carbon atom singly bonded to four other carbon atoms.

$(\text{C}-(\text{C})_2(\text{H})_2) \times 1$  One group consisting of one carbon atom singly bonded to two carbon atoms and two hydrogen atoms.

$(\text{C}-(\text{C})_3\text{H}) \times 1$  One group consisting of one carbon atom singly bonded to three carbon atoms and one hydrogen atom.

Each of these groups has a characteristic contribution to specific heat (and hence enthalpy and entropy). These values are available in tabulated form up to temperatures of 1000 or 1500K in Benson (1976) or Côme Côme (2001), for example. As iso-octane is an alkane (i.e. has only single bonds) there are no corrections required for *cis* and *trans* isomers. Using the values tabulated in Benson for the above groups, the specific heat of iso-octane at  $T = 300\text{K}$  was found to be  $\bar{c}_{p,300} = 45.4\text{cal/mole-K}$ , which agrees within 0.2% of the true value (Scott 1974).

## A.2 Example using the Ignition Correlation

Below is an example of how the ignition correlation given in equation 5.14 can be used to determine the conditions for a specific ignition timing. In particular, this example will discuss how the initial temperatures were determined for the discussion in section 5.4

### A.2.1 Problem Statement

Given the following engine parameters, determine initial mixture temperature such that ignition will occur at TDC.

Table A.1: Summary of the engine parameters used in validating the ignition correlation.

	Engine Speed	
	2000rpm	4000rpm
Equivalence Ratio	0.7	0.7
EGR Fraction	0	0
Octane Number	0	0
Compression Ratio	11	11
Piston Stroke	11.4cm	11.4cm
IVC Angle	34 CAD aTDC	34 CAD aTDC
Initial Pressure	100kPa	100kPa
Req. Initial Temp.	?	?

### A.2.2 Solution

Using the ignition criteria, equation 5.14:

$$t_{TDC} = \frac{\theta_{TDC} - \theta_{IVC}}{6N} = \frac{146^\circ}{6N} = \begin{cases} 1.217 * 10^{-2} & \text{At 2000rpm} \\ 6.083 * 10^{-3} & \text{At 4000rpm} \end{cases} \quad (\text{A.1})$$

The required initial conditions can be determined using equation 5.14 and

## APPENDIX A: SAMPLE CALCULATIONS

---

substituting the values specific to this operation:

$$t_{\text{TDC}} = 1.217 * 10^{-2} = 432.4 \frac{\Delta c_v^{0.295} (\Delta m)^{1/3}}{T_o^{0.295} P_o^{1/3} S_p^{0.924}} \quad (\text{A.2})$$

The determination of each of the variables on the right hand side is discussed in further detail below.

### Relative Fuel Mass

The definition of  $\Delta m$  from equation 5.9 is:

$$\Delta m = m_{\text{O}_2} - m_{\text{fuel}} \quad (\text{5.9})$$

or in molar terms:

$$\Delta m = N_{\text{O}_2} M_{\text{O}_2} - N_{\text{fuel}} M_{\text{fuel}} \quad (\text{A.3})$$

Where  $M_{\text{O}_2}$  and  $M_{\text{fuel}}$  are the molar masses of oxygen and the fuel being considered, respectively. As the mixture composition is generally only known in terms of concentration, equation A.3 can be expressed using the mole fraction,  $Y_i$ :

$$\Delta m = (Y_{\text{O}_2} M_{\text{O}_2} - Y_{\text{fuel}} M_{\text{fuel}}) N_{\text{total}} \quad (\text{A.4})$$

The total number of moles,  $N_{\text{total}}$  can be determined from the ideal gas law, equation 3.58, while the mole fractions are determined using the stoichiometric coefficients described in section 3.5.1:

$$Y_i = \frac{\beta_i}{\sum \beta_i} \quad (\text{A.5})$$

## APPENDIX A: SAMPLE CALCULATIONS

---

By combining equations A.4, A.5, and the ideal gas law, the relative fuel mass is defined by:

$$\Delta m = (\beta_{O_2} M_{O_2} - \beta_{fuel} M_{fuel}) \frac{P_o V_o}{R_u T_o \sum \beta_i} \quad (A.6)$$

In the case of this example, the relative fuel mass is then:

$$\Delta m = \frac{40.34}{T_o} \quad (A.7)$$

### EGR

The change in the mixture specific heat capacity due to the addition of EGR is represented numerically using:

$$\Delta c_v = (1 + EGR) \quad (A.8)$$

Thus for this example,  $\Delta c_v$  has a value of unity.

### Initial Pressure

The initial pressure of the mixture is represented using the cylinder pressure at IVC. For this example this leads to:

$$P_o = 100\text{kPa} \quad (A.9)$$

### Mean Piston Speed

The mean piston speed is defined by:

$$\bar{S}_p = \frac{LN}{30} \quad (A.10)$$

## APPENDIX A: SAMPLE CALCULATIONS

---

Where  $L$ , the piston stroke length, is given in centimeters. The mean piston speed is 762cm/s and 1524cm/s at 2000rpm and 4000rpm, respectively.

### Compression Temperature

The mixture temperature at the end of compression is estimated using the adiabatic compression relationship:

$$T_c = T_o C R^{k-1} \quad (\text{A.11})$$

The ratio of specific heat capacities,  $k$ , was defined as being 1.36 during the derivation of equation A.2 and the same value will be used here.

### A.2.3 Determining the Required Temperature

The temperature required for TDC ignition timing, given the operating conditions outlined in table A.1, can be determined by combining equations A.2, A.7, A.8, A.9, A.10, and A.11. The initial temperatures required for TDC ignition, estimated using the ignition correlation, are:

$$T_o = 416K \quad \text{at 2000rpm}$$

$$T_o = 454K \quad \text{at 4000rpm}$$

### A.3 Calculation Specific Heats

In order to investigate the thermal effect of EGR (see section 2.2.7), the specific heat capacity of a fuel/air mixture and the corresponding exhaust mixture was calculated. In addition, the ratio of specific heats were also compared.

#### A.3.1 Combustion Equation

The mixture composition is described using the balanced combustion equation for a stoichiometric mixture of iso-octane and air:



The specific heat of mixture,  $c_{p,m}$ , can be determined using:

$$c_{p,m} = \sum_i m f_i c_{p,i} \quad (\text{A.13})$$

Where  $m f_i$  is the mass fraction of the  $i^{\text{th}}$  specie and  $c_{p,i}$  is the specific heat capacity of the  $i^{\text{th}}$  specie. Using the following values, the specific heat of the fuel/air mixture at 300K,  $c_{p,f/a}$ , was found to be:

$$m f_{\text{C}_8\text{H}_{18}} = 0.0623 \quad c_{p,\text{C}_8\text{H}_{18}} = 1.65 \frac{\text{kJ}}{\text{kgK}} \quad \text{from Heywood (1988)} \quad (\text{A.14})$$

$$m f_{\text{O}_2} = 0.219 \quad c_{p,\text{O}_2} = 0.918 \frac{\text{kJ}}{\text{kgK}} \quad \text{from Glassman (1996)} \quad (\text{A.15})$$

$$m f_{\text{N}_2} = 0.719 \quad c_{p,\text{N}_2} = 1.04 \frac{\text{kJ}}{\text{kgK}} \quad \text{from Glassman (1996)} \quad (\text{A.16})$$

$$c_{p,f/a} = 1.05 \frac{\text{kJ}}{\text{kgK}} \quad (\text{A.17})$$

## APPENDIX A: SAMPLE CALCULATIONS

---

The ratio of specific heat capacities can be determined using:

$$k_{f/a} = \frac{c_p}{c_p - R_m} \quad (\text{A.18})$$

Where  $R_m$  is the real gas constant of the mixture and is defined by:

$$R_m = \frac{R_u}{M_m} = \frac{R_u}{\frac{m_m}{N_m}} \quad (\text{A.19})$$

Then for this example, the ratio of specific heats is:

$$k_{f/a} = \frac{c_p}{c_p - \frac{R_u}{m_m/N_m}} = \frac{1.05}{1.05 - \frac{8.31}{1830/60.5}} = 1.36 \quad (\text{A.20})$$

To calculate the specific heat capacity of the exhaust gases, the following values were used:

$$mf_{\text{CO}_2} = 0.192 \quad c_{p,\text{CO}_2} = 0.846 \frac{\text{kJ}}{\text{kgK}} \quad \text{from Glassman (1996)} \quad (\text{A.21})$$

$$mf_{\text{H}_2\text{O}} = 0.0885 \quad c_{p,\text{H}_2\text{O}} = 1.87 \frac{\text{kJ}}{\text{kgK}} \quad \text{from Glassman (1996)} \quad (\text{A.22})$$

$$mf_{\text{N}_2} = 0.719 \quad c_{p,\text{N}_2} = 1.04 \frac{\text{kJ}}{\text{kgK}} \quad \text{from Glassman (1996)} \quad (\text{A.23})$$

Resulting in the following values:

$$c_{p,EGR} = 1.08 \frac{\text{kJ}}{\text{kgK}} \quad (\text{A.24})$$

$$k_{EGR} = 1.37 \quad (\text{A.25})$$

## Appendix B

# Extrapolated $c_p$ Fits

The following figures represent the estimations of the specific heat capacities using the methods presented in section 3.3. The points in each figure represent the specific heat capacities estimated using the NIST implementation (Stein & Brown 2003) of the Benson Additivity Rules (Benson 1976). These values were extrapolated to 5000K using the Wilhoit polynomials (equation 3.27) (Burcat 1984), the coefficients of which are given on each figure.

## APPENDIX B: EXTRAPOLATED $C_P$ FITS

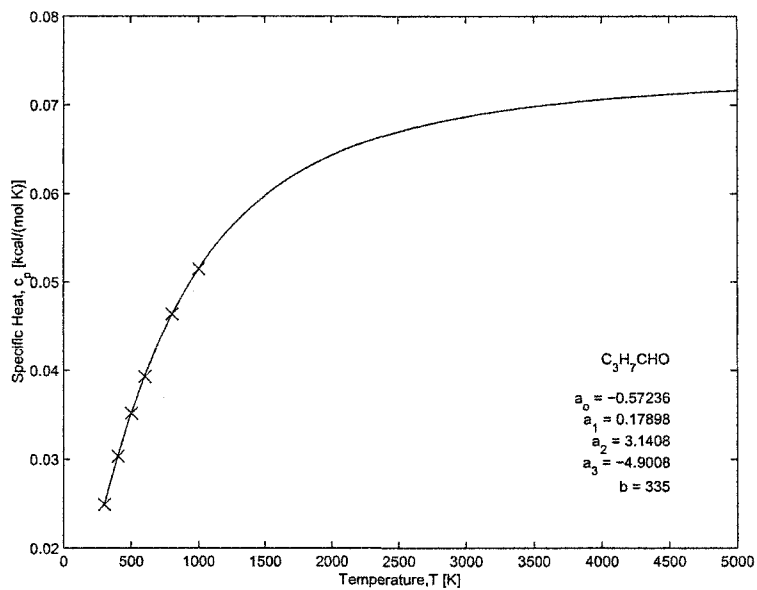


Figure B.1: Estimation of the specific heat of  $C_3H_7CHO$ .

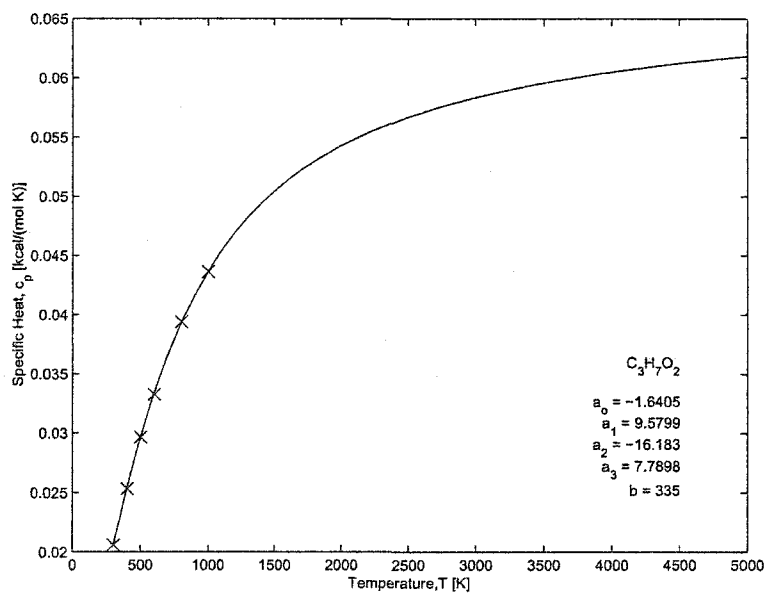


Figure B.2: Estimation of the specific heat of  $C_3H_7O_2$ .

APPENDIX B: EXTRAPOLATED  $C_P$  FITS

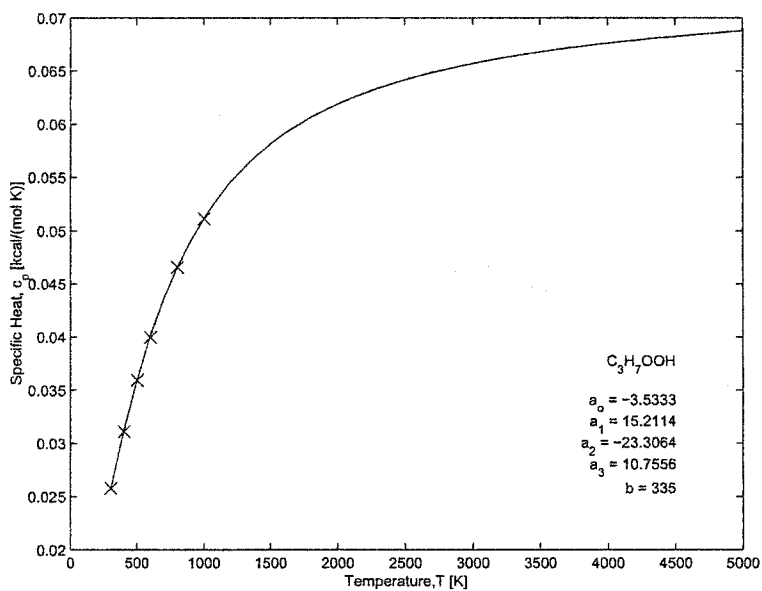


Figure B.3: Estimation of the specific heat of  $C_3H_7OOH$ .

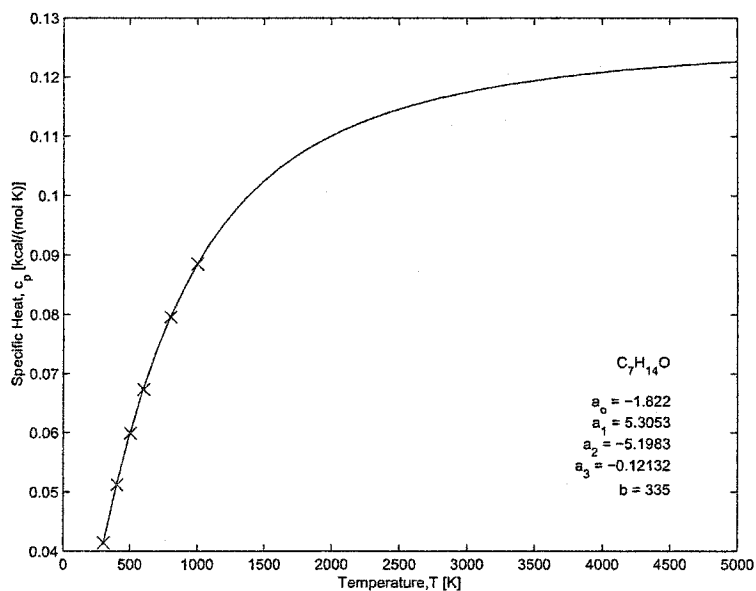


Figure B.4: Estimation of the specific heat of  $C_7H_{14}O$ .

APPENDIX B: EXTRAPOLATED  $C_P$  FITS

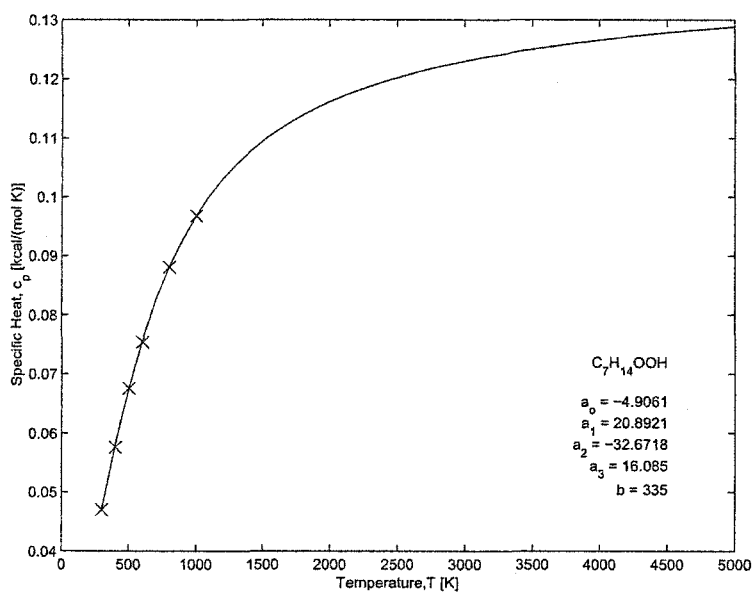


Figure B.5: Estimation of the specific heat of  $C_7H_{14}OOH$ .

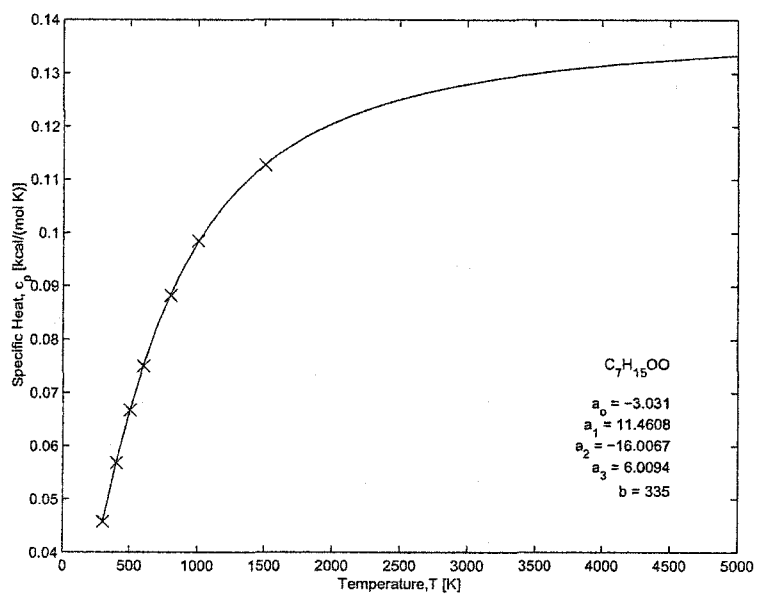


Figure B.6: Estimation of the specific heat of  $C_7H_{15}OO$ .

APPENDIX B: EXTRAPOLATED  $C_P$  FITS

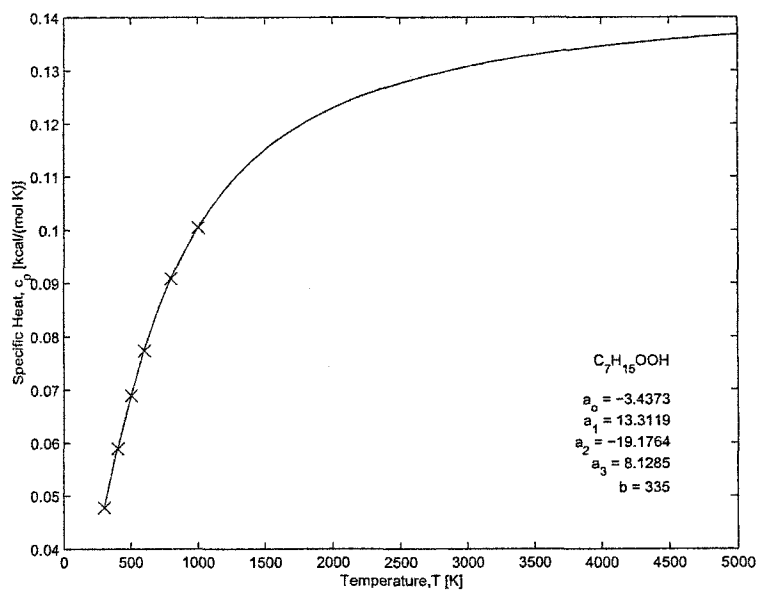


Figure B.7: Estimation of the specific heat of  $C_7H_{15}OOH$ .

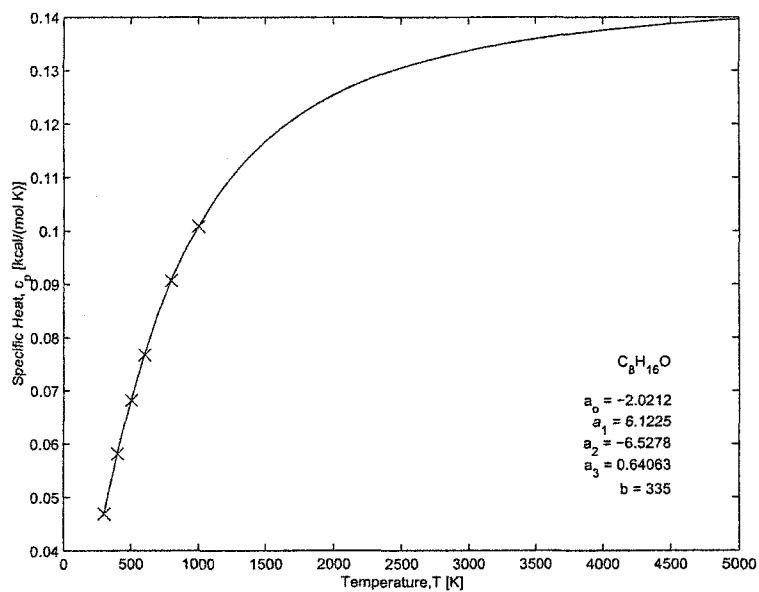


Figure B.8: Estimation of the specific heat of  $C_8H_{16}O$ .

APPENDIX B: EXTRAPOLATED  $C_P$  FITS

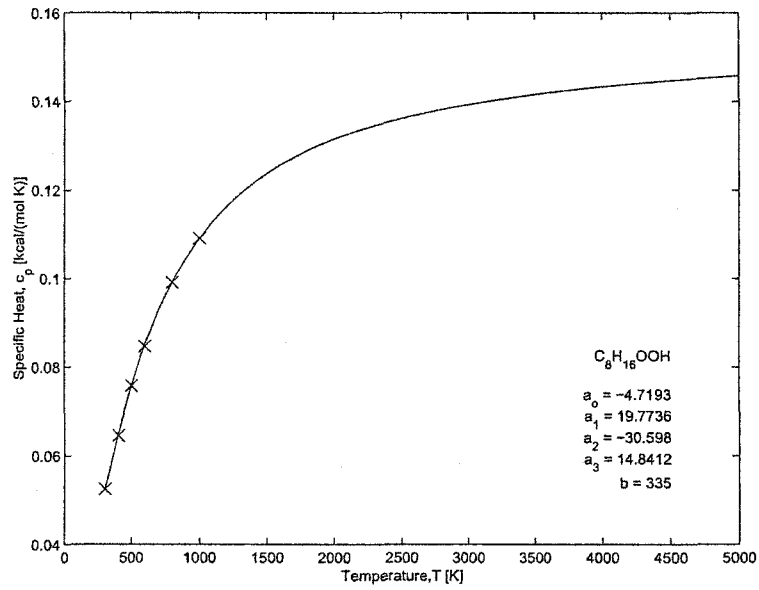


Figure B.9: Estimation of the specific heat of  $C_8H_{16}OOH$ .

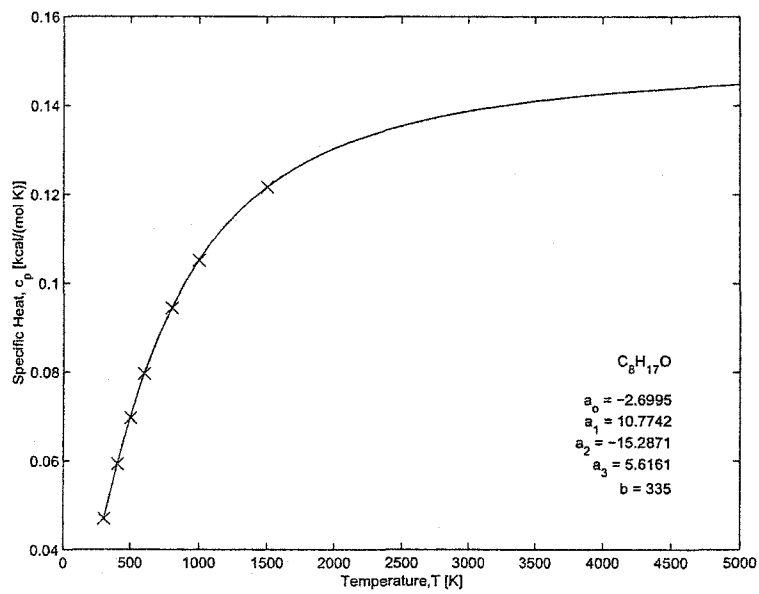


Figure B.10: Estimation of the specific heat of  $C_8H_{17}O$ .

APPENDIX B: EXTRAPOLATED  $C_P$  FITS

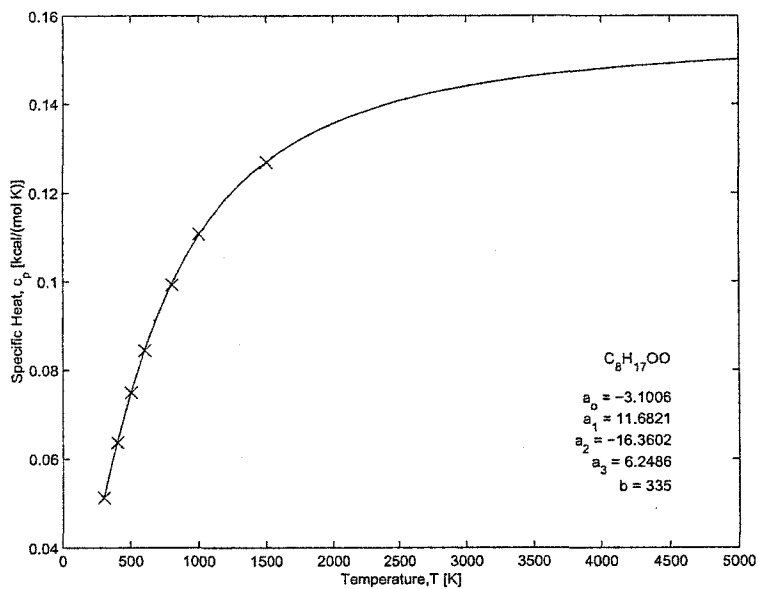


Figure B.11: Estimation of the specific heat of  $C_8H_{17}OO$ .

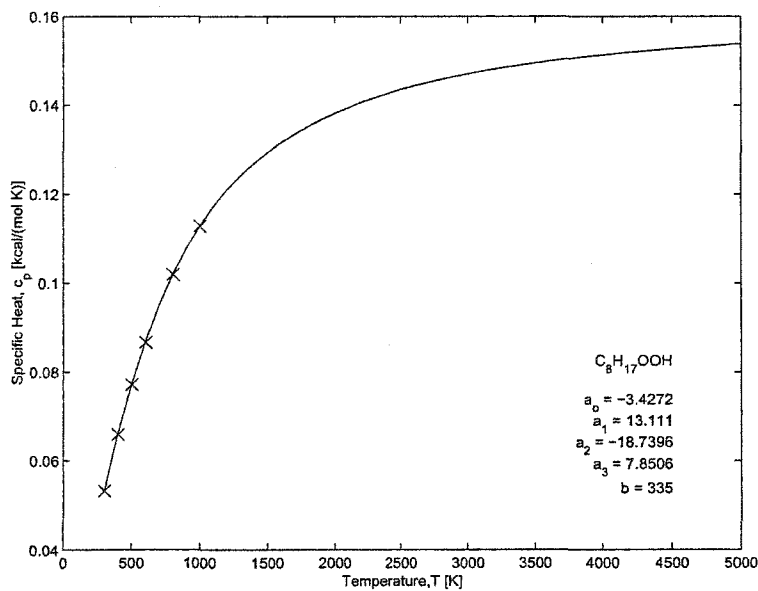


Figure B.12: Estimation of the specific heat of  $C_8H_{17}OOH$ .

APPENDIX B: EXTRAPOLATED  $C_p$  FITS

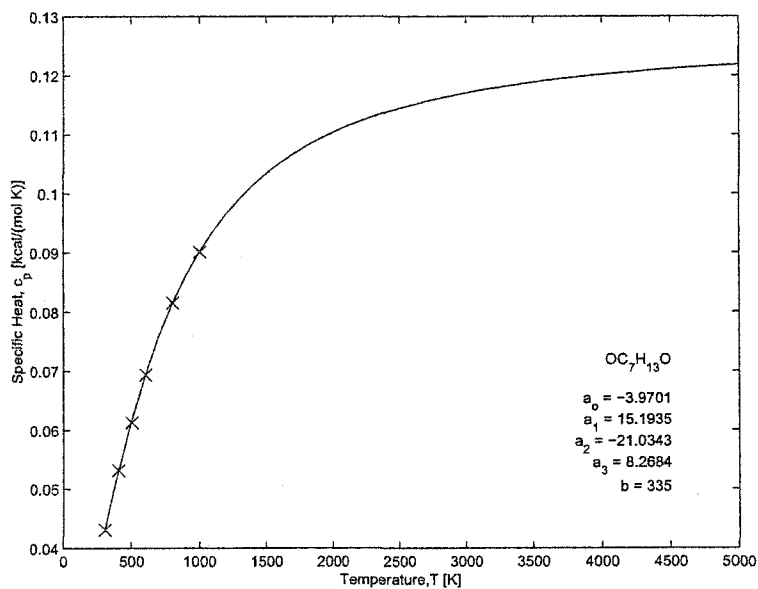


Figure B.13: Estimation of the specific heat of OC<sub>7</sub>H<sub>13</sub>O.

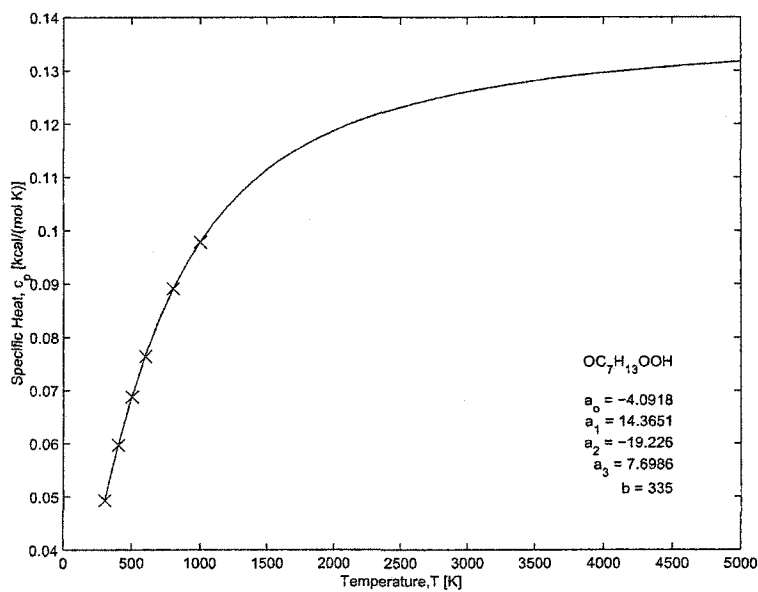


Figure B.14: Estimation of the specific heat of OC<sub>7</sub>H<sub>13</sub>OOH.

APPENDIX B: EXTRAPOLATED  $C_P$  FITS

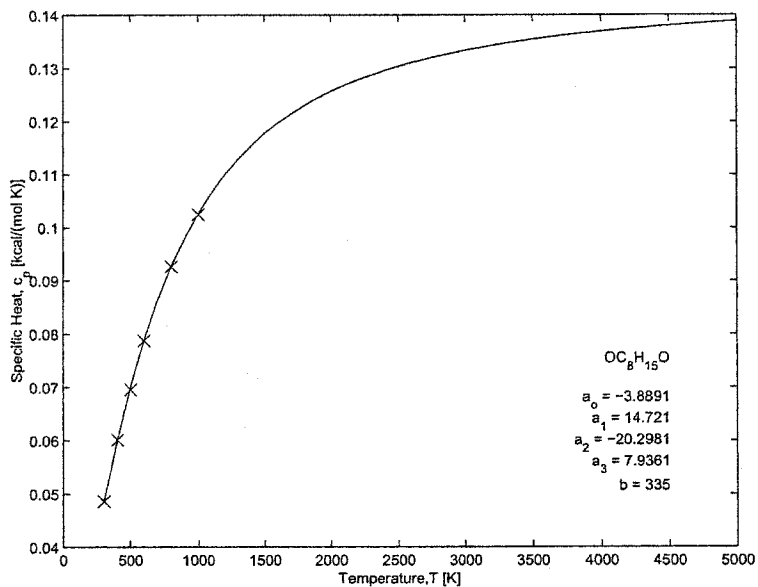


Figure B.15: Estimation of the specific heat of OC<sub>8</sub>H<sub>15</sub>O.

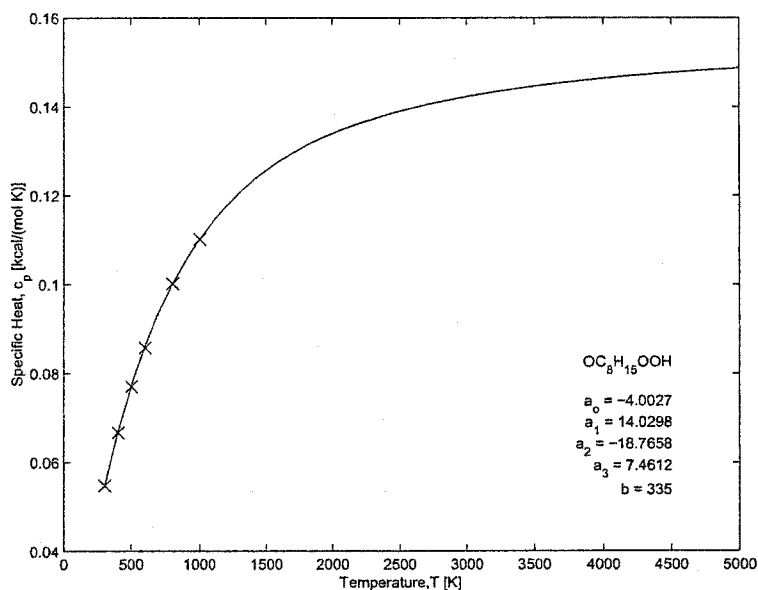


Figure B.16: Estimation of the specific heat of OC<sub>8</sub>H<sub>15</sub>OOH.

APPENDIX B: EXTRAPOLATED  $C_P$  FITS

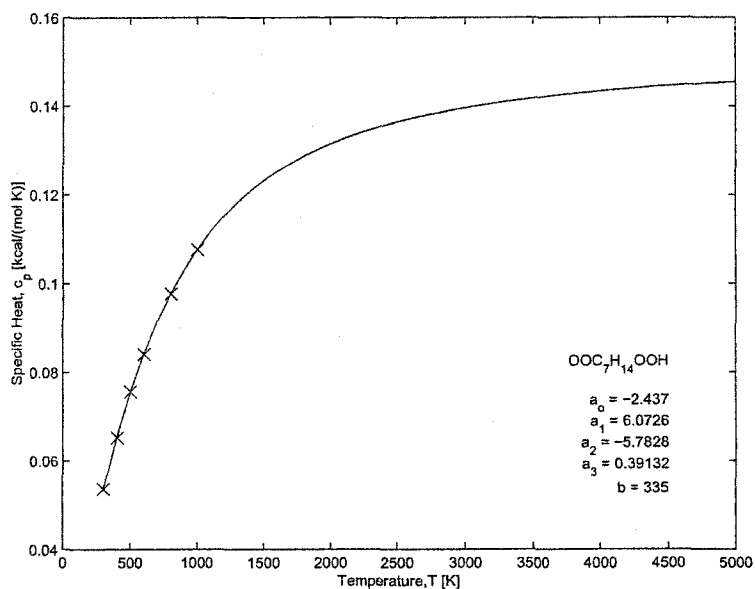


Figure B.17: Estimation of the specific heat of  $\text{OOC}_7\text{H}_{14}\text{OOH}$ .

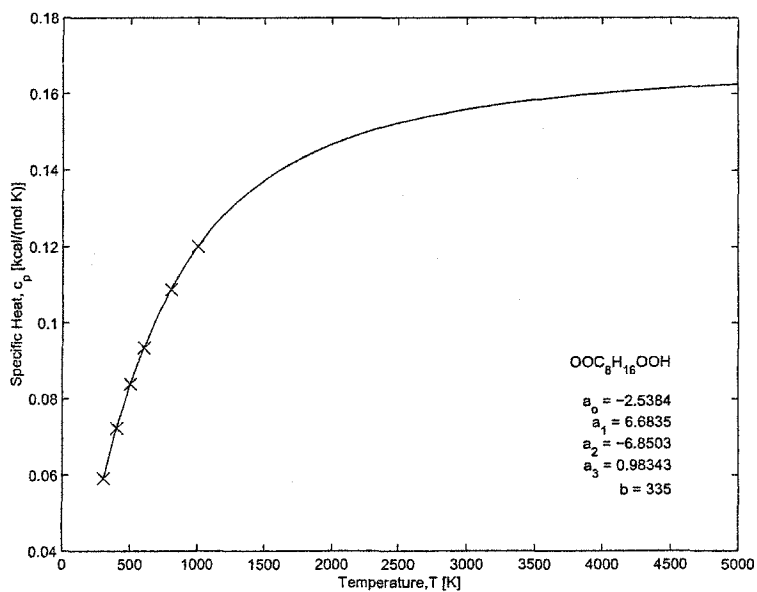


Figure B.18: Estimation of the specific heat of  $\text{OOC}_8\text{H}_{16}\text{OOH}$ .

## Appendix C

# Computer Programs

The following table briefly describes the major files used during the investigation presented in this thesis. The files are presented in alphabetical order and classified as to what type of file they are (function, script, or otherwise) and by how they are called (either by another program or by the user from the Base workspace).

Table C.1: List of computer programs used. All programs were written and executed with Matlab.

Name	Description	Type	Called By
calcPi_v35New.m	Evaluates the 2 parameters from the dimensional analysis (equation 5.12). Results from the parameter variations can either be read in from a directory specified by the user (slow) or provided in the from a previous run in the form of a .mat file (faster).	Function	Base
compParam_v1.m	Plots a comparison of the parameters, indicating what the conditions were for each point. Can also be used to filter which parameters are plotted (for example, only those with a given engine speed).	Function	Base
conditions.m	Displays the current parameter values used by the simulation.	Function	Base
engine_parameters_*.m	Engine parameter file describing the geometry of the engine.	Function	kinetics_fun.m
exothermic.mdl	Simulink model used to run the simulation. Specifies solver and tolerances to be used.	Simulink	start_exothermic.m
expMeanPress.m	Calculates the mean pressure history from the experimental results.	Function	postprocess_exp.m
expSimCompare.m	Plots comparisons of the experimental and simulated HCCI pressure histories. Can accept more than one set of simulation results (all within the same structure).	Function	Base
			<i>continued on next page...</i>

Name	Description	Type	Called By
finset.m	Inserts a desired string at the desired location in a specified file.	Function	makeKinTable.m
kinetics_fun.m	The implementation of the thermokinetic model. Solves the the differential equations as well as determines the discrete pressure state.	S-Function	exothermic.mdl
kinetics_fun_EGR.m	Version of kinetics_fun.m used for the investigation of the thermal effects of EGR. Suitable for only stoichiometric ( $\Phi = 1.0$ ) mixtures and sets the specific heat capacity of the mixture such that it is only that of the fuel/air mixture, regardless of the EGR rate.	S-Function	exothermic.mdl
lma_dyn_fields.m	Derives the differential equations describing specie concentrations in the format required for kinetics_fun.m	Function	Base
makeInput.m	Generates input files for kinetics_fun.m	Function	Base
makeKinTable.m	Creates source for a table showing the chemical kinetic mechanism (see table 3.2).	Function	Base
plotScriptHighLow.m	Plots a comparison of the experimental and simulation RCM ignition delays (see figure 4.3). Experimental ignition delays from Park & Keck (1990) are hard coded.	Script	postprocessRCM.m
plotScriptShockTube.m	Plots a comparison of the experimental and simulation shock tube ignition delays (see figure 4.5). Experimental ignition delays from Fieweger et al. (1997) are hard coded.	Function	Base
<i>continued on next page...</i>			

Name	Description	Type	Called By
plotScriptSJ.m	Plots a comparison of the STANJAN and simulation combustion temperatures (see figure 4.1). STANJAN combustion temperatures are hard coded.	Function	Base
postprocess_exp.m	Postprocessing routine for experimental results from Atkins (2004). Determines mean and cycle specific ignition timing. Prompts user for a directory in which the experimental results are located.	Function	Base
postprocessHCCI.m	Postprocessing routine for HCCI simulation results. Outputs a standard structure containing ignition timing and crank angle resolved states. Prompts user for a directory in which all .mat files will be processed.	Function	Base
postprocessRCM.m	Postprocessing routine for RCM validation simulations. Determines ignition delay based on the method outline by Park & Keck (1990).	Function	Base
postprocessShockTube.m	Postprocessing routine for shock tube validation simulations. Ignition timing is determined based on the method outlined by Fieweger et al. (1997)	Function	Base
postprocessSJ.m	Postprocessing routine for STANJAN validation simulations.	Function	Base
pressFilt.m	Filters the pressure trace to minimize noise amplification during differentiation.	Function	runExothermicBatch.m
			<i>continued on next page...</i>

Name	Description	Type	Called By
rassWith.m	Implementation of the Rassweiler & Withrow (1938) method to determine the exothermicity from a given pressure history.	Function	Base
reactions.mat	Contains the chemical reactions described by the differential equations. Used to determine equilibrium constants.	Binary Data	kinetics_fun.m
renameInput.m	Renames the files in a given directory to simplify file sorting.	Function	Base
runBatch.m	Carries out simulations with exothermic.mdl for all input files in the inputFiles directory.	Script	Base
runExothermicBatch.m	Runs the model using the currently specified parameters (generally defined using an input file).	Function	runBatch.m
spList.mat	Contains the standard index for the species described using the differential equations.	Binary Data	kinetics_fun.m
start_exothermic.m	Initializes the model and specifies a generic set of parameters. Prompts user for an engine parameter file.	Script	Base
THERM.txt	Comprehensive compilation of NASA polynomial coefficients. Does not include approximations for unknown species	Text file	kinetics_fun.m
therm_thergas.txt	Comprehensive compilation of NASA polynomial coefficients, including approximations for unknown properties determined using THERGAS (Muller et al. 1995).	Text file	kinetics_fun.m
			<i>continued on next page...</i>

Name	Description	Type	Called By
therm_unix.txt	Compilation of the NASA polynomial coefficients in Unix format for use with Westgrid. Includes approximations for unknown species determined using methods outlined in chapter 3.	Text file	kinetics_fun.m
THERMpk.txt	Compilation of NASA polynomial coefficients with approximations for unknown species determined using methods outlined in chapter 3.	Text file	kinetics_fun.m
time2cad.m	Resamples the time based simulation results to crank angle domain at 0.1CAD resolution.	Function	runExothermicBatch.m